Mutational scanning reveals substrate-assisted autoregulation of the WNT destruction complex

Murugesh Padmanarayana[1,2,3,8], Saira Sakalas[4], Parijat Sarkar[1,2,3], Mengxiao Ma[1,2,3], Ethan R. Garvin[2,3,5,6], Ethan Lee[7], Steven M. Corsello[2,3,6], Sebastian Guettler[4], Ganesh V. Pusapati[1,2,3,8]* and Rajat Rohatgi[1,2,3,9]*

[1]Department of Biochemistry, Stanford University School of Medicine, Stanford, CA 94305, USA
[2]Department of Medicine, Stanford University School of Medicine, Stanford, CA 94305, USA
[3]Stanford Cancer Institute, Stanford, CA 94305, USA
[4]Divisions of Structural Biology and Cell and Molecular Biology, The Institute of Cancer Research, London, UK
[5]Department of Genetics, Stanford University School of Medicine, Stanford, CA 94305, USA
[6]Department of Chemical and Systems Biology, Stanford University School of Medicine, Stanford, CA 94305, USA
[7]Department of Cell and Developmental Biology, Vanderbilt University, Nashville, TN 37232, USA
[8]These authors contributed equally
[9]Lead contact

*Correspondence: rrohatgi@stanford.edu (R.R.) and ganesh22@stanford.edu (G.V.P)

Abstract

The β-catenin destruction complex (BDC) is a central node in WNT/β-catenin signaling, governing embryonic development and adult tissue homeostasis. Although recognized as a prime therapeutic target in colorectal cancer (CRC) for three decades, its dynamic architecture and biochemical complexity have hindered mechanistic understanding. Here, we systematically mapped the sequence-function landscape of the BDC using tiled base editor screens across four endogenous components—*CTNNB1*, *AXIN1*, *APC*, and *GSK3B*. Validation studies identified ~150 previously unreported mutations across these genes that affected WNT/β-catenin signaling. In addition to known cancer-associated mutations, we discovered rare gain-of-function and separation-of-function alleles of *AXIN1* and *CTNNB1* that provide mechanistic insights into complex assembly and regulation. We describe a region in β-catenin that regulates its binding to TCF/LEF transcription factors and demonstrate that the AXIN1–β-catenin interface is critical for controlling signaling flux through the oncogenic BDC. Mechanistic studies revealed that assembly of the oncogenic BDC is scaffolded by its own substrate β-catenin, establishing an autoregulatory mechanism that represents an unexploited vulnerability in cancers harboring common APC truncations. Our comprehensive mutational resource provides a foundation for understanding WNT/β-catenin signaling mechanisms in health and disease, while revealing strategies for therapeutic intervention in WNT-driven cancers.

Introduction

The WNT/β-catenin pathway is a cell-cell communication system that coordinates the patterning and morphogenesis of most tissues during development[1,2]. Even minor defects in signaling strength cause multiorgan birth defects in humans[3]. In adults, WNT/β-catenin signaling maintains tissue homeostasis by guiding regeneration and repair and has been implicated in chronic degenerative diseases of multiple tissues, including the brain, bone and gastrointestinal

system[1]. Unchecked WNT/β-catenin signaling is a major cause of human cancer morbidity and mortality, yet we lack a single FDA-approved agent targeting this pathway in any cancer[4]. Truncating mutations in the tumor suppressor gene Adenomatous Polyposis Coli (*APC*) lead to ligand-independent, oncogenic signaling that drives >80% of human colorectal cancer (CRC), the second leading cause of cancer deaths[5–9].

APC is a component of the β-catenin destruction complex (BDC), a multi-protein complex that limits WNT/β-catenin signaling by promoting the degradation of β-catenin, a multi-functional protein that coordinates the WNT gene expression program[10–12]. The BDC is composed of two scaffolding proteins (APC and AXIN1), two kinases (CK1α and GSK3β), and β-catenin. In the absence of WNTs, the BDC keeps signaling off by promoting the sequential phosphorylation of β-catenin by CK1α and GSK3β, thus marking it for ubiquitination and degradation[13] (**Fig.1a**). WNTs promote inactivation of the BDC by the receptor complex[14]. As a result, β-catenin accumulates and assembles an activating enhanceosome complex, including BCL9 and TCF/LEF factors, at target gene promoters[15].

Three decades of structural and biochemical studies have mapped multiple, overlapping and seemingly redundant protein-protein interactions (PPIs) between the BDC components[2,10,11,16] (**Fig.1b**). β-catenin contains a structured central armadillo (ARM) domain composed of 12 repeats and flexible N- and C-terminal segments. β-catenin engages both AXIN1 and APC (and the TCF/LEF family of transcription factors in the nucleus) in a groove that extends along the ARM superhelix. While AXIN1 binds at ARM repeats 3-4, APC and the TCF/LEF proteins bind along a much longer extent of this groove. APC can bind to β-catenin through four 15aa (15R A-D) and six 20aa (20R 1-7, excluding 20R2) peptide motifs. These motifs in APC can bind β-catenin *in vitro* with varying affinities. Phosphorylation of the 20R repeats by CK1α and GSK3β can enhance their affinities for β-catenin by ~1000-fold[17,18]. APC contains three SAMP motifs that allow it to independently interact with an N-terminal RGS domain in AXIN1[19]. AXIN1 recruits the kinases CK1α and GSK3β into the BDC complex, bringing them into the proximity of their substrates β-catenin and APC[20–22]. The above picture is further complicated by the fact that other proteins occupy the same groove along the β-catenin ARM domain: the TCF/LEF family of transcription factors in the nucleus, cadherins at adherens junction, and ICAT (inhibitor of β-catenin and TCF4) (reviewed in [11]). Thus, β-catenin participates in at least three cellular assemblies: adherens junction, the BDC in the cytoplasm that regulates its destruction, and the transcriptional complex in the nucleus that shapes the WNT/β-catenin gene expression program.

The complex biochemistry of the BDC has presented obstacles to both mechanistic understanding and therapeutic targeting. For example, we lack information about which sequence elements and protein surfaces are relevant for the activity of the wild-type and oncogenic BDC *in vivo* under endogenous expression levels. Current models are based predominantly on structural or biochemical data with purified protein fragments or overexpression studies in cells (with the notable exception of causal disease variants identified through genetics). The issue of abundance is particularly relevant for the BDC since its size and composition can vary as concentrations of the individual components change[16]. Here we report adenine and cytosine base editor screens to evaluate the WNT signaling phenotype of mutations introduced across endogenous gene loci encoding BDC components[23–27]. Our screens identified classes of mutations that are highly informative (and thus sought after) in sequence-function studies: activating mutations, separation-of-function mutations and mutations that nominate

novel regulatory sites. This strategy enabled the identification of surfaces in component proteins that can be used to regulate the activity of the wild-type and oncogenic BDC.

Results

Tiled base editor screens targeting endogenous destruction complex genes

We used promiscuous PAM-flexible (NG-PAM Cas9n) adenine and cytosine base editors (NG-ABE8e and NG-BE3) to generate transition mutations across all exons of endogenous *APC, AXIN1, CTNNB1* (encoding β-catenin) and *GSK3B* (encoding GSK3β) in a pooled format[25–28]. Our ABE and CBE libraries are predicted to generate missense mutations at 80-90% of amino acid residues encoded by each gene (**Extended Data Fig.1a, Supplementary Table 1**). Both libraries also generated silent and splice site mutations, since the design strategy allowed single-guide RNAs (sgRNAs) to extend ~20 nucleotides into introns at each intron-exon junction (**Extended Data Fig.1b**). However, nonsense mutations will only be generated in the CBE library. The sgRNA library covers each exon in a tiled fashion (**Extended Data Fig.1c**).

Mutagenesis was conducted in haploid human cells (eHAP1) stably expressing our fluorescent transcriptional reporter of WNT/β-catenin signaling strength (7TS, **Fig.1c**)[29]. HAP1 cells, previously established as a powerful model for genetic screens targeting the WNT/β-catenin pathway[29], only possess one allele of each gene and hence simplify the phenotypic evaluation of endogenous mutations[30–32]. Pooled ABE and CBE mutant cell libraries were treated (separately, in duplicate) with the ligand Wnt-3a. Cells with 7TS fluorescence intensities in the top 10% or bottom 15% of the mutant population were isolated using fluorescence activated cell sorting (FACS) to enrich cells carrying mutations that increased or decreased signaling strength, respectively[29] (**Fig.1d**). We sequenced the top 10% sorted (Top 10%), bottom 15% sorted (Bottom 15%), and unsorted cell populations using the Illumina platform. (**Extended Data Fig.1d, Supplementary Table 1**). Two z-scores for each sgRNA (for enrichment in the Top 10% and Bottom 15% gates) were calculated based on a distribution of 282 non-targeting control sgRNAs (**Supplementary Table 1**). sgRNAs that cause mutations that elevate signaling would be depleted from the Bottom 15% gate (negative z-score) and enriched in the Top 10% gate (positive z-score). Conversely sgRNAs that reduce signaling would be enriched in the Bottom 15% gate but depleted from the Top 10% gate. Full results of the screen, including plots showing the position of statistically significant sgRNAs along the protein sequence of each BDC component are shown in **Supplementary Table 1** and **Extended Data Figs.2 and 3**. Our untargeted screens identified many known functional sites, including the phosphodegron in β-catenin and the tankyrase, β-catenin and Dishevelled (DVL) binding sites in AXIN1 (**Extended Data Figs.2 and 3).**

Some of the most statistically significant sgRNAs in our screen encode mutations that drive oncogenic WNT/β-catenin signaling in human cancer[7,33]. Over 80% of sporadic and familial CRC cases are driven by truncating mutations that map to a ~250 amino-acid segment in the central Intrinsically Disordered Region (IDR) of APC known as the Mutation Cluster Region or MCR[34–40] (**Fig.1e)**. Mutant *APC^{mcr}* alleles in human cancer produce a truncated protein rather than eliminating APC from the cell. APC^{mcr} lacks all three SAMP repeats that mediate the direct interaction of APC with AXIN1 (**Fig.1b** and **1e**), thus forming a compromised, oncogenic BDC that cannot fully suppress β-catenin abundance and WNT target gene expression in the absence of ligand stimulation[16,41,42]. Multiple CBE sgRNAs predicted to introduce nonsense mutations in APC were enriched in the Top 10% gate, but all these targeted residues are located before the

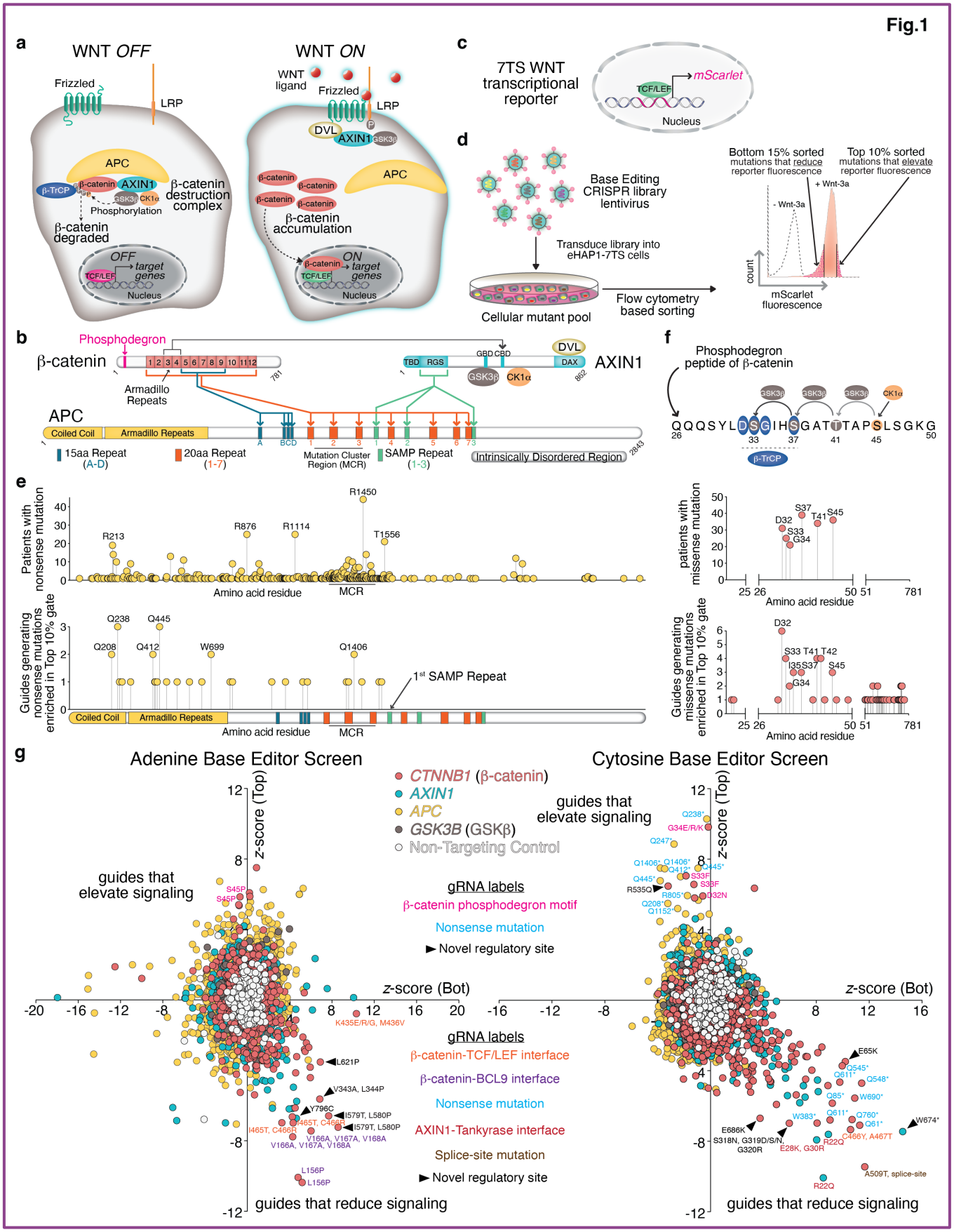
Fig.1
a
WNT OFF
Frizzled
LRP
APC
β-TrCP
β-catenin
AXIN1
GSK3β
CK1α
Phosphorylation
β-catenin destruction complex
β-catenin degraded
OFF
TCF/LEF
target genes
Nucleus
WNT ON
WNT ligand
Frizzled
LRP
DVL
AXIN1
GSK3β
APC
β-catenin
β-catenin accumulation
ON
TCF/LEF
target genes
Nucleus
c
7TS WNT transcriptional reporter
TCF/LEF
mScarlet
Nucleus
d
Base Editing CRISPR library lentivirus
Transduce library into eHAP1-7TS cells
Cellular mutant pool
Flow cytometry based sorting
Bottom 15% sorted mutations that reduce reporter fluorescence
Top 10% sorted mutations that elevate reporter fluorescence
- Wnt-3a
+ Wnt-3a
count
mScarlet fluorescence
b
Phosphodegron
β-catenin
Armadillo Repeats
APC
Coiled Coil
Armadillo Repeats
15aa Repeat (A-D)
20aa Repeat (1-7)
Mutation Cluster Region (MCR)
SAMP Repeat (1-3)
Intrinsically Disordered Region
GBD CBD
DVL
DAX
TBD RGS
GSK3β
CK1α
AXIN1
f
Phosphodegron peptide of β-catenin
GSK3β
CK1α
β-TrCP
QQQSYLDSGIHSGATTAPSLSGKG
e
Patients with nonsense mutation
R213
R876
R1114
R1450
T1556
Amino acid residue
MCR
Guides generating nonsense mutations enriched in Top 10% gate
Q238
Q445
Q208
Q412
W699
Q1406
1st SAMP Repeat
Coiled Coil
Armadillo Repeats
Amino acid residue
MCR
patients with missense mutation
D32
S33
G34
S37
T41
S45
Amino acid residue
Guides generating missense mutations enriched in Top 10% gate
D32
S33 T41 T42
I35 S37
S45
G34
Amino acid residue
g
Adenine Base Editor Screen
Cytosine Base Editor Screen
CTNNB1 (β-catenin)
AXIN1
APC
GSK3B (GSKβ)
Non-Targeting Control
z-score (Top)
z-score (Bot)
guides that elevate signaling
guides that reduce signaling
gRNA labels
β-catenin phosphodegron motif
Nonsense mutation
Novel regulatory site
gRNA labels
β-catenin-TCF/LEF interface
β-catenin-BCL9 interface
Nonsense mutation
AXIN1-Tankyrase interface
Splice-site mutation
Novel regulatory site
S45P
K435E/R/G, M436V
L621P
V343A, L344P
Y796C
I579T, L580P
I465T, C466R
V166A, V167A, V168A
L156P
E65K
E686K
S318N, G319D/S/N, G320R
E28K, G30R
R22Q
A509T, splice-site
W674*
C466Y, A467T

Fig. 1. Base editor screens identify mutational hotspots in the β-catenin destruction complex. a, Inactivation of the β-catenin destruction complex (BDC) by WNTs leads to the accumulation of β-catenin and activation of WNT target genes. **b,** The BDC (composed of APC, β-catenin, AXIN1 and the AXIN1-bound kinases CK1α and GSK3β) is assembled by multivalent, redundant interactions between folded domains (armadillo repeats, RGS) and linear peptide motifs (15R, 20R, or SAMP). Colored lines indicate previously mapped PPIs between AXIN1-APC, APC-β-catenin, and AXIN1-β-catenin. Most oncogenic mutations in APC truncate the protein in the Mutation Cluster Region (MCR), eliminating all direct contacts with AXIN1 and a subset of contacts with β-catenin. TBD, Tankyrase Binding Domain; DVL, Dishevelled; CBD, β-catenin Binding Domain; GBD, GSK3β Binding Domain, DAX, Domain present in DVL and AXIN. **c,** The transcriptional reporter used to measure WNT/β-catenin signaling strength contains a TCF-responsive element (7 TCF binding sites) driving mScarlet expression (abbreviated 7TS). **d,** Strategy for pooled base-editing screens in human haploid cells carrying the fluorescent WNT reporter (eHAP1-7TS) shown in **c**. **e,** Lollipop plots compare the position (x-axis) and frequency (y-axis) of nonsense mutations in APC from The Cancer Genome Pan-Cancer Atlas (top) with the position of nonsense mutations enriched in the Top 10% gate of our cytosine base editor (CBE) screen (bottom). Most enriched nonsense mutations were found before the first SAMP repeat (see **b**) in both human cancers and our screens. **f,** Lollipop plots show the high frequency of WNT-activating mutations found in β-catenin phosphodegron motif both in human cancers (top) and missense mutations enriched in the Top 10% gate of our base editing screens (bottom). **g,** Plots showing *z*-scores for enrichment of each sgRNA in the Bottom 15% (Bot, x-axis) and Top 10% (Top, y-axis) gates used for sorting mutant cells with diminished or enhanced WNT/β-catenin signaling strength, respectively (see **d**). Each sgRNAs is represented by a single dot colored according to the targeted gene. Label colors identify guides predicted to cause nonsense mutations, splice-site mutations, or mutations at known residues that mediate key PPI or PTMs. Arrowheads indicate sgRNAs that nominate new regulatory sites.
See also Extended Data Figures 1, 2, and 3; Supplementary Tables 1 and 3.

first SAMP repeat (**Fig.1e**). This result mirrors the observation that truncated APC variants that include the first SAMP are not tumorigenic in mouse models[43].

The most common oncogenic β-catenin mutations across multiple human cancers disrupt an N-terminal degron motif (^{32}DSGIHSGATTAPS^{45}) sequentially phosphorylated by two AXIN1-bound kinases, Casein Kinase 1α (CK1α) and GSK-3β[13] (**Fig.1f**). GSK-3β phosphorylation of Ser33 and Ser37 in this degron generates a high-affinity binding site (^{32}DpSGφXpS^{37}) for the SCF$^{\beta\text{-TrCP}}$ E3 ligase, which ubiquitylates β-catenin and earmarks it for proteasomal degradation[44]. Multiple overlapping sgRNAs targeting nearly all the critical residues in this phosphodegron and β-TrCP binding site (e.g. the invariant Asp32) were enriched in the Top 10% sorted population, consistent with their expected effect of causing mutations that drive constitutive, high-level WNT/β-catenin signaling (**Fig.1f**).

An *x*-*y* plot of sgRNA z-scores for enrichment in the Bottom 15% gate (*x*-axis) vs. Top 10% gate (*y*-axis) identified sgRNAs predicted to make mutations in regions known to be critical for BDC function and regulation (**Fig.1g**). AXIN1 mutations in residues that mediate its interaction with the negative regulator tankyrase are predicted to impair WNT/β-catenin signaling[45]. Indeed, sgRNAs encoding such mutations at the AXIN1-tankyrase interface are depleted from the Top 10% gate and enriched in the Bottom 15% gate. sgRNAs predicted to mutate β-catenin residues at its interfaces with the activating TCF/LEF transcription factors and the BCL9 co-activator are enriched in the Bottom 15% gate but depleted from the Top 10% gate. Conversely, sgRNA that truncate APC or introduce mutations at the β-TrCP-β-catenin interface

are enriched in the Top 10% gate. This bird's eye view of screen results confirmed that our strategy, based on measuring enrichment of each sgRNA in two gates designed to isolate cells with elevated or reduced WNT/β-catenin signaling strength, efficiently identified residues in BDC components required to mediate regulatory PPIs and post-translational modifications (PTMs).

To select missense mutations for deeper mechanistic analysis, we took a systematic approach to validating the results of our base editing screens (diagrammed in **Extended Data Fig.4a**). Preference was given to sgRNAs with z-scores ≥2 that targeted residues not mplicated in prior structural or biochemical studies and residues targeted by multiple different guides (**Extended Data Figs. 2 and 3**). Initial filtering yielded 370 guides across *CTTNB1* (80 sgRNAs), *AXIN1* (73 sgRNAs), *APC* (196 sgRNAs), and *GSK3B* (21 sgRNAs). Each sgRNA was individually re-tested for its effect on WNT/β-catenin signaling strength using the 7TS reporter in eHAP1 cells and, for those guides that showed a significant effect, a second validation test was conducted in HEK293T cells (**Extended Data Fig.4, Supplementary Table 2**). Most of the missense mutations that were successfully validated mapped to β-catenin and AXIN1 (**Extended Data Fig.4b-e**). The z-scores for missense mutations in APC and GSK3β were lower (2<z<3, **Extended Data Fig.3**) compared to β-catenin and AXIN1 (**Extended Data Fig.2**). During validation studies, these mutations in APC and GSK3β had only modest effects (**Extended Data Fig.4f and g**). We speculate that APC engages in redundant interactions that cannot easily be disrupted by point mutations and that inactivating mutations in GSK3β might impair cell growth. Regardless, we focused on the mechanistic analysis of mutations in β-catenin and AXIN1 for the remainder of the study .

The sequence-function landscape of β-catenin

To identify new regulatory sites in the BDC, we first focused on analysis of missense mutations in β-catenin (**Fig.2a, 2b, Extended Data Fig.2a-2d**). For ease of description, we divided β-catenin into 6 regions (Sites 1-6) that mediate specific PPIs or regulatory functions (**Fig.2b, Extended Data Fig.5a**)[11]. Mapping Top 10% and Bottom 15% enrichment z-scores (above a cutoff of 2) onto a structural model[46,47] revealed that our screen identified mutations in β-catenin located at known interaction interfaces with β-TrCP, BCL9, AXIN1, APC and the TCF/LEF transcription factors (**Fig.2a**). A detailed examination of structurally characterized PPI interfaces demonstrated that our screen identified key residues predicted to make contacts (defined as a distance <5 Å) between β-catenin and β-TrCP[44] (**Extended Data Fig.5b**), β-catenin and BCL9[48] (**Extended Data Fig.5c**), β-catenin and LEF1[49] (**Extended Data Fig.5d**), and β-catenin and TCF4[50] (**Extended Data Fig.5e**). Interestingly, we also identified mutations around these interfaces that were beyond the 5 Å distance cutoff for a contact, suggesting that allosteric effects or changes in local conformation can influence these interactions.

Overall, our screen and subsequent directed analysis in two different cell lines provided functional data on endogenous mutations at ~186 residues in β-catenin (**Fig.2b, Extended Data Fig.5a**). While most β-catenin mutations reduced WNT signaling strength, we also identified gain-of-function mutations (e.g. phosphodegron mutations) that elevated signaling (**Fig.2b**). The high quality of these data is demonstrated by the identification of multiple residues that have been previously implicated in β-catenin function (highlighted in bold lettering in **Extended Data Fig.5a** and labeled in **Fig.2b**). Additionally, the tiling design of our libraries (**Extended Data Fig.1c**) allowed the identification of multiple sgRNAs that targeted the same residue, (**Extended Data Figs.2a-2d, 5a**). Our screens also identified unexpected mutations in β-catenin that either

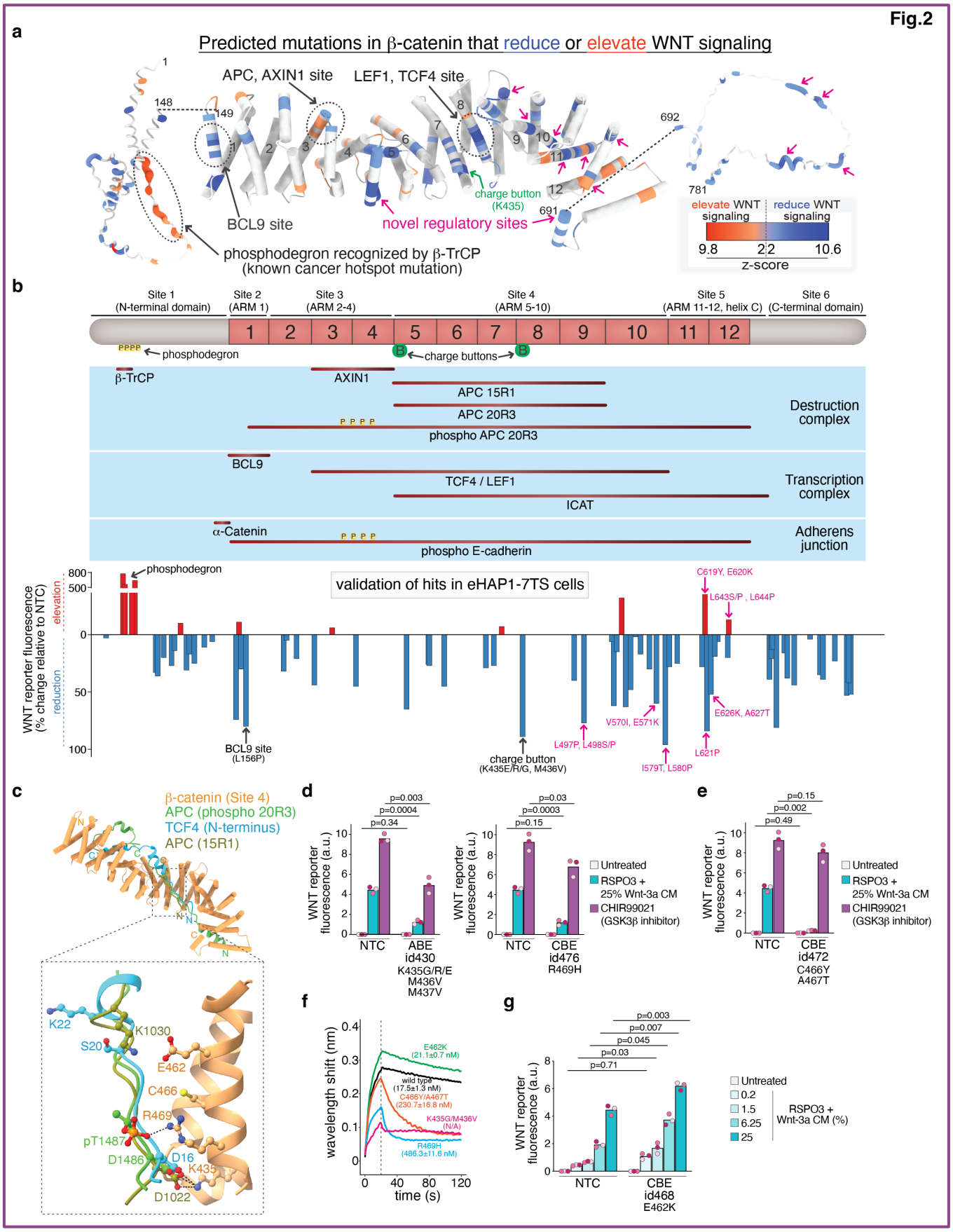
Fig.2
a
Predicted mutations in β-catenin that reduce or elevate WNT signaling
APC, AXIN1 site
LEF1, TCF4 site
BCL9 site
novel regulatory sites
charge button (K435)
phosphodegron recognized by β-TrCP (known cancer hotspot mutation)
elevate WNT signaling
reduce WNT signaling
9.8
2.2
10.6
z-score
b
Site 1 (N-terminal domain)
Site 2 (ARM 1)
Site 3 (ARM 2-4)
Site 4 (ARM 5-10)
Site 5 (ARM 11-12, helix C)
Site 6 (C-terminal domain)
phosphodegron
charge buttons
β-TrCP
AXIN1
APC 15R1
APC 20R3
phospho APC 20R3
Destruction complex
BCL9
TCF4 / LEF1
ICAT
Transcription complex
α-Catenin
phospho E-cadherin
Adherens junction
validation of hits in eHAP1-7TS cells
WNT reporter fluorescence (% change relative to NTC)
elevation
reduction
BCL9 site (L156P)
charge button (K435E/R/G, M436V)
L497P, L498S/P
V570I, E571K
I579T, L580P
L621P
E626K, A627T
C619Y, E620K
L643S/P , L644P
c
β-catenin (Site 4)
APC (phospho 20R3)
TCF4 (N-terminus)
APC (15R1)
K22
S20
K1030
E462
C466
R469
pT1487
D1486
D16
K435
D1022
d
WNT reporter fluorescence (a.u.)
NTC
ABE id430 K435G/R/E M436V M437V
CBE id476 R469H
Untreated
RSPO3 + 25% Wnt-3a CM
CHIR99021 (GSK3β inhibitor)
e
CBE id472 C466Y A467T
f
wavelength shift (nm)
time (s)
E462K (21.1±0.7 nM)
wild type (17.5±1.3 nM)
C466Y/A467T (230.7±16.8 nM)
K435G/M436V (N/A)
R469H (486.3±11.6 nM)
g
CBE id468 E462K
0.2
1.5
6.25
25
RSPO3 + Wnt-3a CM (%)

202

Fig.2. Base editing screens identify known and novel regulatory surfaces on β-catenin. a, A β-catenin backbone structural model (PDB 2Z6H) shows the position of missense mutations predicted (based on an editing window spanning N3-N10 of the protospacer) to be generated by sgRNAs with z-scores ≥ 2 in either the ABE or CBE screens[46]. Coloring denotes whether the predicted mutation increased (red) or decreased (blue) WNT/β-catenin signaling, based on whether the encoding sgRNA was enriched in the Top 10% or Bottom 15% gates used for sorting (see **1d**). Black arrows point to amino acid residues previously implicated in β-catenin function; magenta arrows highlight candidate residues that play a functional role in signaling. The 12 armadillo repeats of β-catenin are numbered on the last helix of each repeat. The N- and C-terminal segments of β-catenin (absent in published structures) were modeled by AlphaFold3 and are represented as worm models with a radius specified by the z-score[84]. **b,** Linear cartoon of β-catenin (top) showing Sites 1-6 and position of key charge button residues is aligned with a graphic showing regions of the ARM superhelix that interact with various partner proteins (brown lines in middle panel). The bar graph (bottom, aligned to the top cartoon) shows the position of sgRNAs that increased (red) or decreased (blue) WNT/β-catenin signaling strength (relative to a non-targeting control sgRNA, NTC) when individually introduced into eHAP1-7TS cells. Black arrows denote sgRNAs that target known β-catenin interaction interfaces and magenta arrows show sgRNAs selected for mechanistic analysis. **c,** Superimposed structural models showing the interaction of phosphorylated APC 20R3 (PDB 1TH1, green), TCF4 (PDB 1JDH, blue), and APC 15R1 (PDB 1JPP, olive) with β-catenin (PDB 2Z6H, sandy brown)[46,50,54,55]. In the zoomed view, a ball-and-stick depiction is used to show side chains of β-catenin residues identified as functionally significant in our screens. Electrostatic interactions are indicated with dashed black lines. **d,e,g,** WNT/β-catenin signaling strength (measured using the 7TS reporter, see **1c**) in HEK293T-7TS cells carrying various screen-identified mutations in β-catenin. Cells were treated with the indicated concentrations of Wnt-3a conditioned media (always in the presence of the potentiator RSPO3) or a GSK3β inhibitor (CHIR99021) for 24 h. Bars represent the mean of three biological replicates (n=3, corresponding points from each replicate are colored a different shade of pink). Each point represents the mean fluorescence from approximately 10,000 cells in a single biological replicate. Note that **d** and **e** show experiments that were conducted together (with the same control) but are depicted separately for clarity. Statistical significance was determined using multiple unpaired Student's t-tests with Welch's correction. P-values were adjusted using the two-stage step-up method (Benjamini, Krieger, and Yekutieli) to control the false discovery rate (FDR) at Q = 0.01. **f,** Biolayer interferometry (BLI) was used to assess association and dissociation kinetics between a GST-tagged TCF4 fragment (a.a. 1-53, immobilized on the BLI probe at 50 nM) and untagged, full-length β-catenin variants (1 μM). One representative curve is shown, with the affinity constant (K_D ± s.d.) calculated from three independent replicates. See also Extended Data Figures 4 and 5 and Supplementary Table 2.

increase or decrease WNT/β-catenin signaling strength (but cannot be readily predicted by prior structural or biochemical studies). While we can explore only a small fraction of this dataset in this study, we hope that it serves as a valuable resource for the field to understand the function of β-catenin, a target for drugs being tested in CRC.

As an illustration of how scanning mutagenesis can be used to probe a structurally defined protein interaction interface, we focused on β-catenin Site 4, which forms an extended groove along the ARM superhelix between repeats 5-10 (**Fig.2b,2c**). The groove in Site 4 can bind (in a mutually exclusive manner based on structural data) to APC 20R and 15R repeats, TCF/LEF proteins, the negative regulator ICAT, and E-cadherin[49,51–57] (**Fig.2c**). Our screen identified a column of mutations along one face of a helix that frames the Site 4 groove: K435G/M436G, R469H, C466Y/A467T, and E462K (**Fig.2c**). K435 is a well-characterized “charge button” residue known to be critical for multiple β-catenin interactions[11]. Indeed, sgRNAs targeting β-

215 catenin K435 or a nearby basic residue R469 reduced signaling strength in response to WNTs
216 or the GSK3-β inhibitor CHIR99021, consistent with their roles in anchoring β-catenin to
217 TCF4[51,52] (**Fig.2d**). Mutations at β-catenin C466/A467, implicated in nonpolar contacts with both
218 APC and TCF4[58,59], also markedly reduced signaling strength in response to WNTs (**Fig.2e**). β-
219 catenin C466Y/A467T was fully active when signaling was initiated using CHIR99021,
220 demonstrating these mutations did not compromise β-catenin integrity. Biolayer interferometry
221 (BLI) binding assays using purified proteins confirmed that the R469H and C466Y/A467T
222 mutations in β-catenin reduced its affinity for TCF4 by >10-fold (**Fig.2f**).
223 We also identified β-catenin mutations in this crowded PPI region that had effects only on
224 specific interaction partners. E462K unexpectedly enhanced signaling strength in cells (**Fig. 2g**),
225 suggesting selectively impaired interactions with the negative regulator APC. In binding assays
226 with purified proteins, E462K did not change the affinity of the β-catenin-TCF4 interaction
227 (**Fig.2f**). E462 likely forms an electrostatic interaction with K1030 in APC 15R1, though the
228 K1030 side chain is disordered in the β-catenin-APC 15R-A crystal structure[54] (**Fig.2c**). The
229 residue at the position corresponding to APC K1030 in TCF4 points in the opposite direction
230 (TCF4 K22) and thus cannot make a salt bridge with β-catenin E462, explaining why β-catenin
231 E462K is a separation-of-function mutation that can discriminate between APC and TCF/LEF
232 binding.
233
234 **New gain- and loss-of-function mutations in β-catenin**
235 Several mutations in Sites 4-6 identified in our screen targeted residues not previously implicated
236 in β-catenin function (sgRNAs highlighted in magenta lettering in **Fig.2b**, individual mutations
237 shown in **Extended Data Fig.5a**). Mechanistic analysis was conducted in pooled HEK293T cell
238 lines established after introduction of the base editor and specific sgRNA. Mutant allele
239 frequencies in all cell lines were measured using Illumina sequencing to identify the dominant β-
240 catenin mutation (**Extended Data Fig.6a**).
241 In β-catenin Site 4 (ARM5-10), three mutations (L497P/L498P, E571K and I579T/L580P,
242 **Fig.3a**) reduced Wnt-3a-induced activation of both the 7TS reporter (**Fig.3b**) and transcription
243 of the endogenous target gene *AXIN2* (**Extended Data Fig.7a**). Mutations in these residues
244 impair signaling to the same extent as mutations that include the critical charge button
245 (K435G/M436V), but they are not predicted to make contacts with any known interaction
246 partners. To measure in-cell PPIs, β-catenin was immunoprecipitated (IP) from extracts of
247 untreated cells or cells treated with Wnt-3a or CHIR99021 (**Fig.3c**). Importantly, these loss-of-
248 function mutations did not decrease the abundance of β-catenin or abolish the interaction of β-
249 catenin with AXIN1, APC or E-cadherin. However, these mutations decreased the interaction
250 between β-catenin and multiple members of the TCF/LEF family of transcriptional activators. We
251 propose that these mutations have allosteric or indirect effects selectively on the β-catenin-
252 TCF/LEF interaction or that the published structures (which use N-terminal fragments of
253 TCF/LEF) did not capture the full extent of this critical activating interaction.
254 The E571K mutation was distinguished by the property that it inhibited Wnt-3a-driven
255 signaling but had little effect on signaling initiated by CHIR99021 (**Fig.3b**). Consistent with
256 activity assays, the interaction between β-catenin E571K and TCF/LEF proteins was partially
257 restored by CHIR99021 (**Fig.3c**). *In vitro* interaction assays (BLI) demonstrated that purified β-
258 catenin E571K could still bind to purified TCF4, though its affinity was reduced by ~7-fold relative
259 to wild-type β-catenin (**Fig.3d**). The E571K mutation did not change the affinity between β-

catenin and ICAT, a negative regulator that also binds in this region. In comparison, the β-catenin K435G/M436V charge button mutant had no detectable affinity for TCF4 and reduced affinity for ICAT (**Fig.3d**). Interestingly, E571K was the only mutant with a defect in Wnt-3a-induced accumulation of β-catenin (provisionally defined as the pool unphosphorylated at the N-terminal phosphodegron, **Extended Data Fig.7b**). Thus, the E571K mutation, in addition to impairing TCF/LEF binding, may cause a defect in BDC inactivation by WNTs.

We next turned to mutations in Site 5 (ARM11-12) that both decreased (**Fig.4a**, **Extended Data Fig.7c**) and increased (**Fig.4b**) WNT ligand sensitivity, without substantially altering protein abundance (**Fig.4c**). The reduction-of-function L621P and D624N/E626K/E628K mutations

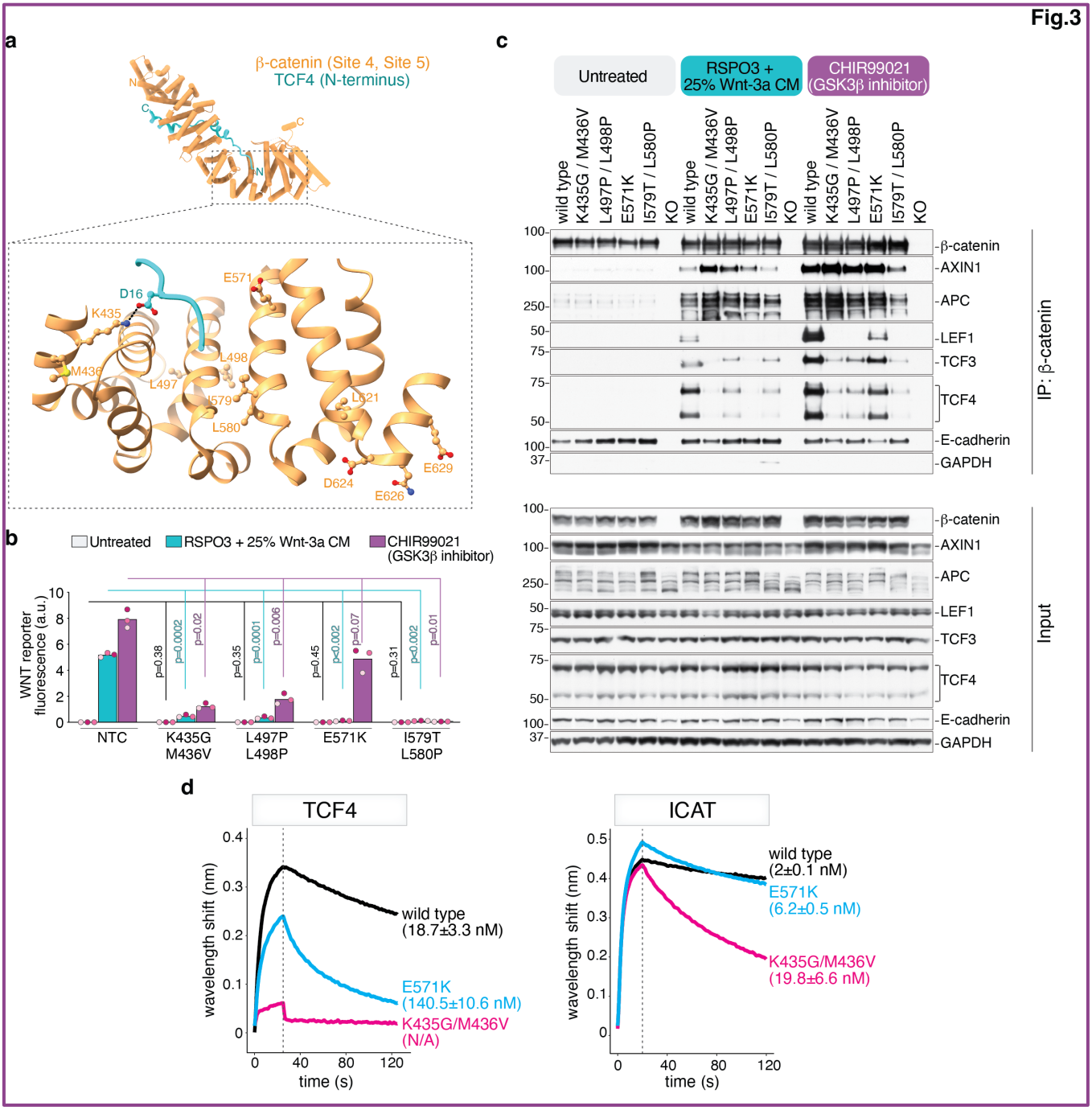

Fig. 3. Mutations in β-catenin Site 4 affect interactions with the TCF/LEF transcription factors. a, Structure of β-catenin (PDB 2Z6H, sandy brown) in complex with the N-terminus of TCF4 (PDB 1JDH, blue)[50]. Zoomed view of Site 4 (ARM5-10) shows side chains of β-catenin residues identified as significant hits in our screen in ball-and-stick representation, including the key charge button K435 (see **Fig. 2b**). **b,** WNT/β-catenin signaling strength in HEK293T-7TS reporter cells carrying various mutations in β-catenin (confirmed by deep sequencing, **Extended Data Fig.6**) after treatment (24h) with RSPO3+Wnt-3a or CHIR99021. The bars represent the mean of three biological replicates (*n*=3, each in a different pink shade). Each data point is the mean 7TS fluorescence from ~10,000 cells. Statistical significance was determined by Brown-Forsythe and Welch ANOVA followed by Dunnett's T3 multiple comparisons test for pairwise comparisons between groups. **c,** Association of β-catenin with the indicated interaction partners assessed by co-immunoprecipitation (IP) from extracts of cell lines shown in **b** (*n*=2**,** one representative immunoblot shown). β-catenin knock-out (KO, *CTNNB1*$^{-/-}$) cells serve as a specificity control for the IPs, association of β-catenin mutants with E-cadherin demonstrates protein integrity, and GAPDH is a loading control. **d,** BLI was used to assess association and dissociation kinetics between β-catenin variants and a GST-TCF4 fragment (left, same as **Fig.2f**) and GST-ICAT (right). All GST-tagged proteins were immobilized on the BLI probe at 50 nM and β-catenin variants were used at 1 μM (TCF4) and 0.5 μM (ICAT). One representative curve is shown, with the affinity constant (K_D ± s.d.) calculated from three independent replicates.
See also Extended Data Figures 5, 6 and 7.

reduced the association between β-catenin and TCF/LEF proteins in cell lysates (**Fig.4c**), but did not affect Wnt-3a-induced accumulation of β-catenin (**Extended Data Fig.7d**). In purified binding assays, the D624K/E626K/E628K mutations reduced the affinity between β-catenin and both TCF4 and ICAT by ~10-fold (**Fig.4f**). In comparison, both β-catenin mutations (C619Y/E620K and L643S/P, L644P) that increased the potency of Wnt-3a ligands also enhanced association with TCF4 in cell extracts (**Fig.4c**). This effect can be most clearly seen at low, subsaturating Wnt-3a concentrations (**Fig.4c**) and explains why cells carrying these mutations are hyper-responsive to WNTs (**Fig.4b**).

The C619 and E620 residues are located in a region at the end of the β-catenin ARM superhelix that interacts with a helical bundle of the negative regulator ICAT (**Fig.4d**). Introduction of a bulky residue in C618Y or a charge reversal in E620K could disrupt this interface. In a purified binding assay, C619Y/E620K did not change the affinity of β-catenin with TCF4, but profoundly impaired the β-catenin-ICAT interaction (**Fig.4f**). Since ICAT and TCF4 bind to β-catenin in a mutually exclusive manner, the enhanced association of β-catenin C619Y/E620K with TCF/LEF factors in cell extracts (**Fig.4c**) is likely to be a secondary consequence of the impaired association of ICAT or other negative regulators[53,56,60]. The second activating mutation (β-catenin L643S/P, L644P) is not at the direct interface with ICAT but could potentially impact the interaction via an allosteric effect (**Fig.4e**). However, we were unable to produce this mutant protein in bacteria to measure affinities. This example further highlights the ability of base editing screens to identify useful separation-of-function mutations, especially important in analysis of proteins like β-catenin which have multiple interaction partners.

The isolation of mutations that can either increase or decrease WNT/β-catenin signaling strength in β-catenin ARM10-12 nominate this region as a largely unexplored regulatory site for the association of β-catenin with TCF/LEF transcription factors. Interestingly, a stapled peptide that binds in this region was shown to block the interaction between β-catenin and TCF4, but the functional effects on WNT/β-catenin signaling were not reported[61]. Several of these novel

Fig.4

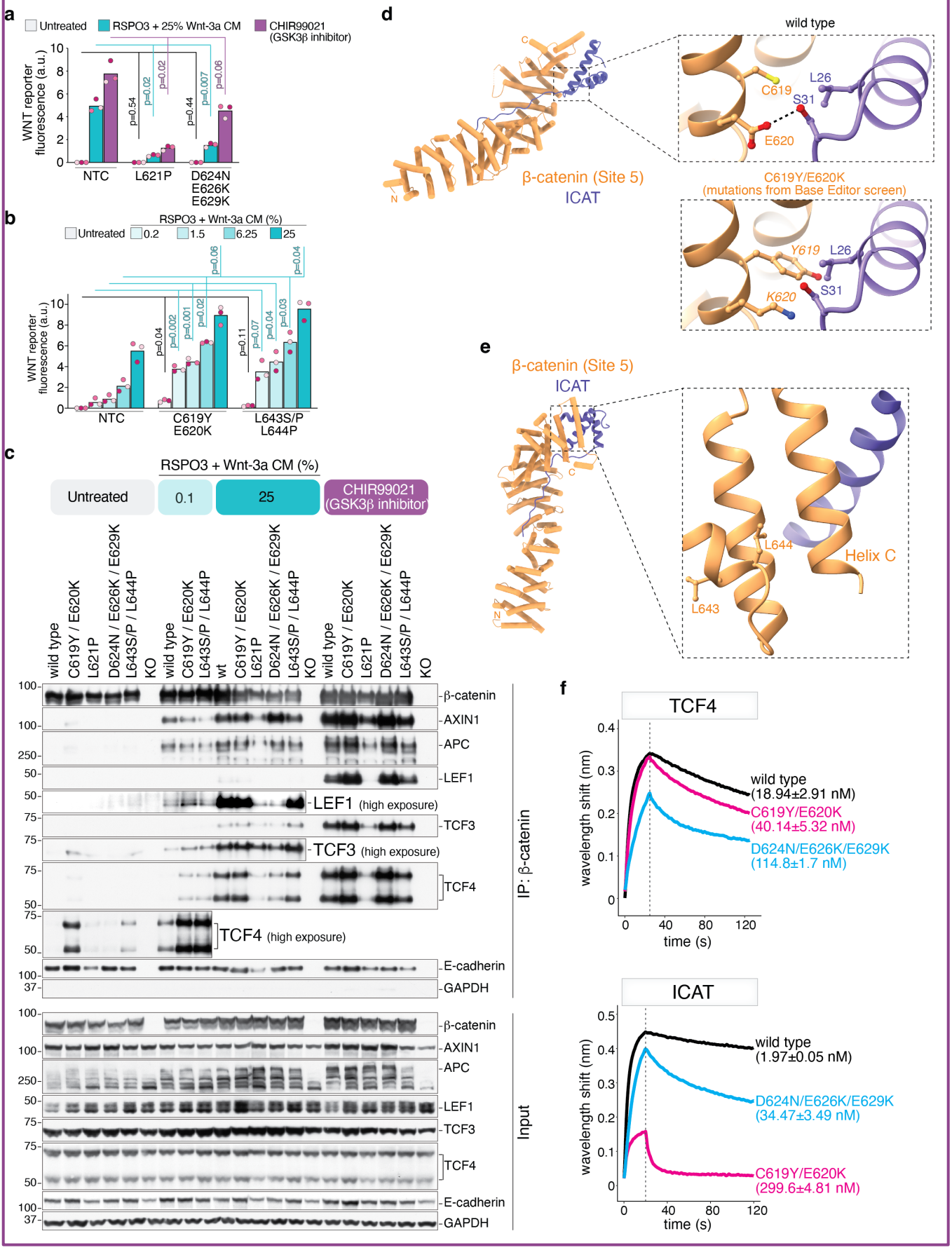
a
Untreated
RSPO3 + 25% Wnt-3a CM
CHIR99021 (GSK3β inhibitor)
WNT reporter fluorescence (a.u.)
NTC
L621P
D624N E626K E629K
b
RSPO3 + Wnt-3a CM (%)
Untreated
0.2
1.5
6.25
25
NTC
C619Y E620K
L643S/P L644P
c
RSPO3 + Wnt-3a CM (%)
Untreated
0.1
25
CHIR99021 (GSK3β inhibitor)
wild type
C619Y / E620K
L621P
D624N / E626K / E629K
L643S/P / L644P
KO
wt
β-catenin
AXIN1
APC
LEF1
LEF1 (high exposure)
TCF3
TCF3 (high exposure)
TCF4
TCF4 (high exposure)
E-cadherin
GAPDH
IP: β-catenin
Input
d
β-catenin (Site 5)
ICAT
wild type
C619
S31
L26
E620
C619Y/E620K
(mutations from Base Editor screen)
Y619
K620
e
β-catenin (Site 5)
ICAT
L644
L643
Helix C
f
TCF4
wild type
(18.94±2.91 nM)
C619Y/E620K
(40.14±5.32 nM)
D624N/E626K/E629K
(114.8±1.7 nM)
wavelength shift (nm)
time (s)
ICAT
wild type
(1.97±0.05 nM)
D624N/E626K/E629K
(34.47±3.49 nM)
C619Y/E620K
(299.6±4.81 nM)

Fig. 4. Mutations in β-catenin Site 5 (ARM 11-12) can reduce or enhance WNT/β-catenin signaling. a,b, WNT/β-catenin signaling strength in HEK293T-7TS reporter cells carrying mutations in β-catenin (confirmed by deep sequencing, **Extended Data Fig.6**) predicted to reduce (**a**) or enhance (**b**) WNT/β-catenin signaling. WNT/β-catenin signaling in cells carrying reduction-of-function mutations (**a**) was assessed after treatment with a saturating concentration of RSPO3+Wnt-3a or CHIR99021 (24h). Dose-response analysis (**b**) was used to assess sensitivity to Wnt-3a in HEK293T-7TS cells carrying putative gain-of-function mutations in β-catenin. The bars represent the mean of three biological replicates (*n*=3, each in a different pink shade). Each data point is the mean 7TS fluorescence from ~10,000 cells. Statistical significance was determined by Brown-Forsythe and Welch ANOVA followed by Dunnett's T3 multiple comparisons test for pairwise comparisons between groups. **c**, Association of β-catenin with the indicated interaction partners assessed by co-immunoprecipitation from extracts of cell lines shown in **a** and **b**, depicted as in **Fig.3c** (*n*=2, one representative immunoblot shown). **d,e,** Structural model of β-catenin (PDB 2Z6H, sandy brown) in complex with ICAT (purple) from PDB 1LUJ[46,56]. Zoomed region in **d** shows a potential steric clash created by the β-catenin C619Y/E620K gain-of-function mutation at the interface with ICAT. Zoom in **e** shows that the other gain-of-function mutations in β-catenin (L643S/P, L644P) are not directly at the PPI interface with ICAT. **f,** Association and dissociation kinetics between β-catenin variants and a GST-TCF4 fragment (top, same as **Fig.2f**) and GST-ICAT (bottom, same as **Fig.3d**). GST-tagged TCF4 and ICAT were immobilized on the BLI probe at 50 nM and β-catenin variants were used at 1 μM (TCF4) or 0.5 μM (for ICAT). Representative binding curves are shown, with the affinity constant (K_D ± s.d.) derived from three biological replicates.
See also Extended Data Figures 6 and 7.

mutations in β-catenin also reduced the constitutively high level of WNT reporter activity in cancer cell lines carrying the CRC-driving APC^{mcr} oncoprotein (which cannot bind directly to AXIN1) (**Extended Data Fig.7e-h**). This activity profile is consistent with the model that these reduction-of-function mutations decrease WNT/β-catenin signaling downstream of the BDC at the level of the WNT transcriptional complex. Small molecules that bind in ARM10-12 may represent a useful strategy to disrupt the interaction between β-catenin and TCF4 in CRC.

The sequence-function landscape of AXIN1

Base editing screens identified both gain- and loss-of-function missense mutations in AXIN1. Since AXIN1 is a negative regulator, gain-of-function mutations (**Fig.5a**, blue bars) suppress WNT/β-catenin signaling and loss-of-function mutations elevate WNT/β-catenin signaling (**Fig.5a**, red bars). Gain-of-function mutations in AXIN1 were considerably more common than those identified in β-catenin (**Fig.2b**, red bars) and were clustered in the DAX domain (**Fig.5a**, blue bars and **Extended Data Fig.2e-2h**).

The AXIN1 DAX domain has been implicated in two opposing roles[16,62–66]. DAX-mediated AXIN1 oligomerization is thought to increase the efficiency of β-catenin targeting by the BDC, thus keeping basal signaling low. However, in the presence of WNTs, the DAX domain mediates the recruitment of AXIN1 to DVL proteins at the receptor complex, ultimately resulting in inactivation of the BDC. Mutations enriched in the Bottom 15% gate were distributed throughout the DAX domain, including at the structurally-defined interface with the DIX domain of DVL[67] (**Fig.5b**). Validation studies on a subset of these mutations revealed that they reduced Wnt-3a-induced reporter activation, but (in an important control) did not affect CHIR99021-induced signaling (**Extended Data Fig.8a)**. This reduction in WNT/β-catenin signaling strength was even observed for mutations (F810P/L, Y822H/Y823H) that reduced the abundance of AXIN1

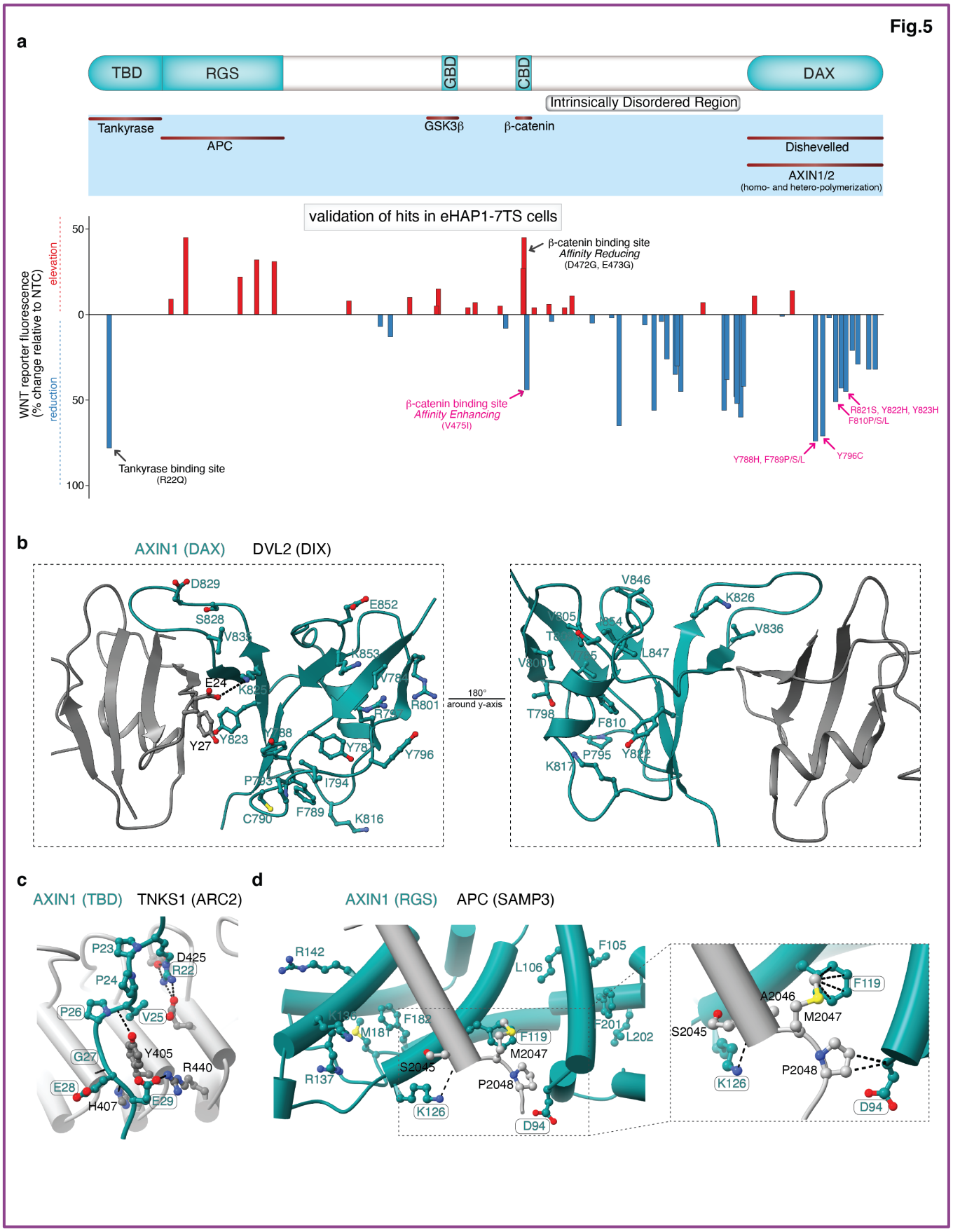
Fig.5
a
TBD
RGS
GBD
CBD
DAX
Intrinsically Disordered Region
Tankyrase
APC
GSK3β
β-catenin
Dishevelled
AXIN1/2
(homo- and hetero-polymerization)
validation of hits in eHAP1-7TS cells
WNT reporter fluorescence
(% change relative to NTC)
elevation
reduction
50
0
50
100
β-catenin binding site
Affinity Reducing
(D472G, E473G)
β-catenin binding site
Affinity Enhancing
(V475I)
Tankyrase binding site
(R22Q)
R821S, Y822H, Y823H
F810P/S/L
Y788H, F789P/S/L
Y796C
b
AXIN1 (DAX)
DVL2 (DIX)
D829
S828
V835
E852
K853
E24
K825
R801
Y27
Y823
Y788
Y787
Y796
P793
I794
C790
F789
K816
180°
around y-axis
V846
K826
V836
L847
T798
F810
P795
Y822
K817
c
AXIN1 (TBD)
TNKS1 (ARC2)
P23
D425
R22
P24
P26
V25
G27
Y405
R440
E28
H407
E29
d
AXIN1 (RGS)
APC (SAMP3)
R142
F105
L106
F182
M181
F119
M2047
F201
L202
S2045
R137
P2048
K126
D94
A2046
F119
M2047
S2045
P2048
K126
D94

320

Fig. 5. Base editing screens identify known and novel regulatory regions on AXIN1. a, Linear cartoon of AXIN1 (top) showing known regions that interact with partner proteins (middle). The bar graph (bottom, aligned to the cartoon at the top) shows the position of sgRNAs that increased (red) or decreased (blue) WNT/β-catenin signaling strength (relative to a non-targeting control sgRNA, NTC) when individually introduced into eHAP1-7TS cells. Black arrows denote sgRNAs that target known AXIN1 interaction interfaces and magenta arrows show sgRNAs selected for mechanistic analysis. TBD, Tankyrase Binding Domain; RGS, Regulator of G-Protein Signaling; GBD, GSK3β Binding Domain; CBD, β-catenin Binding Domain; DAX, Domain present in DVL and AXIN. **b,c,d,** Structural models showing PPI interfaces between various domains of AXIN1 (always in teal, defined in **a**) and the DIX domain of Dishevelled (DVL2, **b**)[67], the Ankyrin repeat cluster 2 (ARC2) domain of Tankyrase 1 (TNKS1, **c**)[68], and the SAMP3 repeat of APC (**d**)[19]. In **b**-**d**, ball-and-stick depiction is used to show side chains of AXIN1 residues predicted (located within the N3-N10 region of the protospacer) to be targeted by sgRNAs that were enriched (*z*-score of ≥ 2) in the Bottom 15% (**b**, **c**) or Top 10% (**d**) gates used for sorting (see **Fig.1d**). Rounded rectangles are drawn around residues previously identified as being critical for the depicted interaction and dotted lines show putative hydrophobic or electrostatic interactions.
See also Extended Data Figures 2, 4 and 8.

(**Extended Data Fig.8b**). Surprisingly, none of these mutations in the DAX domain elevated basal signaling in the absence of Wnt-3a.

As with β-catenin, sgRNAs predicted to make mutations at known AXIN1 interaction interfaces were top hits in our screens (labeled in **Fig.5a**). Amongst the mutations enriched in the Bottom 15% gate, we identified several located at the known interface between AXIN1 and tankyrase enzymes (**Fig.5c, Extended Data Fig.2e-2h**). Tankyrases reduce AXIN1 abundance by poly-ADP-ribosylation-mediated ubiquitination[45,68]. These mutations (e.g. R22Q) increase AXIN1 abundance and consequently suppress WNT/β-catenin signaling (**Extended Data Fig.8**). Conversely, mutations at the interface between the AXIN1 RGS domain and Ser-Ala-Met-Pro (SAMP) motif on APC (**Fig.5d, Extended Data Fig.2g**) were highly enriched in the Top 10% gate, consistent with the prediction that they would increase WNT/β-catenin signaling strength by disrupting a key stabilizing PPI in the BDC[19].

Repairing an oncogenic BDC by affinity enhancing mutations in AXIN1

The fourth major region of AXIN1 highlighted by the mutations identified in our screens was the catenin binding domain (CBD), a peptide that binds to Site 3 in β-catenin as a short α-helix (**Extended Data Fig. 2h, Fig.6a**). This region was notable for mutations that both increased and decreased WNT/β-catenin signaling strength, a hallmark of regulatory sites in many proteins (**Fig.5a**). Two different mutations at the same residue (AXIN1 V475) had opposing effects on WNT/β-catenin signaling strength: V475A enhanced signaling while V475I diminished signaling (**Fig.6b, Extended Data 9a**). Binding assays using purified proteins revealed that the affinity of β-catenin for an AXIN1 CBD peptide carrying the V475I mutation was ~2 fold higher (~450 nM) compared to a WT CBD peptide (1 μM), while the affinity of AXIN1 V475A for β-catenin was markedly diminished (**Fig.6d**). This bi-directional correlation between affinity and activity suggested that quantitative changes in affinity between AXIN and β-catenin likely drive the observed cellular changes in WNT/β-catenin signaling strength.

This observation presented an opportunity to probe the AXIN1-β-catenin interaction in cells by tuning its affinity using mutations. Our goal was to compare the impact of these mutations on AXIN1-β-catenin affinity *in vitro* to their effect on WNT/β-catenin signaling and BDC

integrity in cells. To further magnify affinity differences we combined V475I with L479W, identified in a phage display campaign to identify high-affinity β-catenin-binding stapled peptides[69,70] (**Fig.6c**). The V475I/L479W double mutant AXIN1 CBD peptide demonstrated a 25-fold increase in affinity for β-catenin compared to the WT CBD (40 nM vs. 1 μM) in binding assays with purified proteins (**Fig.6d, Extended Data Fig.9b**). The increased affinity was almost completely driven by a ~20-fold decrease in the rate constant for dissociation (k_{off}) of β-catenin from an AXIN1 V475I/L479W CBD peptide (compared to a wild-type peptide). Thus, the half-life of a β-catenin-AXIN1 V475I/L479W complex is predicted to be ~60 seconds, compared to ~3 seconds for the wild-type complex. To disrupt the AXIN1-β-catenin interaction, we combined

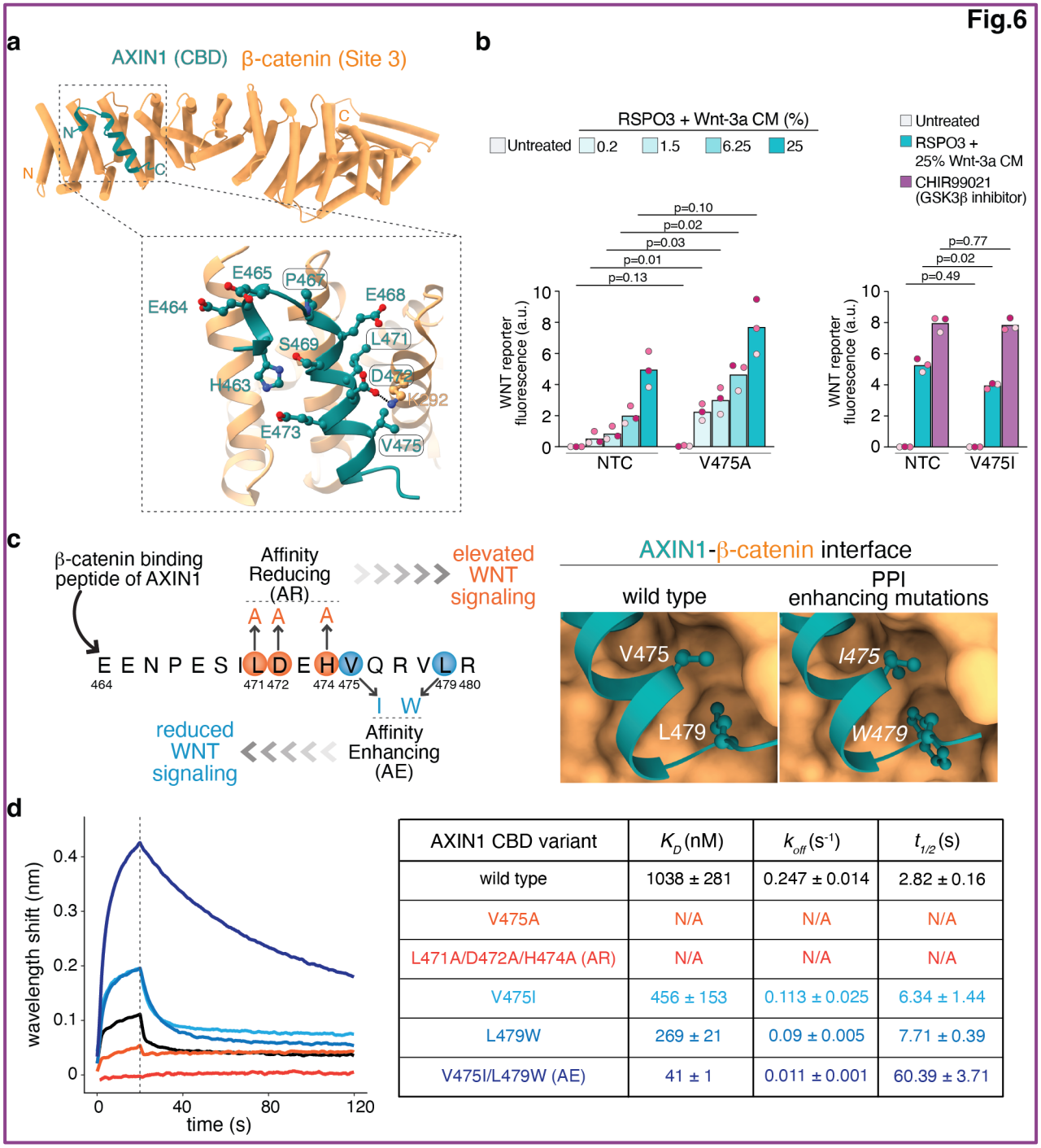

AXIN1 CBD variant	K_D (nM)	k_{off} (s^{-1})	$t_{1/2}$ (s)
wild type	1038 ± 281	0.247 ± 0.014	2.82 ± 0.16
V475A	N/A	N/A	N/A
L471A/D472A/H474A (AR)	N/A	N/A	N/A
V475I	456 ± 153	0.113 ± 0.025	6.34 ± 1.44
L479W	269 ± 21	0.09 ± 0.005	7.71 ± 0.39
V475I/L479W (AE)	41 ± 1	0.011 ± 0.001	60.39 ± 3.71

Fig. 6. Base editing screens identify AXIN1 mutations that either increase or decrease its affinity for β-catenin. a, AlphaFold3 model of the AXIN1 CBD (green) bound in Site 3 (ARM3-4) of β-catenin (PDB 2Z6H, sandy brown). In the zoomed view of this largely hydrophobic interface, ball-and-stick depiction is used to show side chains of AXIN1 residues predicted (i.e. located within the N3-N10 region of the protospacer) to be targeted by sgRNAs that were enriched (*z*-score of ≥ 2) in the Top 10% gate used for sorting (see **Fig.1d**). Rounded rectangles are drawn around residues previously identified as being critical for the depicted interaction. **b,** WNT/β-catenin signaling strength in HEK293T-7TS reporter cells carrying mutations in AXIN1 (confirmed by deep sequencing, **Extended Data Fig.6**) predicted to enhance (left) or reduce (right) WNT/β-catenin signaling (assay identical to **Fig.4a,4b**). The bars represent the mean of three biological replicates (*n*=3, each in a different pink shade). Each data point is the mean 7TS fluorescence from ~10,000 cells. Statistical significance was determined using multiple unpaired Student's t-tests with Welch's correction. P-values were adjusted using the two-stage step-up method (Benjamini, Krieger, and Yekutieli) to control the false discovery rate (FDR) at Q = 0.01. **c**, Mutations in the AXIN1 CBD peptide used to generate affinity-enhancing ($AXIN1^{AE}$) and affinity-reducing ($AXIN1^{AR}$) variants of AXIN1. **d**, K_D, k_{off}, and half-life ($t_{1/2}$) values for purified β-catenin binding to variant GST-tagged AXIN1 CBD peptides shown in **b** and **c** were measured using BLI. GST-AXIN1 CBD peptides were immobilized at a concentration of 50 nM on the BLI probe and β-catenin was used at 1 μM in solution. Representative binding curves are shown, with the affinity constant (K_D ± s.d.) derived from three biological replicates presented on the right.

three mutations (L471A/D472A/H474A) in the AXIN1 CBD[71] (**Fig.6c-d**) and established that this variant showed no detectable binding to purified β-catenin (**Fig.6d, Extended Data Fig.9b**). We hereafter refer to these mutations in AXIN1 as affinity enhancing ($AXIN1^{AE}$: V475I/L479W) or affinity reducing ($AXIN1^{AR}$: L471A/D472A/H474A) to distinguish them from wild-type AXIN1 ($AXIN1^{WT}$) (**Fig.6c**).

To understand the consequences of increasing or decreasing the lifetime of the AXIN1-β-catenin complex in cells, we introduced the AE and AR mutations at the endogenous *AXIN1* locus in two isogenic HAP1 cell lines, one carrying an unmodified *APC* allele and a second with an oncogenic APC^{mcr} allele (predicted to express an APC^{mcr} protein truncated at amino acid 1337 or APC 1337*) (**Extended Data Fig.10**). AXIN1 targeted co-IP experiments were used to assess BDC integrity. In cell lines expressing full-length APC, all three AXIN1 variants were associated with β-catenin and APC to a comparable extent under conditions of no or low Wnt-3a exposure (**Fig.7a, Extended Data Fig.9c**). Since $AXIN1^{AR}$ has no measurable direct affinity for β-catenin (**Fig.6d**), it likely associates with β-catenin indirectly through APC[16,72]. In the presence of saturating Wnt-3a or CHIR99021 (both conditions that maximally inhibit GSK3β and activate signaling), $AXIN1^{AE}$ pulled down much greater amounts of both β-catenin and APC compared to $AXIN1^{WT}$ (**Fig.7a, Extended Data Fig.9c**). Thus, increasing the *in vitro* AXIN1-β-catenin affinity (**Fig.6d**) increased their association in cell only under conditions of high WNT exposure or GSK3β inhibition (both of which lead to high-amplitude signaling).

In APC^{mcr} cells, which express a truncated APC (APC 1337*) protein that lacks all three of the AXIN1-binding SAMP repeats, $AXIN1^{AE}$ bound much greater amounts of β-catenin and APC compared to $AXIN1^{WT}$ under all conditions tested. Conversely, the interaction between $AXIN1^{AR}$ and both β-catenin and APC was abolished. Thus, in the absence of the RGS-SAMP mediated interaction between AXIN1 and APC^{mcr}, β-catenin can bridge the two proteins by simultaneously binding to APC^{mcr} (through its 15R A-D repeats) and AXIN1 (through its CBD)[16,72]. Reconstitution experiments using purified proteins support the idea that β-catenin

Fig.7

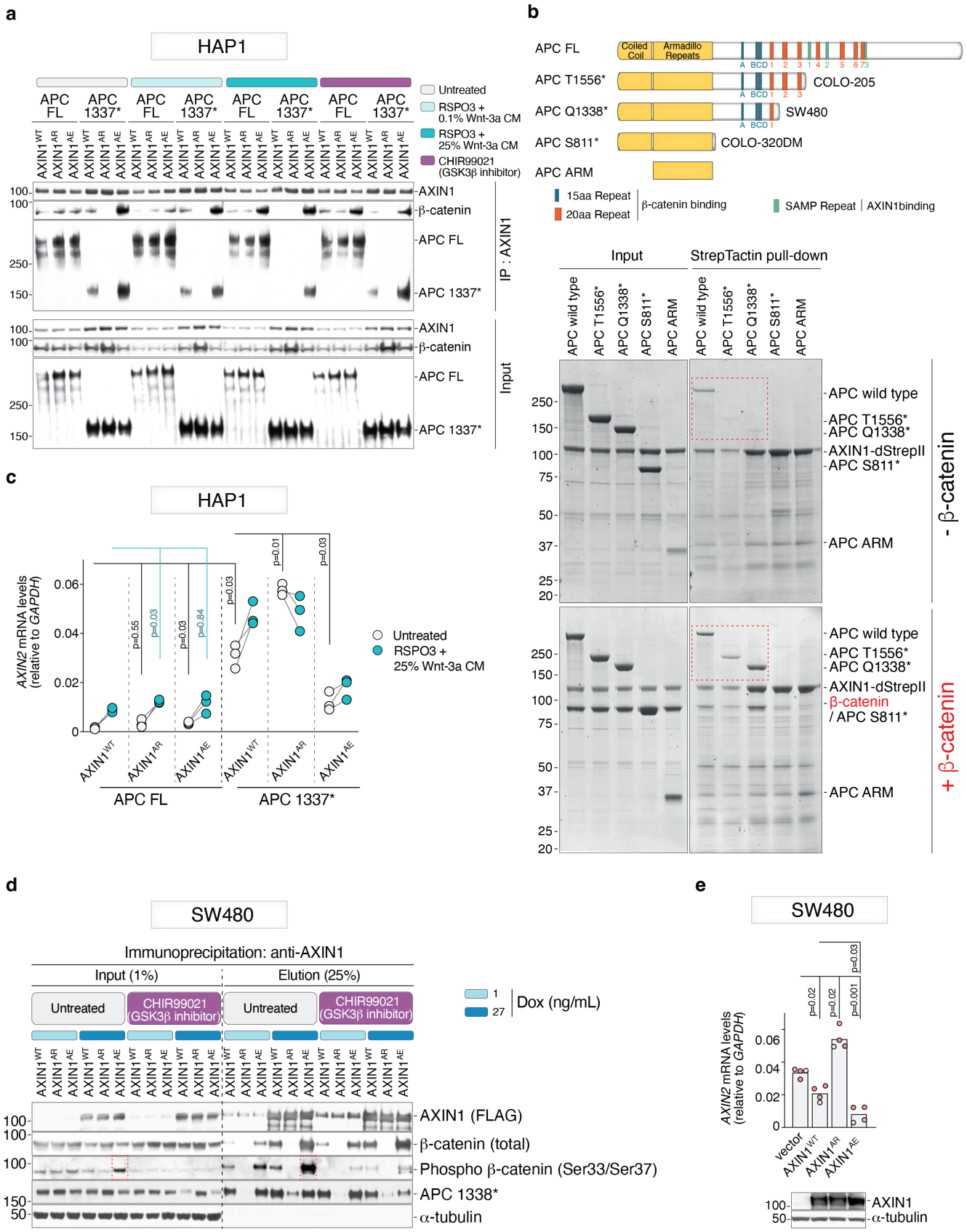
a
HAP1
APC FL
APC 1337*
Untreated
RSPO3 + 0.1% Wnt-3a CM
RSPO3 + 25% Wnt-3a CM
CHIR99021 (GSK3β inhibitor)
AXIN1
β-catenin
APC FL
APC 1337*
IP : AXIN1
Input
b
APC FL
APC T1556*
APC Q1338*
APC S811*
APC ARM
Coiled Coil
Armadillo Repeats
COLO-205
SW480
COLO-320DM
15aa Repeat
20aa Repeat
β-catenin binding
SAMP Repeat
AXIN1binding
Input
StrepTactin pull-down
APC wild type
APC T1556*
APC Q1338*
AXIN1-dStrepII
APC S811*
APC ARM
- β-catenin
+ β-catenin
β-catenin / APC S811*
c
HAP1
AXIN2 mRNA levels (relative to GAPDH)
Untreated
RSPO3 + 25% Wnt-3a CM
APC FL
APC 1337*
d
SW480
Immunoprecipitation: anti-AXIN1
Input (1%)
Elution (25%)
Untreated
CHIR99021 (GSK3β inhibitor)
Dox (ng/mL)
AXIN1 (FLAG)
β-catenin (total)
Phospho β-catenin (Ser33/Ser37)
APC 1338*
α-tubulin
e
SW480
AXIN2 mRNA levels (relative to GAPDH)
Vector
AXIN1

Fig. 7. The AXIN1-β-catenin interaction is critical for the assembly of the oncogenic BDC. a, Association of endogenous AXIN1 with APC and β-catenin in extracts from clonal eHAP1 cells measured using an AXIN1 IP followed by immunoblotting. Sequence verified clonal cell lines (**Extended Data Fig.10**) contained the indicated combinations of full-length APC (APC FL) or truncated APC (APC 1337*) and one of three AXIN1 variants-- $AXIN1^{WT}$, $AXIN1^{AE}$ (V775I/L479W) and $AXIN1^{AR}$ (L471A/D472A/H474A)-- with varying affinities for β-catenin (see **Fig.6d**). Extracts were made from untreated cells or cells treated (1h) with low-dose Wnt-3a, high-dose Wnt-3a or CHIR99021. **b,** A coomassie-stained gel depicts the association between purified, Strep II-tagged AXIN1 (bait) and purified APC variants (schematically shown above the gel) in the absence (top gel) or presence (bottom gel) of purified β-catenin. APC^{mcr} variants only associate with AXIN1 in the presence of β-catenin (dotted red boxes). **c,** The abundance of *AXIN2* mRNA, encoded by a WNT target gene, was used to measure the strength of signaling in response to Wnt-3a in HAP1 cells lines carrying the indicated combination of *APC* and *AXIN1* alleles (described in **a**). Three independent clonal cell lines were used for each *AXIN1* and *APC* allelic combination, with a line used to link data points from the same cell line. **d,** Association of doxycycline (Dox)-inducible, FLAG-tagged AXIN1 variants ($AXIN1^{WT}$, $AXIN1^{AE}$ or $AXIN1^{AR}$) with endogenous truncated APC (APC 1338*) and endogenous β-catenin was measured using a FLAG IP from extracts of untreated or CHIR99021 treated SW480 CRC cells. Dotted red boxes show that expression of $AXIN1^{AE}$ increases the abundance of phosphorylated β-catenin in both cell extracts and BDC IPs. **e,** WNT/β-catenin signaling strength in SW480 CRC cells stably expressing FLAG-tagged AXIN1 variants. The bars represent the mean of four biological replicates (*n*=4, each in a different pink shade). Each data point represents the mean *AXIN2* mRNA abundance (relative to a control housekeeping mRNA) from three technical replicates. In panels **c** and **e**, statistical significance was determined by Brown-Forsythe and Welch ANOVA followed by Dunnett's T3 multiple comparisons test for pairwise comparisons between groups. Experiments in **a**, **b**, and **d** were repeated at least twice (*n*=2) and one representative gel or immunoblot is shown.
See also Extended Data Figures 9 and 10.

functions as the linchpin of the oncogenic BDC[16] (**Fig.7b**). Oncogenic APC variants truncated before the SAMP repeats only associated with AXIN1 in the presence of β-catenin. Further truncations of APC that remove the 15R repeats abolished the capacity of β-catenin to bridge APC and AXIN1 (**Fig.7b**).

There was a notable difference in WNT/β-catenin signaling behavior, as measured by *AXIN2* mRNA abundance, between cell lines expressing full-length APC or truncated APC (APC 1337*). In the context of full-length APC, basal and Wnt-3a-induced signaling in cell lines carrying any of the three AXIN1 variants was comparable. However, the results were different in APC^{mcr} cells: $AXIN1^{AR}$ led to a further increase in *AXIN2* mRNA levels and nuclear β-catenin abundance while the $AXIN1^{AE}$ variant had the opposite effect (**Fig.7c**, **Extended Data Fig.9d**). Thus, cells carrying an oncogenic APC^{mcr} allele were more sensitive to changes in the affinity between AXIN1 and β-catenin than those carrying WT APC.

To test this concept in a cancer cell line, we stably expressed $AXIN1^{WT}$, $AXIN1^{AE}$ or $AXIN1^{AR}$ in the human CRC cell line SW480 using an inducible expression system. SW480 carries a mutant *APC* allele that encodes a protein truncated at amino acid residue 1338 (nearly identical to the APC 1337* protein expressed in our engineered HAP1 cells). SW480 cells have elevated WNT/β-catenin signaling and *AXIN2* expression due to impaired BDC function, leading to a defect in β-catenin phosphorylation and degradation[73]. In co-IP experiments, $AXIN1^{AE}$ showed enhanced association with β-catenin, while $AXIN1^{AR}$ failed to associate with β-catenin (consistent with HAP1 results) (**Fig.7d**). More importantly, β-catenin phosphorylated at its N-

406 terminal degron motif (and thus marked for degradation) was considerably more abundant in
407 cells expressing AXIN1^{AR}, showing that enhancing the affinity of AXIN1 and β-catenin can
408 improve the activity of an oncogenic BDC complex (**Fig.7d**). Accordingly, *AXIN2* mRNA
409 abundance, a metric of WNT/β-catenin signaling strength, was suppressed to a greater extent
410 in SW480 cells expressing AXIN1^{AE} compared to cells expressing AXIN1^{WT}. Interestingly,
411 WNT/β-catenin signaling was hyperactivated in SW480 cells expressing AXIN1^{AR}, likely because
412 replacement of the endogenous WT AXIN1 with AXIN1^{AR} resulted in disassembly and complete
413 inactivation of the BDC (**Fig.7e**). Taken together, these data show that the AXIN1-β-catenin
414 interaction is a rate-limiting step in oncogenic WNT/β-catenin signaling that can be manipulated
415 to increase or decrease the activity of the impaired BDC found in cells that carry *APC^{mcr}* alleles
416 (**Fig.7e**).
417

418 ## Discussion

419 In this work, base editing screens provided mechanistic insights into the BDC, a complex
420 signaling machine that functions as the nerve center of WNT/β-catenin signaling, one of the most
421 important developmental and stem cell signaling systems that also drives the majority of human
422 CRCs. A longstanding, unresolved challenge in WNT signalling is understanding the biochemical
423 differences between the wild-type, ligand-regulated BDC and the oncogenic BDC, hobbled by
424 truncating mutations in APC. Human cancer genetics first revealed that oncogenic WNT/β-
425 catenin signaling is not driven by the complete loss of APC function, as might be expected if it
426 were a simple gatekeeper[37,74]. Instead, at least one *APC* allele in both sporadic and familial CRC
427 cases is truncated such that it loses all three SAMP repeats required for its interaction with
428 AXIN1 but retains at least one of the 20R repeats that can mediate a high affinity interaction with
429 β-catenin (**Fig.1b, Extended Data Fig.7e**). This arrangement results in an intermediate level of
430 ligand-independent WNT/β-catenin signaling that drives tumorigenesis but avoids senescence
431 or cell death[74,75]. Understanding the detailed biochemistry of how the oncogenic BDC calibrates
432 this just-right level of signaling flux also is central to therapeutic development. Given the
433 pervasive role of WNT/β-catenin signaling in tissue homeostasis, a clinically viable WNT inhibitor
434 must differentiate between mutation-driven oncogenic signaling and ligand-driven physiological
435 signaling.

436 We propose that BDC assembly and regulation is fundamentally different in cells
437 expressing full-length APC and APC^{mcr}. These insights emerged from experiments that allowed
438 us to increase or decrease the affinity of a specific PPI, the AXIN1-β-catenin interaction, using
439 mutations at endogenous gene loci (thus avoiding the potentially confounding consequences of
440 overexpression). In the presence of full-length APC, increasing or decreasing the AXIN1-β-
441 catenin affinity across a >50-fold range above and below the native K_D (~1 μM), had very little
442 effect on BDC assembly or target gene induction under basal, ligand-free conditions. This is
443 likely because the APC 20R repeats are phosphorylated by GSK3β under basal conditions,
444 drastically increasing their affinity (K_D ~1 nM *in vitro*) for the same groove (ARM 3-4) in β-catenin
445 occupied by the AXIN1 CBD (**Fig.8a**)[55,58]. Thus, β-catenin is not available to interact with even
446 the high affinity (K_D ~40 nM) AXIN1^{AE} variant used in our experiments. Essentially, the
447 phosphorylation of APC by GSK3β makes the AXIN1-β-catenin interaction dispensable for β-
448 catenin recruitment into the BDC or for the assembly of the BDC itself (**Fig.8b**). Consistent with
449 this view, when GSK3β is inhibited either by CHIR99021 or by high Wnt-3a addition, the AXIN1-
450 β-catenin affinity becomes relevant: AXIN1^{AE} pulls down much more β-catenin and APC

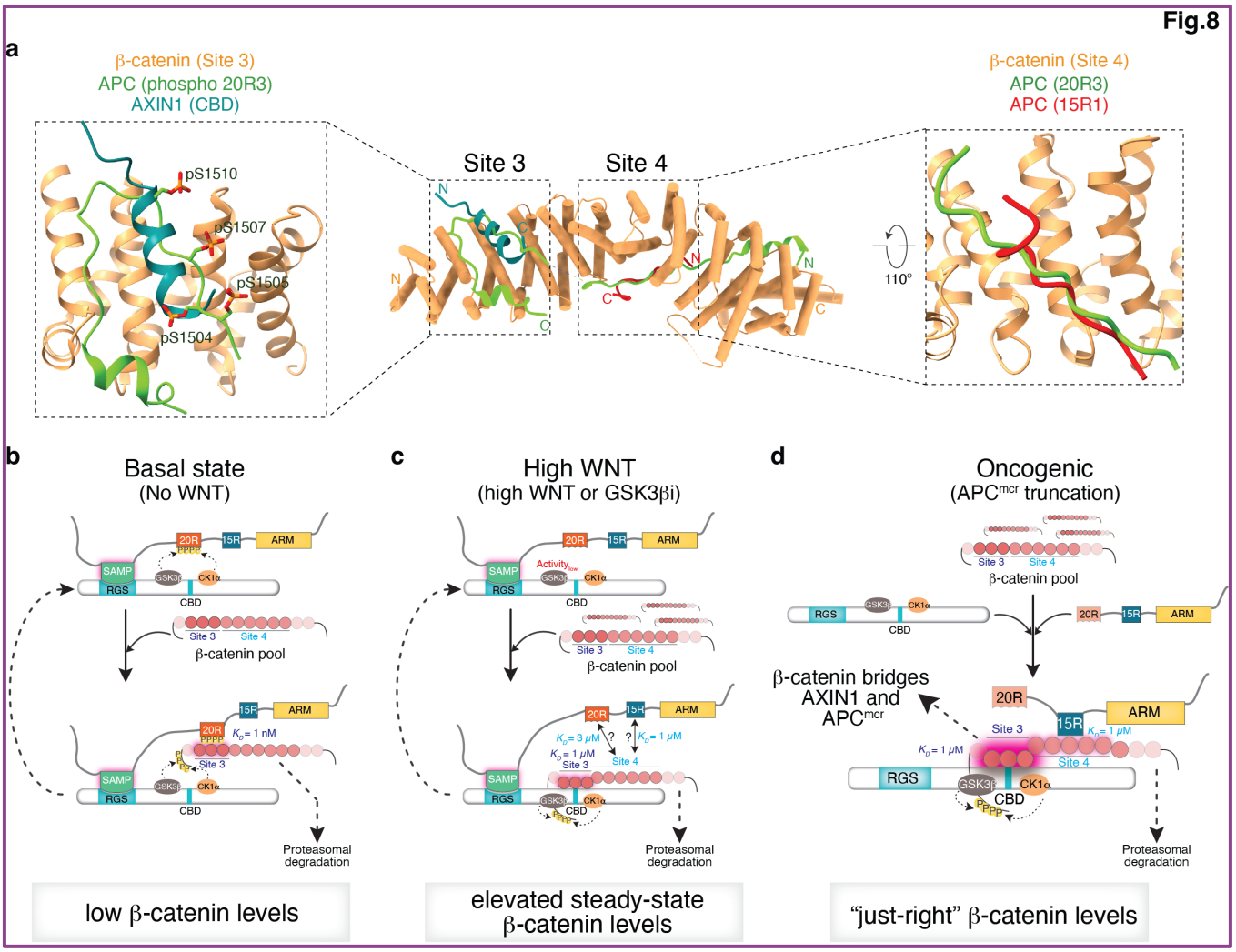

Fig. 8. Different modes of β-catenin recognition by the wild-type and oncogenic BDC. See text for details. **a,** Structural superposition shows that the AXIN1 CBD (PDB 1QZ7) and phosphorylated APC 20R (p20R; PDB 1TH1) both bind to overlapping (and hence mutually exclusive) surfaces in β-catenin (PDB 2Z6H) Site 3, though the affinities are vastly different (K_D~1 nM for APC p20R and K_D~1 μM for AXIN1)[17,18,46,58,71]. APC 15R motifs (PDB 1JPP) and the extended regions of 20R motifs (PDB 1TH1) can also bind in β-catenin (PDB 2Z6H) Site 4, but AXIN1 only binds in Site 3[46,54,58]. **b,** In the presence of full-length APC, APC and AXIN1 can associate directly, allowing phosphorylation of the APC 20R motifs by the AXIN1-bound kinases and thus creating a high affinity (K_D~1 nM) binding site for β-catenin Site 3. In this regime, AXIN1 cannot directly bind to β-catenin, and the steady state concentration of β-catenin is kept low (limited by the APC p20R-β-catenin affinity). **c,** Inhibition of GSK3β by WNTs or CHIR99021 reduces APC phosphorylation, thus sharply decreasing the affinity of 20R motifs for β-catenin Site 3. Thus, β-catenin is recruited into the BDC primarily through its moderate affinity interaction (K_D~1 μM) with AXIN1 (or APC via Site 4), which requires a higher steady state β-catenin concentration for significant association. **d,** When APC is truncated in CRC, β-catenin becomes the linchpin, recruiting AXIN1 and APC via moderate affinity interactions with Site 3 and Site 4, respectively. Unlike the case where APC is intact (**b**, **c**), there are no cycles of β-catenin recruitment and degradation; each oncogenic BDC disassembles when β-catenin is phosphorylated and degraded. The steady-state β-catenin level is autoregulated-- an increase in the β-catenin concentration increases BDC assembly and hence enhances the degradation rate while a decrease reduces BDC assembly and hence decreases the degradation rate.

452 (**Fig.7a**). Under these conditions, APC phosphorylation drops, reducing the affinity of the 20R
453 repeats for β-catenin by ~300-1000-fold and thus vacating the ARM3-4 groove for the AXIN1
454 CBD (**Fig.8c**)[17,18].
455 In cells with APC^{mcr}, the AXIN1-β-catenin interaction becomes a critical determinant of
456 BDC assembly for two key reasons: APC^{mcr} cannot bind directly to AXIN1 because it has lost its
457 SAMP motifs and, as a consequence, the remaining 20R repeats in APC^{mcr} cannot be
458 phosphorylated by GSK3β to generate a high-affinity β-catenin binding site (**Fig.8d**). Indeed,
459 point mutations at the interface between AXIN1 CBD and β-catenin ARM 3-4 ($AXIN1^{AR}$)
460 prevented the association between AXIN1 and both β-catenin and APC^{mcr}. Our data support the
461 model that β-catenin serves as the linchpin of the oncogenic BDC, bridging AXIN1, which binds
462 to ARM 3-4 via its CBD, and APC^{mcr}, which binds to the extended ARM5-9 region via its 15R
463 repeats (**Fig.8d**). Accordingly, the interaction of purified AXIN1 with APC^{mcr} depends on the
464 presence of β-catenin. Full-length APC binds to AXIN1 regardless of the presence of β-catenin
465 because its SAMP motifs can directly engage the RGS domain of AXIN1. Conversely, more
466 extensive APC truncations that lack the 15R repeats fail to associate with AXIN1 regardless of
467 β-catenin (**Fig.7b**). These data are consistent with prior work showing that disruption of β-catenin
468 in cells prevents the co-precipitation of AXIN1 and truncated APC from cell extracts[72].
469 We propose that β-catenin becomes both a substrate and a key assembly factor for the
470 oncogenic BDC, thus promoting its own degradation and limiting its own abundance to achieve
471 the just-right signaling flux necessary for CRC development. This mode of autoregulation is
472 conceptually analogous to substrate-assisted catalysis, where the concentration and affinity of
473 the substrate (β-catenin) for the enzyme (BDC) determines catalytic efficiency. Thus, steady-
474 state β-catenin abundance in CRC cells is self-regulated by its own availability and critically
475 dependent on its affinities for AXIN1 and APC^{mcr}. In support of this idea, increasing or decreasing
476 the AXIN1-β-catenin affinity has a corresponding effect on the abundance of phosphorylated β-
477 catenin, the immediate product of the reaction catalyzed by the BDC (**Fig.7d**). Changes in the
478 affinity between β-catenin and APC^{mcr} would also be predicted to have analogous effects on the
479 catalytic efficiency of the oncogenic BDC, though such mutations were not identified in our
480 screens. In the presence of full-length APC, β-catenin is simply recruited as a substrate to the
481 BDC, which is optimized for suppressing basal signaling by minimizing β-catenin abundance
482 (**Fig.8a**).
483 The substrate-assisted model of the oncogenic BDC has therapeutic implications. Small
484 molecule drugs that slow the first-order dissociation of β-catenin from AXIN1 or APC^{mcr} (thus
485 mimicking of the affinity-enhancing mutations identified in our screens) may partially repair the
486 activity of the oncogenic BDC (without significantly affecting the native BDC). Similarly, drugs
487 that disrupt these interactions should super-activate WNT/β-catenin signaling, also a detrimental
488 outcome given the just-right model for CRC development[74,75]. Substrate affinity and substrate
489 turnover can be competing properties that would need to be balanced in any such strategy. If
490 the affinity between β-catenin and the oncogenic BDC is too high, product inhibition may limit
491 BDC activity if phosphorylated β-catenin cannot be efficiently ubiquitinated or extracted for
492 proteasomal degradation.
493 We finish by noting that base editing screens, which now enable the installation and
494 functional evaluation of point mutations across endogenous proteins, have distinct advantages
495 over loss-of-function and overexpression screens. Beyond gene identification, genetic screens
496 in model organisms have provided insights into biochemical mechanisms of protein function by

enabling the isolation of alleles that carry mutations at one or a small number of amino acid residues. These point mutations, often on protein surfaces, can identify enzyme active sites, protein-protein or protein-ligand interaction interfaces, and allosteric sites. The most informative (but rare) alleles are gain-of-function and separation-of-function alleles. Gain-of-function alleles can identify positive or instructive (rather than permissive) functions of a protein, identify rate limiting steps, and bypass genetic redundancy. We identified several such mutations in both β-catenin and AXIN1: mutations that increased the in-cell association of β-catenin with TCF/LEF proteins and mutations in the CBD and C-terminal disordered region of AXIN1 that suppress WNT/β-catenin signaling. A key signature of a regulatory site, identified both for the AXIN1 CBD and the ARM 11-12 region of β-catenin, are distinct mutations that have opposite effects on signaling strength. Second, separation-of-function mutations are especially valuable in mapping sequence-function relationships in multi-functional proteins (like β-catenin). Even in the very congested PPI interfaces on β-catenin, our screens identified mutations that distinguished between interactions with APC, TCF/LEF, and ICAT. Finally, our analysis of residues at known interfaces between β-catenin and its binding partners showed that the functional impact of mutations at endogenous genes can sometimes be difficult to predict from purely structural proximity considerations or *in vitro* binding assays. Hence, *in situ* base-editing screens can be used for the in-cell functional annotation of PPI interfaces identified by structural and biochemical studies.

Methods

Reagents and antibodies

Wnt-3a conditioned medium was produced as described previously[29]. Recombinant human R-Spondin 3 (RSPO3) was purchased from R&D Systems (Cat#3500-RS-025). CHIR99021 was purchased from Cayman Chemical (Cat#13122). The following primary antibodies were used for immunoblotting and immunofluorescence: β-catenin (BD Biosciences, Cat#610154, 1:3,000 for immunoblotting), Non-phospho (Active) β-Catenin (Ser33/37/Thr41) (Cell Signaling Technology, Cat#8814, 1:1,000 for immunoblotting, 1:200 for immunofluorescence), Phospho β-Catenin (Ser33/37) (Cell Signaling Technology, Cat#2009, 1:1000 for immunoblotting), AXIN1 (Cell Signaling Technology, Cat#2074, 1:1,000 for immunoblotting), APC (Millipore-Sigma, Cat#OP44, 1:200 for immunoblotting), LEF1 (Cell Signaling Technology, Cat#2230, 1:1,000 for immunoblotting), TCF3 (Cell Signaling Technology, Cat#2883, 1:1,000 for immunoblotting), TCF4 (Cell Signaling Technology, Cat#2569, 1:1,000 for immunoblotting), E-Cadherin (Cell Signaling Technology, Cat#3195, 1:1,000 for immunoblotting), GAPDH (Proteintech, Cat#60004-1-Ig, 1:10,000 for immunoblotting), α-Tubulin (Proteintech, Cat#66031-1-Ig, 1:10,000 for immunoblotting), and GST (Bethyl Laboratories, Cat#A190-122A, 1:1000 for immunoblotting). The following secondary antibodies were used: Peroxidase conjugated donkey anti-mouse/rabbit IgG (Jackson ImmunoResearch), IRDye 800CW donkey anti-mouse/rabbit IgG (LICORbio), and Alexa Fluor 488 conjugated donkey anti-mouse/rabbit IgG (Thermo Fisher Scientific).

Cell culture

HAP1, a near haploid human cell line and eHAP1, a fully haploid human cell line[32], were gifts from Jan Carette, Stanford University. These cell lines were authenticated by morphology and ploidy analysis as described below to confirm identity. HEK293T, RKO, DLD-1, and SW480 were

542 obtained from American Type Culture Collection (ATCC) and their identity was authenticated by
543 the vendor using STR profiling. All cell lines were confirmed to be mycoplasma-free using an
544 isothermal PCR-based assay (InvivoGen, Cat#rep-mys-10). Experiments were performed using
545 cells between passages 3 and 25. HAP1 and eHAP1 cells were grown in Iscove's Modified
546 Dulbecco's Medium (IMDM) containing L-Glutamine (cytiva, Cat#SH30243FS) and
547 supplemented with 10% fetal bovine serum (FBS) (MilliporeSigma, Cat #F0926), extra glutamine
548 (2 mM) (cytiva, Cat#SH3003401), and penicillin-streptomycin (50 U/mL) (Thermo Fisher
549 Scientific, Cat #15140163). HEK293T, RKO, DLD-1, and SW480 cells were grown in Dulbecco's
550 Modified Eagle Medium (DMEM) containing high glucose, with 4.0mM L-glutamine, and sodium
551 pyruvate (cytiva, Cat #SH30243) and supplemented with 10% FBS, 1x MEM non-essential
552 amino acids solution (Thermo Fisher Scientific, Cat #11140076), and penicillin-streptomycin (50
553 U/mL). Cells were subcultured every 3 days at a splitting ratio of 1:10 using 0.25% Trypsin-EDTA
554 (Thermo Fisher Scientific, Cat #25200072) for HAP1 and eHAP1 cells or 0.05% Trypsin-EDTA
555 (Thermo Fisher Scientific, Cat# 25300062) for HEK293T, RKO and DLD-1 cells. All cell lines
556 were cultured in a humidified atmosphere containing 5% CO2 at 37 °C. HAP1 and eHAP1 cells
557 were routinely tested for ploidy state every fifth passage by flow cytometry with propidium iodide
558 staining as described previously[76].
559
560 **Generation of WNT transcriptional reporter cell lines**
561 Clonal WNT transcriptional reporter cell lines were generated in eHAP1, HEK293T, RKO, and
562 DLD-1 cells. These lines contain a fluorescent reporter construct downstream of a WNT-
563 responsive element. For RKO and DLD-1 lines, the lentiviral plasmid 7xTcf-eGFP (7TG) was
564 used. This plasmid contains seven repeats of an optimized TCF/LEF binding site driving
565 expression of eGFP. It was generated from 7xTcf-eGFP//SV40-PuroR[77] by digestion with BsrGI
566 and SalI to remove the SV40-PuroR cassette, creating a selection marker-free backbone that is
567 compatible with CRISPR base editor plasmids. For eHAP1 and HEK293T lines, the 7xTcf-
568 mScarlet (7TS) lentiviral plasmid was used, in which the eGFP cassette was replaced with the
569 coding sequence for mScarlet. Lentivirus was produced by co-transfecting the respective
570 reporter plasmid (7TG or 7TS) with the packaging plasmids psPAX2 (Addgene Plasmid #12260)
571 and pMD2.G (Addgene Plasmid #12259) into 293FT (Thermo Fisher Scientific) cells using
572 polyethylenimine (PEI; Polysciences, Inc., Cat# 23966-2). Supernatant containing lentivirus was
573 collected at 48 h post-transfection and filtered (0.45 µm). Recipient clonal cell lines were
574 transduced at an MOI of ~0.5 in the presence of polybrene (8 µg/mL; Millipore-Sigma,
575 Cat#H9268). Two days post-transduction, cells were treated with 50% Wnt-3a conditioned
576 medium for 24 h followed by FACS to isolate eGFP/mScarlet positive single cells using a
577 SH800S cell sorter (Sony Biotechnology) into 96-well plates. Multiple individual clones (~24)
578 were picked and expanded for each reporter line. Reporter activity was validated in expanded
579 clonal lines after 24 h treatment with 50% Wnt-3a conditioned medium. Reporter fluorescence
580 (eGFP or mScarlet) was measured by flow cytometry using a 488 nm laser and FL2 525/50 nm
581 bandpass filter (eGFP) or a 561 nm laser and FL3 600/60 nm bandpass filter (mScarlet). Clonal
582 lines with optimal growth rate, morphology, and a high dynamic range of reporter fluorescence
583 were selected for downstream assays. High dynamic range was defined as achieving at least
584 100-fold induction of reporter fluorescence upon Wnt-3a stimulation compared to control.
585
586 **FACS-based pooled CRISPR Base Editing Screens**

587 *Library construction*
588 For tiled sgRNA library design, we used the Beagle tool from the Broad Institute Genetic
589 Perturbation Platform. The resulting library was filtered to exclude guide sequences containing
590 *BsmBI* restriction sites. The Ensembl transcript IDs used for guide design were: *CTNNB1*
591 (ENST00000349496), *APC* (ENST00000257430), *AXIN1* (ENST00000262320), and *GSK3B*
592 (ENST00000264235). *BsmBI* recognition sites and appropriate overhangs were appended to
593 each targeting sequence sequence for Golden Gate cloning into base editor plasmids (pRDA
594 429, Addgene#179098 expressing ABE8e Cas9-NG and pRDA 336, Addgene #179095
595 expressing BE3.9 Cas9-NG). Primer sites were included for amplification of subsets from the
596 same synthesis pool. The final oligonucleotide sequence was as follows 5'-[Forward
597 Primer]*CGTCTCACACCG*[targeting sequence, 20 nt]*GTTTCGAGACG*[Reverse Primer]-3'.
598 Oligonucleotide pools were synthesized by CustomArray. PCR amplification of the
599 oligonucleotide pools used 25 µL of 2x NEBNext PCR Master Mix (New England Biolabs, Cat#
600 M0541S), 2 µL of the oligonucleotide pool (~2 ng), 5 µL of primer mix at a final concentration of
601 0.5 µM, and 18 µL of nuclease-free water. PCR cycling conditions were: (1) Initial denaturation:
602 98 °C for 1 min; (2) 98 °C for 10 s; (3) 62 °C for 10 s; (4) 72 °C for 20 s; (5) cycle through steps
603 2-4 for 18 cycles; (6) Final extension: 72 °C for 2 min. The following primer (5'-3') pairs were
604 used for amplification:
605 APC-ABE: Forward: GGTCGTCGCATCACAATGCG, Reverse: TCTCGAGCGCCAATGTGACG
606 APC-CBE: Forward: GTGTAACCCGTAGGGCACCT, Reverse: GTCGAGAGCAGTCCTTCGAC
607 CTNNB1-ABE: Forward: CATGTTGCCCTGAGGCACAG, Reverse: CCGTTAGGTCCCGAAAGGCT
608 CTNNB1-CBE: Forward: AGGCACTTGCTCGTACGACG, Reverse: ATGTGGGCCCGGCACCTTAA
609 AXIN1-ABE: Forward: GTCGCTAGCTAGGTCCGAAC, Reverse: TGTGCTGCGCAAGACCACGT
610 AXIN1-CBE: Forward: CAGCGCCAATGGGCTTTCGA, Reverse: AGCCGCTTAAGAGCCTGTCG
611 GSK3B-ABE: Forward: ACATGGCGCTGTCCCAGATG, Reverse: AACCTACGCCATGGTGCGTG
612 GSK3B-CBE: Forward: CTACAGGTACCGGTCCTGAG, Reverse: GTACCTAGCGTGACGATCCG
613 Control: Forward: TTACTAGACTGCGGGGCCAC, Reverse: CGGCTCGATCTGCGACGAAT
614 The resulting amplicons were resolved on a 2% TAE gel and purified by Zymoclean Gel DNA
615 Recovery Kit (Zymo Research, Cat#D4008) and ligated into the pre-digested base editor
616 plasmids using Esp3I (Thermo Fisher Scientific, Cat# ER1281) and T4 DNA ligase (New
617 England Biolabs, Cat# M0202S) following the Golden Gate cloning method. The ligation product
618 was isopopanol precipitated and electroporated into Stbl4 electrocompetent cells (Invitrogen,
619 Cat# C751003) and grown at 30 °C. Plasmid DNA (pDNA) was prepared (HiSpeed Plasmid Maxi
620 Kit, Qiagen, Cat# 12662) and pooled. Library representation and distribution were confirmed by
621 next-generation sequencing.
622
623 *Mutant library cell preparation*
624 Lentivirus for pooled library production was generated by transfecting HEK293T cells (20×1e6)
625 in a 225 cm^2 flask with a DNA mixture containing pMD2.G (5 µg), psPAX2 (50 µg), and 40 µg of
626 the library vector, using PEI (1 mg/mL) at a 1:3 ratio. The viral supernatant was collected 48 h
627 post-transfection. To determine lentiviral titer, eHAP1-7TS cells were transduced with varying
628 volumes of lentivirus. After 48 h, puromycin (5 µg/mL; Sigma-Aldrich, Cat# P8833) was added,
629 and after five days, cell viability was assessed to determine the viral dose that resulted in a
630 transduction efficiency of 30-50%, corresponding to a multiplicity of infection (MOI) of
631 approximately 0.35-0.70. To generate mutant library cells, eHAP1-7TS cells were transduced in

632 two biological replicates at a low MOI of approximately 0.5. Briefly, cells were seeded at a density
633 of 1.5×10^6 cells per well in a 12-well plate containing IMDM. 24 h post seeding, plates were
634 subjected to spinfection with lentivirus mixed with polybrene (8 µg/mL) at 640xg for 2 h to
635 enhance transduction efficiency, followed by a 4-6 h incubation after which cells were trypsinized
636 and seeded into 225-cm^2 flasks. Two days post-transduction, puromycin (5 µg/mL) was added
637 and maintained for seven days to eliminate non-transduced cells.
638
639 *FACS-based phenotype enrichment for pooled screens*
640 For each biological replicate screen, mutant library cells were thawed in 15-cm dishes, split and
641 seeded for the FACS sorting stage. Cells were treated with 50% Wnt-3a conditioned medium for
642 24 h and then sorted by flow cytometry to isolate the top 10% and bottom 15% of the reporter
643 population, with unsorted cells collected as a reference for log-fold change normalization.
644
645 *Next Generation Sequencing*
646 Genomic DNA (gDNA) was isolated from sorted and unsorted cell populations using the Mag-
647 Bind Blood & Tissue DNA HDQ Kit (Omega Bio-Tek, Cat# M6393). For PCR amplification of the
648 integrated sgRNA sequences, 10 µg of gDNA was combined with a 100 µL reaction mixture
649 containing 2x NEBNext Master Mix and primers containing adaptor sequences with unique
650 barcoded i7 and i5 indices for Illumina sequencing. PCR cycling conditions were: (1) Initial
651 denaturation: 95 °C for 1 min; (2) Denaturation: 94 °C for 30 s; (3) Annealing: 52.5 °C for 30 s;
652 (4) Extension: 72 °C for 30 s; (5) cycle through steps 2-4 for 25 cycles; (6) Final extension: 72
653 °C for 5 min. PCR products were resolved on a 2% TAE gel, purified and library concentrations
654 were estimated using qRT-PCR with PhiX (Illumina, Cat# FC-110-3001) as a standard. The
655 samples were then sequenced on an Illumina NextSeq 550 platform with a 20% spike-in of PhiX.
656
657 *Data analyses*
658 Data analysis was performed using R (v4.3.2). Raw sequencing reads were demultiplexed and
659 converted to FASTQ files using the bcl2fastq module (v2.20.0), with each file assigned to a
660 condition based on the 8-nt P5 and P7 primers. These FASTQ files were then preprocessed to
661 extract the 20-nt guide RNA sequences using the PreprocessReads function from the QuasR
662 package (v1.36.0)[78]. The guide RNA reads were subsequently aligned to a custom reference file
663 containing all possible guide RNA sequences in the library using the Subread algorithm from the
664 Rsubread package (v2.16.2)[79]. Following alignment, a read count matrix was generated[80]. The
665 raw read counts were normalized to reads per million (RPM) for each condition using the formula:
666 RPM=(reads per guide RNA / total reads per condition)×1e6. To prevent issues with zero counts,
667 a $\log_2$ transformation was applied to the RPM values after adding a pseudocount of 1 to all
668 counts. We filtered out any sgRNAs with $\log_2$-normalized reads per million in the unsorted
669 sample falling outside 1.5 times the interquartile range (IQR) from the first and third quartiles,
670 effectively removing outliers and guides with extremely low or high representation. The log-fold
671 change (LFC) between sorted and unsorted populations was then calculated for each sgRNA.
672 To provide a standardized score (z-score) of enrichment or depletion, we used the LFC values
673 from control sgRNAs (non-targeting) to compute a mean and standard deviation, which were
674 then used to calculate z-scores for each sgRNA in the respective sorted populations as
675 described previously[27]. Predicted base editing mutations (N3-N10 window) were categorized
676 using custom R functions. Each mutation was assigned a category—including "missense,"

677 "nonsense," "splice-site," "silent,"—by parsing annotation strings derived from the library design.
678 These categories were stored in a new column within the dataset for subsequent analysis and
679 plotting. All analyses were conducted in R, and the complete code and analysis pipelines are
680 available on GitHub to ensure reproducibility and transparency.
681
682 **Validation of base editor gRNA hits**
683 To validate the top hits from the base editing screens, sgRNAs with z-scores ≥2 were selected.
684 Individual targeting sequences were cloned into either the pRDA 429 or pRDA 336 plasmids.
685 Screen hits were validated in two independent cell lines, eHAP1-7TS and HEK293T-7TS, with
686 reporter line generation and culture conditions described in the preceding sections.
687
688 *Validation in eHAP1-7TS cells*
689 Lentivirus was produced as described above. For each sgRNA, 1.5×1e6 eHAP1-7TS reporter
690 cells were seeded per well in a 12-well plate. 24 h post cell seeding, cells were transduced with
691 1.5 mL of lentivirus in a growth medium containing polybrene (8 µg/mL). The plates were
692 centrifuged at 640×g for 2 h before being transferred to a 37 °C incubator. After 4–6 h, cells were
693 trypsinized and transferred to a 10-cm dish. Puromycin selection was initiated 48 h post-
694 transduction by replacing the growth medium with fresh medium containing puromycin (5 µg/mL)
695 and continued for 5–7 days. Following selection, cells were split into two conditions: one in
696 growth medium without WNT conditioned media and a second supplemented with 50% WNT
697 conditioned media. After 24 h of treatment, cells were trypsinized, suspended in growth medium,
698 and mScarlet fluorescence was measured by flow cytometry using a SH800S cell sorter.
699
700 *Validation in HEK293T-7TS cells*
701 sgRNAs that resulted in ≥50% reduction in reporter fluorescence (for hits from the bottom 15%
702 sorted gate) and ≥10% elevation in reporter fluorescence (for hits from the top 10% sorted gate)
703 were selected for an independent round of validation in HEK293T-7TS reporter cells. Cells were
704 seeded at 3×10^5 cells per well in a 12-well plate. 24 h post-seeding, cells were transfected with
705 1 µg of the pRDA plasmid using the PEI transfection reagent. 48 h after transfection, cells were
706 trypsinized and seeded into 6-cm dishes. Puromycin selection was started 24 h later at 5 µg/mL
707 and continued for 5–6 days. Cells were then subjected to WNT ligand treatment for 24 h and
708 mScarlet fluorescence was measured as described for the eHAP1-7TS cells.
709
710 *Data analysis and hit selection*
711 Due to the large scale of the initial validation screen (370 sgRNAs), measurements were
712 conducted as a single experiment in both eHAP1-7TS and HEK293T-7TS reporter cell lines. The
713 selection of sgRNAs for subsequent, more detailed characterization was based on the criterion
714 that a given sgRNA showed the same phenotype (either a reduction or an elevation in
715 fluorescence) in both cell lines. sgRNAs that met this criterion were then subjected to detailed
716 characterization in at least three independent experiments.
717
718 **FACS-based phenotype enriched mutant cell generation**
719 Following the selection of hits for detailed characterization, mutant cell populations were
720 generated through FACS-based enrichment. The procedure was performed on HEK293T-7TS

721 mutant cells as described in the previous section. Two distinct protocols were followed based on
722 the observed phenotype:
723 For hits that resulted in a reduction of reporter fluorescence, cells were treated with 25% Wnt-
724 3a conditioned medium and 10 ng/mL RSPO3 for 24 h. Cells with the lowest mScarlet
725 fluorescence peak were then sorted using flow cytometry.
726 For hits that resulted in an elevation of reporter fluorescence, cells were treated with 5% Wnt-3a
727 conditioned medium and 10 ng/mL RSPO3 for 24 h. Cells with the highest mScarlet fluorescence
728 peak were then sorted.
729 In both cases, approximately 1×10^6 cells were sorted, expanded, and frozen for future analysis.
730 To determine the enriched mutational signature that resulted in the phenotype, deep sequencing
731 of the target region was conducted. This was performed as described in the 'Next Generation
732 Sequencing' section, with the key difference being a two-step PCR protocol. The first step used
733 primers with appended Illumina adapters, and the second PCR step incorporated primers with
734 adapters and barcodes for demultiplexing (Supplementary Table 3). Reads were analyzed with
735 CRISPResso2[81] to determine allele frequencies in the pooled sorted cells.
736
737 **Recombinant *Sp*Cas9 and sgRNA purification and Ribonucleoprotein (RNP) complex**
738 **assembly**
739 Recombinant *Streptococcus pyogenes* Cas9 (*Sp*Cas9) protein was purified using a protocol
740 adapted from the previously described method[82]. The expression plasmid pMJ915 (Addgene,
741 plasmid#69090), which encodes *Sp*Cas9 with an N-terminal His-MBP-TEV tag and a C-terminal
742 2xSV40NLS sequence, was transformed into Rosetta 2(DE3)pLysS Competent *E. coli* cells
743 (Millipore-Sigma,Cat#71403). *E. coli* were cultured in terrific broth (Thermo Scientific,
744 Cat#H26824.36) at 37 °C. Protein expression was induced with 0.25 mM IPTG at a cell density
745 of OD_{600}=0.6, followed by incubation at 18 °C for 16 h. Cell pellets were harvested by
746 centrifugation and resuspended in lysis buffer (20 mM Tris pH 8.0, 500 mM NaCl, 1 mM TCEP,
747 5% glycerol, 5 mM imidazole, 0.5 mM PMSF, and 1x protease inhibitor cocktail (Millipore-Sigma,
748 Cat#S8820). Resuspended cells were homogenized using an EmulsiFlex-C5 (Avestin) at 20,000
749 psi. Lysates were clarified by centrifugation at 50,000xg for 30 minutes and the supernatant was
750 incubated with His-Tag Purification Resin (Roche, Cat#5893682001) for batch binding. The resin
751 was washed with ten column volumes of wash buffer (lysis buffer excluding PMSF and protease
752 inhibitor cocktail). Bound protein was eluted with an elution buffer (wash buffer supplemented
753 with 250 mM imidazole). TEV protease (homemade) was added to the eluted protein, and the
754 mixture was dialyzed overnight against Ion-Exchange Buffer A (20 mM HEPES pH 7.5, 150 mM
755 KCl, 1 mM TCEP, and 5% glycerol) using a 10 MWCO dialysis cassette (Thermo Fisher
756 Scientific, Cat#66453) to cleave the His-MBP tag. The cleaved sample was then applied to a
757 HiTrap SP HP column (cytiva) equilibrated in 15% Ion-Exchange Buffer B (20 mM HEPES pH
758 7.5, 1 M KCl, 1 mM TCEP, and 5% glycerol). *Sp*Cas9 was eluted with a linear gradient from 15%
759 to 50% Ion-Exchange Buffer B. Peak fractions were pooled, concentrated using an Amicon
760 ultracentrifugal filter, 30 kDa MWCO (Millipore-Sigma, Cat#UFC9030), and subjected to size
761 exclusion chromatography on a HiLoad 16/60 Superdex 200 prep grade column (cytiva)
762 equilibrated in Size Exclusion Buffer (20 mM HEPES pH 7.5, 150 mM KCl, 1 mM TCEP, and
763 10% glycerol). Peak fractions containing purified *Sp*Cas9 were pooled, aliquoted, flash frozen in
764 liquid nitrogen, and stored at -80 °C. sgRNA template assembly, amplification, *in vitro*
765 transcription, and purification were performed as described previously[82]. Target sequences that

766 are part of the T7FwdVar oligo in the sgRNA template assembly step are listed in the "APCmcr
767 truncation in HAP1 cells" and "PGE of AXIN1 in HAP1 cells" sections. *In vitro* transcription was
768 carried out using the HiScribe T7 High yield RNA Synthesis Kit (New England Biolabs,
769 Cat#E2040S) following the manufacturer's instructions. Transcription reactions were
770 subsequently treated with RNase-free DNase I (Thermo Fisher Scientific, Cat EN0521) to
771 remove DNA template, followed by Quick CIP (New England Biolabs, Cat#M0525). sgRNAs
772 were purified using the RNeasy Mini kit (Qiagen, Cat#74104) following a modified protocol[82]. For
773 CRISPR/Cas9 mediated non-homologous end joining (NHEJ) and homology-directed repair
774 (HDR) experiments, Cas9 ribonucleoprotein (RNP) complexes were assembled immediately
775 before use. A 20 µL reaction volume was prepared containing 100 pmol of purified *Sp*Cas9
776 protein and 120 pmol of sgRNA in Cas9 buffer (20 mM HEPES pH 7.4, 150 mM KCl, 1 mM
777 $MgCl_2$, 1 mM TCEP, and 10% glycerol).
778
779 **APC^{mcr} truncation in RKO and HAP1 cells**
780 Truncations within the mutation cluster region (MCR) of the endogenous APC gene were
781 introduced into RKO and HAP1 cells using CRISPR/Cas9-mediated gene editing. RKO cells
782 were prepared for electroporation using the Cell Line Nucleofector Kit R (Lonza Bioscience,
783 Cat#VCA-1001). For electroporation reaction, 1 µg of the plasmid pSpCas9(BB)-2A-GFP
784 (Addgene, Cat#48138), encoding *Sp*Cas9 and sgRNA targeting the APC^{mcr} (APC sg1320; 5'-
785 ACTGCTGGAACTTCGCTCAC-3'), was added to the cell suspension. Electroporation was
786 carried out using the Amaxa Nucleofector II system following the manufacturer's instructions with
787 program A-024. APC^{mcr} truncation mutation was generated in HAP1 cells by delivering pre-
788 assembled Cas9 ribonucleoprotein (RNP) complexes via electroporation. The RNP complexes
789 were assembled using purified *Sp*Cas9 protein and *in vitro* transcribed sgRNA targeting the
790 APC^{mcr} (APC sg1336, 5'- ACCAAATCCAGCAGACTGCA-3'). HAP1 cells were electroporated
791 with the assembled RNP complexes using the NEPA21 Electro-Kinetic transfection system
792 (Bulldog-Bio). The specific electroporation parameters used were: poring pulse of 190 V, poring
793 length of 5 ms, and the remaining parameters being default settings. Approximately 24 h after
794 electroporation, the cell culture medium was replaced with fresh growth medium. On the
795 following day (approximately 48 h post-electroporation), live single cells were sorted into
796 individual wells of a 96-well plate containing growth medium using a SH800 Cell Sorter. Single-
797 cell clones were subsequently expanded in culture. Successful introduction of APC^{mcr} truncation
798 mutations in clonal cell lines was confirmed by both Sanger sequencing of the targeted APC
799 locus and immunoblotting to assess the size of APC.

800 **Validation of base editor sgRNA hits in APC^{mcr} truncated cells**
801 sgRNAs that passed the hit selection criteria from the "Validation of base editor sgRNA hits"
802 section were cloned into either the pRDA 429 or pRDA 336 plasmids. Lentivirus production and
803 transduction was performed as described in the 'Generation of WNT transcriptional reporter
804 lines' section. The recipient clonal cell lines (RKO-7TG 1320* and DLD-1-7TG) were transduced
805 at a multiplicity of infection (MOI) of approximately 0.5 in the presence of polybrene (8 µg/mL).
806 Transduced cells were subjected to puromycin selection at a concentration of 5 µg/mL for 5-7
807 days, or until all non-transduced control cells had died.
808
809 **Precise genome editing (PGE) of *AXIN1* locus in HAP1 cells**

sgRNAs and single-stranded oligonucleotide (ssODN) donor templates for precise genome editing of the *AXIN1* locus via homology directed repair (HDR) were designed using the CRISPR HDR Design Tool (Integrated DNA Technologies). The targeting sequences for *AXIN1* were 5'-GGAGAACCCTGAGAGCATCC-3' (L471A/D472A/H474) and 5'-CAGCGTGTGCTGAGGACACC-3' (L479W). ssODN donor templates were designed to introduce either the L471A/D472A/H474A or the L479W mutations into the *AXIN1* gene. The sequences of the ssODN templates are listed in the Supplementary Table 3. A silent mutation designed to introduce a *Pst*I restriction site was incorporated into the ssODN for the *AXIN1* L471A/D472A/H474A mutation to facilitate screening, designed using the silent mutagenesis tool (molbiotools). A mutation-specific forward primer was designed to screen for the *AXIN1* L479W mutant allele. HAP1 cells, both wild-type for APC (full length) and those harboring the APCmcr truncation, were subjected to electroporation to deliver the CRISPR/Cas9 RNP complex and ssODN donor templates for HDR. Electroporation was performed as described in the "generation of APCmcr truncation in HAP1 cells" section using the NEPA21 Electro-Kinetic transfection system. For each reaction, 100 pmol of pre-assembled *Sp*Cas9 RNP complex, 100 pmol of the respective ssODN donor template, and 1 µM of HDR Enhancer v2 (Integrated DNA Technologies, Cat#10007910) were added to the cell suspension immediately prior to electroporation. Single-cell sorting was performed approximately 72 h post-electroporation to isolate individual cells for clonal expansion, as described in the "single-cell sorting and clonal expansion" section. Sorting was performed based on viability gating. Putative positive clones were screened and confirmed for the presence of the desired *AXIN1* mutations. For clones putatively carrying the *AXIN1* L471A/D472A/H474A mutation, genomic DNA was extracted, and a region of the *AXIN1* locus was amplified by PCR. The PCR product was then digested with the *Pst*I restriction enzyme (New England Biolabs) to confirm the introduction of the silent mutation and thus the intended HDR event. Clones putatively carrying the *AXIN1* L479W mutation were screened by PCR using a mutation-specific forward primer (see Supplementary Table 3) followed by analysis of the PCR product size on an agarose gel. Positive clones identified by these screening methods were further confirmed by Sanger sequencing of the targeted *AXIN1* locus. To generate HAP1 cells harboring the *AXIN1* V475I/L479W double mutation, a clonal line previously established with the *AXIN1* L479W single mutation was used. This clonal line was transduced with a lentivirus generated from the plasmid pRDA 336 expressing a CBE targeting the *AXIN1* locus with the targeting sequence sequence 5'-CTGTACGTGCTCGTCCAGGA-3'. Following transduction, antibiotic selection was applied to enrich for transduced cells. Single-cell sorting, clonal expansion, and positive clone identification were performed as described earlier in the "single-cell sorting and clonal expansion" and "genotype confirmation" sections, respectively.

Generation of doxycycline-inducible FLAG-AXIN1 stable SW480 cell lines

These cell lines were generated using the PiggyBac transposon system. Briefly, FLAG-AXIN1 wild-type, Affinity-Reducing (AR) mutant (L471A/D472A/H474A), and Affinity-Enhancing (AE) mutant (V475I/L479W) constructs were cloned into the PB-TAC-ERP2 (Addgene Cat#80478) plasmid. For transfection, 300,000 SW480 cells were seeded per well in a 6-well plate. Approximately 24 h later, the cells were transfected with 1 µg of the PB-TAC-ERP2 plasmid and 1 µg of the Super PiggyBac Transposase expressing plasmid using X-tremeGENE DNA 9 transfection reagent (Millipore-Sigma Cat#6365787001). At 48 h post-transfection, cells were

855 trypsinized and re-plated for puromycin selection. Selection was performed with a concentration
856 of 5 µg/mL of puromycin for 5 days.
857
858 **Generation of FLAG-AXIN1 stable SW480 cell lines by lentiviral transduction**
859 FLAG-AXIN1 wild-type, Affinity-Reducing (AR) mutant (L471A/D472A/H474A), and Affinity-
860 Enhancing (AE) mutant (V475I/L479W) constructs were cloned into the pRDA 336 plasmid by
861 swapping the Cas9-NG sequence to retain the P2A-puromycin selection cassette. Lentivirus
862 production and transduction was performed as described in the 'Generation of WNT
863 transcriptional reporter lines' section. Recipient clonal cell lines were transduced at a multiplicity
864 of infection (MOI) of approximately 0.5 in the presence of polybrene (8 µg/mL). Transduced cells
865 were subjected to puromycin selection at a concentration of 5 µg/mL for 5 days.
866
867 **Immunoblotting**
868 All cells were harvested by scraping. Samples were lysed according to the target protein to
869 ensure optimal extraction. Protein concentrations were determined using the BCA Protein Assay
870 Kit (Thermo Fisher Scientific, Cat#23225) with bovine serum albumin (BSA) as the standard.
871 For the analysis of soluble (non-phosphorylated, active) β-catenin, cells were lysed in hypotonic
872 buffer (10 mM Tris pH 7.5, 10 mM KCl, 5 mM EDTA) supplemented with a Protease and
873 Phosphatase Inhibitor cocktail (Thermo Fisher Scientific, Cat#78442) and 1 µM Bortezomib.
874 After a 10-minute incubation on ice, cells were lysed via a freeze-thaw cycle using liquid nitrogen.
875 Lysates were then centrifuged at 20,000 x *g* for 30 minutes at 4 °C to separate the soluble
876 fraction, and the supernatant was collected for analysis. For the analysis of AXIN1, cells were
877 lysed in a Cell Lysis Buffer with Ionic and Non-Ionic Detergents (CLB-wIND; 50 mM Tris pH 8.0,
878 150 mM NaCl, 1% Triton X-100, 0.1% SDS, 0.1% Deoxycholate, 10% glycerol) containing a
879 Protease and Phosphatase Inhibitor cocktail. Samples were vortexed for 30 minutes at 4 °C to
880 ensure complete lysis. Lysates were then clarified by centrifugation at 20,000 x *g* for 30 minutes
881 at 4 °C, and the resulting supernatant was collected for analysis. For immunoblotting, 20–30 µg
882 of total protein was separated by SDS-PAGE using 4–12% gradient NuPAGE Bis-Tris Protein
883 Gels (Thermo Fisher Scientific). Separated proteins were transferred to a nitrocellulose
884 membrane (Bio-Rad, Cat#1620112). Membranes were blocked for 30 minutes at room
885 temperature in either LI-COR Odyssey Blocking Buffer (0.2x PBS, 0.1% casein, and 0.01%
886 sodium azide) for β-catenin blots or Blocking Buffer M (Tris-buffered saline (TBS) containing
887 0.1% Tween-20 (TBS-T) and 5% non-fat dry milk) for AXIN1 blots. Primary antibodies were
888 incubated overnight at 4 °C. After three washes with TBS-T, membranes were incubated for 1 h
889 at room temperature with the appropriate secondary antibody: IRDye 800CW (LICORbio) for β-
890 catenin or HRP-conjugated (Jackson ImmunoResearch) for AXIN1. Blots were washed three
891 times with TBS-T. β-catenin blots were imaged using an Odyssey CLx Imaging System
892 (LICORbio). Chemiluminescence for AXIN1 was detected using SuperSignal West Pico PLUS
893 chemiluminescent substrate (Thermo Fisher Scientific, Cat#34580), and signals were captured
894 on film.
895
896 **Co-immunoprecipitation**
897 Cells were harvested by scraping and lysed in a Cell Lysis Buffer with Non-Ionic Detergent (CLB-
898 wND; 50 mM Tris pH 7.4, 150 mM NaCl, 1% Triton X-100, 1 mM DTT, 10% glycerol)
899 supplemented with a Protease and Phosphatase Inhibitor cocktail (Thermo Fisher Scientific,

Cat#78442), 1 μM Bortezomib, 2 mM $MgCl_2$, and 50 U/mL Benzonase. Lysates were rotated on a nutator for 1 h at 4 °C and then clarified by centrifugation at 20,000 x *g* for 30 minutes at 4 °C. For the immunoprecipitation of endogenous proteins (β-catenin and AXIN1), 3–4 mg of clarified cell lysate was pre-cleared with Dynabeads Protein A/G (Thermo Fisher Scientific, Cat#10002D and Cat#10004D) for 1 h at 4 °C to remove proteins that non-specifically bind to the beads. Following this, the pre-cleared lysates were incubated overnight at 4 °C on a nutator with pre-conjugated antibody-bead complexes. For β-catenin immunoprecipitation, 2 μg of β-catenin antibody was conjugated to Dynabeads Protein G. For AXIN1 immunoprecipitation, 2 μg of AXIN1 antibody was conjugated to Dynabeads Protein A. The resulting immunocomplexes were captured and washed three times with wash buffer (CLB-wND without inhibitors). Immunocomplexes were then eluted in 2x Laemmli sample buffer. For the immunoprecipitation of FLAG-tagged AXIN1 in SW480 cells, the procedure was identical, with the exception that anti-FLAG M2 magnetic beads (Sigma-Millipore, Cat#M8823) were used instead of the antibody-bead conjugation step and the pre-clearing step was omitted due to the low non-specific binding of the beads. Eluted proteins from all immunoprecipitation experiments were analyzed by immunoblotting.

Immunofluorescence

Cells cultured on glass coverslips were fixed with 4% paraformaldehyde (PFA) in PBS for 10 min at room temperature (r/t) . Following fixation, cells were permeabilized and blocked for 30 minutes at r/t using Blocking and Permeabilization Buffer (BPB) (1x PBS pH 7.4 containing 1% donkey serum, 1% BSA, and 0.1% Triton X-100). Coverslips were then incubated with the primary antibody against active β-Catenin (diluted in BPB) for 1 h at r/t. After three washes with PBS, cells were incubated with Alexa Fluor 488 conjugated donkey anti-rabbit IgG secondary antibody (Thermo Fisher Scientific) for 45 minutes at r/t in the dark. Coverslips were washed three times with PBS and mounted onto glass slides using ProLong Diamond Antifade Mountant with DAPI (Invitrogen, Cat#P36962) to counterstain nuclei. Images were acquired on a Leica TCS SP8 confocal microscope using a 63× oil-immersion objective. Z-stacks covering the entire cell were collected at 0.5 μm intervals, and maximum intensity projection images were generated for analysis. Nuclear and cytoplasmic fluorescence intensities were quantified using CellProfiler (v4)[83]. Nuclear masks were defined by automated thresholding of the DAPI channel, and cytoplasmic masks were generated by radial expansion of nuclear boundaries while excluding neighboring nuclei. Mean fluorescence intensities were extracted from nuclear and cytoplasmic compartments for downstream analyses.

Quantitative real-time PCR

Total RNA was extracted from cells using TRIzol reagent (Thermo Fisher Scientific, Cat#15596026) following the manufacturer's protocol. The RNA concentration and purity were determined using a Synergy H1 microplate reader (Biotek). cDNA was synthesized from 250 ng of total RNA using the iScript Reverse Transcription Supermix (Bio-Rad, Cat#1708841). Quantitative real-time PCR was performed on a QuantStudio 5 Real-Time System (Agilent) using SYBR Green qPCR Master Mix (Selleck, Cat#B21703) following the manufacturer's instructions. A melt curve analysis was performed at the end of the run to ensure product specificity. The expression of target genes was normalized to the housekeeping gene *GAPDH*. The primers used were: hAXIN2_Fwd: 5' – GTCCAGCAAAACTCTGAGGG – 3', hAXIN2_Rev:

945 5' – CTGGTGCAAAGACATAGCCA – 3', hGAPDH_Fwd: 5' – TGCACCACCAACTGCTTAGC –
946 3', hGAPDH_Rev: 5' – GGCATGGACTGTGGTCATGAG – 3'.
947
948 **Expression and purification of recombinant proteins**
949 Recombinant proteins were expressed in *E. coli* using the same protocol as described for the
950 *Sp*Cas9 protein in the 'Recombinant *Sp*Cas9 and sgRNA purification' section. For the GST-
951 tagged β-catenin binders (AXIN1, a.a. Cys435-His498; TCF4, a.a. Met1-Glu53; ICAT, a.a. Met1-
952 Gln81, cell pellets were resuspended in B-PER Reagent (Thermo Fisher Scientific, Cat#90079)
953 supplemented with lysozyme (100 µg/mL), DNase I (5 U/mL), 1 mM PMSF, and protease
954 inhibitor cocktail (Sigma-Millipore) and incubated for 15 min at room temperature. The lysate
955 was clarified by centrifugation at 50,000 x *g* for 30 minutes at 4 °C. For affinity chromatography,
956 clarified lysates were incubated with Glutathione Sepharose resin (Gold Biotech) for 1 h at 4 °C
957 on a rotator. The mixture was transferred to a gravity-flow chromatography column (Bio-Rad),
958 and the column was washed with 50 column volumes of GST-Wash Buffer (50 mM sodium
959 phosphate buffer pH 7.4, 500 mM NaCl and 1 mM DTT). The GST-tagged proteins were then
960 eluted with GST-Elution Buffer (50 mM sodium phosphate buffer pH 7.4, 150 mM NaCl, 1 mM
961 DTT and 10 mM L-Glutathione). The eluted proteins were buffer exchanged into GST-Storage
962 Buffer (30 mM sodium phosphate buffer pH 7.4, 150 mM NaCl, 1 mM DTT, 5% glycerol) using
963 an Amicon Ultra-15 Centrifugal Filter Unit (Millipore, Cat#UFC901024, 10 kDa MWCO). Protein
964 concentration was determined by measuring the absorbance at 280 nm. To purify GST-
965 brSUMO-tagged full-length β-catenin, cell pellets were resuspended in GST-Lysis Buffer (50 mM
966 Sodium phosphate buffer pH 7.4, 150 mM NaCl, 1 mM DTT) supplemented with 1 mM PMSF,
967 and protease inhibitor cocktail. The cells were lysed by high-pressure homogenization (LM20
968 Microfluidizer) with two passes at 20,000 psi. The lysate was clarified by centrifugation at 50,000
969 x *g* for 30 minutes at 4 °C. The clarified lysate was incubated with Glutathione resin for 1 h at 4
970 °C on a rotator and then transferred to a gravity-flow column. The column was washed with 50
971 column volumes of GST-Wash Buffer, followed by a wash with 10 column volumes of Cleavage
972 Buffer (50 mM Sodium phosphate buffer pH 7.4, 150 mM NaCl and 1 mM DTT). GST-brSUMO
973 tag was cleaved by incubating the sample with 200 nM bdSENP1 (homemade) for 1 h at 4 °C
974 on a rotator. The cleaved protein was then eluted using a gravity-flow column, and the eluate
975 was centrifuged at 20,000 x *g* for 10 minutes at 4 °C. The sample was subjected to a size-
976 exclusion chromatography on a HiLoad 16/60 Superdex 200 prep grade column (cytiva)
977 equilibrated in SEC Buffer (30 mM Sodium phosphate buffer pH 7.4, 150 mM NaCl, 5% glycerol).
978 Fractions containing the purified protein were pooled and concentrated using an Amicon 30 kDa
979 MWCO concentrator. Protein concentration was estimated by measuring the absorbance at 280
980 nm.
981
982 **APC-AXIN1 pull-down assays to explore the contribution of β-catenin**
983 Human AXIN1, β-catenin and APC variants were expressed using the baculovirus expression
984 system in Sf9 cells and purified as described previously[16]. For the *in vitro* binding (pull-down)
985 assay, preys (APC variants, β-catenin) were added to AXIN1-dStrepII (the bait) in equimolar
986 ratios and left to incubate at room temperature for 20 min in binding buffer (50 mM HEPES pH
987 7.5, 150 mM NaCl, 5% glycerol, 1 mM TCEP). Then, 30 µl of packed StrepTactin Sepharose
988 resin (IBA Lifesciences) was added to the binding reactions in the binding buffer to a total volume
989 of 500 µl and left to incubate for 60 min at 4°C rotating. The resin was washed three times with

990 1 ml of binding buffer, allowing 5 min for incubation at each wash step. Finally, 50 µl of 1.5x SDS
991 sample buffer was added to the resin. Samples were boiled and analyzed by SDS-PAGE and
992 Coomassie staining.
993
994 **Pull-down assays**
995 To investigate the *in vitro* binding interaction between GST-AXIN1 CBD and full-length β-catenin,
996 we performed pull-down assays. *In vitro* binding reactions were set up in a total volume of 100
997 µL using a binding buffer containing 20 mM Tris pH 7.5, 150 mM NaCl, 0.1% Triton X-100, and
998 2 mM DTT. A fixed concentration of 1 µM GST-AXIN1 CBD was incubated with increasing
999 concentrations of full-length β-catenin (0.01, 0.1, 0.5, and 2 µM) for 30 min at 22 °C. Following
1000 the initial binding reaction, Glutathione Magnetic Agarose beads (Thermo Fisher Scientific, Cat#
1001 78601) were added to each sample and incubated for an additional 30 min at 22 °C. The beads
1002 were then washed three times with a binding buffer to remove unbound proteins. The protein
1003 complexes were eluted by boiling in a 2x Laemmli sample buffer. Samples, representing 10% of
1004 the total elution volume, were analyzed by SDS-PAGE followed by immunoblotting with
1005 antibodies against GST and β-catenin, as described in the 'Immunoblotting' section.
1006
1007 **Biolayer interferometry-based protein binding assays**
1008 Kinetic binding experiments were performed on an Octet RED96 system (ForteBio, Sartorius) at
1009 30 °C with a plate shaking speed of 1,000 rpm in 96-well black, flat-bottom polypropylene
1010 microplates (Greiner Bio-One, #655209). All assays were conducted in Octet buffer composed
1011 of 30 mM sodium phosphate pH 7.4, 150 mM NaCl, 1 mM DTT, and 5% glycerol, supplemented
1012 with 0.05% Tween-20 and 0.1% BSA to minimize nonspecific binding. Octet GST biosensor tips
1013 were pre-equilibrated in Octet buffer for 10 min prior to use. Sensors were then loaded with GST-
1014 tagged ligands (GST-AXIN1 and its variants, GST-ICAT, and GST-TCF4) at 50 nM, ensuring
1015 measurements remained within the linear range of the BLI signal to avoid overcrowding on the
1016 sensor surface. Following ligand immobilization, sensor tips were washed and baselined in wells
1017 containing only Octet buffer. For analyte binding, full-length β-catenin and its variants were used
1018 at concentrations of 500 nM for GST-ICAT, 1 µM for GST-Axin1 and GST-TCF4. Association
1019 was monitored for 20–25 s, followed by 100 s of dissociation in the Octet buffer. A reference
1020 sensor (ligand-loaded but dipped into buffer only) was included to correct for nonspecific signal
1021 drift and baseline fluctuations. All sensorgrams were reference-subtracted and analyzed using
1022 ForteBio Data Analysis Software 10.0 software. Experimental data from both association and
1023 dissociation phases was simultaneously fit using a 1:1 binding model to estimate k_{on} and k_{off}.
1024 The association phase is modelled using pseudo-first-order kinetics, assuming that the analyte
1025 concentration is effectively constant since we used a ~10–60 fold excess of analyte over
1026 immobilized ligand. The dissociation phase was modeled using first-order decay kinetics. The
1027 equilibrium dissociation constant was calculated as $K_D=k_{off}/k_{on}$. Reported K_D values represent
1028 the average of at least three independent experiments.
1029
1030 **Data visualization, statistics and reproducibility**
1031 Quantitative data were visualized using GraphPad Prism and R. All structural figures were
1032 generated using UCSF ChimeraX (version 1.8rc202405140121). PDB codes for structural
1033 figures are provided in the respective figure legends. Immunoblot panels were processed using
1034 Adobe PhotoShop (for chemiluminescence data) and Fiji (for LI-COR data). Figure panels were

prepared using Adobe Illustrator. Unless otherwise indicated, all experiments were performed with a minimum of three (n≥3) independent biological replicates. Technical replicates were not counted as independent samples for statistical analysis. Data are consistently presented as the mean with individual data points overlaid. For experiments involving comparisons between two groups (e.g., wild-type vs. a single mutant β-catenin variant) within a single treatment condition (untreated, Wnt-3a, or CHIR99021), statistical significance was determined using multiple unpaired Student's *t*-tests with Welch's correction. The rejection thresholds for the *p*-values were adjusted using the two-stage step-up (Benjamini, Krieger, and Yekutieli) method to control the false discovery rate (FDR) at 0.01. For experiments involving comparisons across multiple groups (e.g., wild-type β-catenin and four mutant variants) within a single treatment condition (untreated, Wnt-3a, or CHIR99021), statistical significance was determined using Brown-Forsythe and Welch Analysis of Variance (ANOVA) tests. Subsequent pairwise comparisons between groups were conducted using Dunnett's T3 multiple comparisons test. Specific *p*-values for key comparisons are reported directly in the figure panels.

Use of Artificial Intelligence

The authors used AI assistants to strategically refine different sections of this manuscript. The abstract was improved with the assistance of Claude (Anthropic) to enhance its appeal to a broader audience and convey the work's significance beyond a specialized field. Gemini (Google) was used to ensure the methods and figure legends were detailed, clear, and consistent to promote greater reproducibility. The AI assistants did not perform any scientific analysis, interpretation of results, or contribute to the intellectual content of this research. All information presented is the sole product of the authors' work and judgment.

Data availability

All raw and processed sequencing data supporting the CRISPR-based screening and subsequent analyses are available in the Sequence Read Archive (SRA) repository under BioProject accession number PRJNA1344315. The specific read counts and processed data files derived from the initial base editing screen are listed in Supplementary Table 1. All source data and corresponding raw quantification files used for the validation of sgRNAs in eHAP1-7TS and HEK293T cell lines are provided in Supplementary Table 2, accompanying the paper.

Code availability

The custom R scripts and computational pipelines utilized for the processing and statistical analysis of the base editing screen data were written in R (4.3.2) and are publicly available at the following GitHub repository:https://github.com/RohatgiLab/Murugesh_DC_base_editing_analysis

Acknowledgements

We are grateful to Yuki Yoshida for cloning the GST-TCF4 CBD construct and to Ramin Dubey for generating the DLD-1-7TG WNT transcriptional reporter line. This work was supported by the National Institutes of Health (NIH) grants GM118082 (to R.R.), CA230220 (to S.M.C.), and GM122516, CA281002, and CA236733 (to E.L.). R.R. and E.L. were also supported by an Innovation Fund Award from the Pew Charitable Trusts. M.M. was supported by an American Cancer Society – Jean Perkins Foundation Postdoctoral Fellowship in Cancer Research (Award

PF-20-121-01-TBE). Work in S.G. 's group was funded by a Cancer Research UK Programme Foundation Award (C47521/A28286) and a PhD Studentship by The Institute of Cancer Research to S.S.

Author contributions

R.R. and G.V.P. conceived the study. M.P. optimized the base editing methodology, conducted screens, performed formal analyses, and generated the structure panels. M.P. also performed all Biolayer Interferometry (BLI) experiments, generated the eHAP1-7TS reporter line, and performed validation experiments in eHAP1-7TS cells. G.V.P. designed the experiments, engineered the HAP1 clonal lines using HDR, and performed mechanistic analyses of the engineered cell lines. G.V.P. also designed the sorting strategy for the HEK293T-7TS mutant cells and conducted all validation experiments in the HEK293T-7TS, RKO APC1320*-7TG, and DLD-1-7TG cell lines. M.P. performed the deep sequencing to determine allele frequency in the sorted HEK293T-7TS mutant cells. G.V.P. and R.R. purified recombinant proteins from bacteria. S.S. performed the *in vitro* AXIN1-APC-β-catenin pulldown experiments under the guidance of S.G.. P.S. and M.M. assisted with immunofluorescence staining and immunoblotting experiments. E.L. provided essential reagents. S.M.C. and M.P. contributed to the sgRNA library design. G.V.P. contributed to the data visualization with input from M.P. R.R. drafted the original manuscript with input from G.V.P. and M.P. R.R. and G.V.P. reviewed and edited the manuscript. R.R. supervised the study and acquired funding. All authors reviewed the manuscript.

Competing interests

E.L. is a co-founder and holds equity in StemSynergy Therapeutics, a company developing inhibitors for major signaling pathways (including the WNT pathway) for the treatment of cancer. E.L.'s interests are reviewed and managed by Vanderbilt University in accordance with their conflict of interest policies. The remaining authors declare that they have no competing financial and non-financial interests.

Correspondence and request for materials should be addressed to Rajat Rohatgi.

References

1. Clevers, H., Loh, K. M. & Nusse, R. Stem cell signaling. An integral program for tissue renewal and regeneration: Wnt signaling and stem cell control. *Science* **346**, 1248012 (2014).
2. Maurice, M. M. & Angers, S. Mechanistic insights into Wnt-β-catenin pathway activation and signal transduction. *Nat. Rev. Mol. Cell Biol.* 1–18 (2025).
3. Chai, G. *et al.* A Human Pleiotropic Multiorgan Condition Caused by Deficient Wnt Secretion. *N. Engl. J. Med.* **385**, 1292–1301 (2021).
4. Sanchez-Vega, F. *et al.* Oncogenic signaling pathways in The Cancer Genome Atlas. *Cell* **173**, 321–337.e10 (2018).
5. Cancer Genome Atlas Network. Comprehensive molecular characterization of human colon and rectal cancer. *Nature* **487**, 330–337 (2012).
6. Bray, F. *et al.* Global cancer statistics 2022: GLOBOCAN estimates of incidence and mortality worldwide for 36 cancers in 185 countries. *CA Cancer J. Clin.* **74**, 229–263

1124 (2024).
1125 7. Yaeger, R. *et al.* Clinical Sequencing Defines the Genomic Landscape of Metastatic
1126 Colorectal Cancer. *Cancer Cell* **33**, 125–136.e3 (2018).
1127 8. Dow, L. E. *et al.* Apc Restoration Promotes Cellular Differentiation and Reestablishes
1128 Crypt Homeostasis in Colorectal Cancer. *Cell* **161**, 1539–1552 (2015).
1129 9. Bugter, J. M., Fenderico, N. & Maurice, M. M. Mutations and mechanisms of WNT
1130 pathway tumour suppressors in cancer. *Nat. Rev. Cancer* **21**, 5–21 (2021).
1131 10. Stamos, J. L. & Weis, W. I. The β-catenin destruction complex. *Cold Spring Harb.*
1132 *Perspect. Biol.* **5**, a007898 (2013).
1133 11. Xu, W. & Kimelman, D. Mechanistic insights from structural studies of beta-catenin and its
1134 binding partners. *J. Cell Sci.* **120**, 3337–3344 (2007).
1135 12. Munemitsu, S., Albert, I., Souza, B., Rubinfeld, B. & Polakis, P. Regulation of intracellular
1136 beta-catenin levels by the adenomatous polyposis coli (APC) tumor-suppressor protein.
1137 *Proc. Natl. Acad. Sci. U. S. A.* **92**, 3046–3050 (1995).
1138 13. Liu, C. *et al.* Control of beta-catenin phosphorylation/degradation by a dual-kinase
1139 mechanism. *Cell* **108**, 837–847 (2002).
1140 14. MacDonald, B. T. & He, X. Frizzled and LRP5/6 receptors for Wnt/β-catenin signaling.
1141 *Cold Spring Harb. Perspect. Biol.* **4**, a007880–a007880 (2012).
1142 15. Gammons, M. & Bienz, M. Multiprotein complexes governing Wnt signal transduction.
1143 *Curr. Opin. Cell Biol.* **51**, 42–49 (2018).
1144 16. Ranes, M., Zaleska, M., Sakalas, S., Knight, R. & Guettler, S. Reconstitution of the
1145 destruction complex defines roles of AXIN polymers and APC in β-catenin capture,
1146 phosphorylation, and ubiquitylation. *Mol. Cell* **81**, 3246–3261.e11 (2021).
1147 17. Liu, J., Xing, Y., Hinds, T. R., Zheng, J. & Xu, W. The third 20 amino acid repeat is the
1148 tightest binding site of APC for beta-catenin. *J. Mol. Biol.* **360**, 133–144 (2006).
1149 18. Choi, H.-J., Huber, A. H. & Weis, W. I. Thermodynamics of beta-catenin-ligand
1150 interactions: the roles of the N- and C-terminal tails in modulating binding affinity. *J. Biol.*
1151 *Chem.* **281**, 1027–1038 (2006).
1152 19. Spink, K. E., Polakis, P. & Weis, W. I. Structural basis of the Axin-adenomatous polyposis
1153 coli interaction. *EMBO J.* **19**, 2270–2279 (2000).
1154 20. Rubinfeld, B., Tice, D. A. & Polakis, P. Axin-dependent phosphorylation of the
1155 adenomatous polyposis coli protein mediated by casein kinase 1epsilon. *J. Biol. Chem.*
1156 **276**, 39037–39045 (2001).
1157 21. Yost, C. *et al.* The axis-inducing activity, stability, and subcellular distribution of beta-
1158 catenin is regulated in Xenopus embryos by glycogen synthase kinase 3. *Genes Dev.* **10**,
1159 1443–1454 (1996).
1160 22. Ikeda, S. *et al.* Axin, a negative regulator of the Wnt signaling pathway, forms a complex
1161 with GSK-3beta and beta-catenin and promotes GSK-3beta-dependent phosphorylation of
1162 beta-catenin. *EMBO J.* **17**, 1371–1384 (1998).
1163 23. Lue, N. Z. & Liau, B. B. Base editor screens for in situ mutational scanning at scale. *Mol.*
1164 *Cell* **83**, 2167–2187 (2023).
1165 24. Hanna, R. E. *et al.* Massively parallel assessment of human variants with base editor
1166 screens. *Cell* **184**, 1064–1080.e20 (2021).
1167 25. Komor, A. C., Kim, Y. B., Packer, M. S., Zuris, J. A. & Liu, D. R. Programmable editing of
1168 a target base in genomic DNA without double-stranded DNA cleavage. *Nature* **533**, 420–

1169 424 (2016).
1170 26. Gaudelli, N. M. *et al.* Programmable base editing of A•T to G•C in genomic DNA without
1171 DNA cleavage. *Nature* **551**, 464–471 (2017).
1172 27. Sangree, A. K. *et al.* Benchmarking of SpCas9 variants enables deeper base editor
1173 screens of BRCA1 and BCL2. *Nat. Commun.* **13**, 1318 (2022).
1174 28. Nishimasu, H. *et al.* Engineered CRISPR-Cas9 nuclease with expanded targeting space.
1175 *Science* **361**, 1259–1262 (2018).
1176 29. Lebensohn, A. M. *et al.* Comparative genetic screens in human cells reveal new
1177 regulatory mechanisms in WNT signaling. *Elife* **5**, e21459 (2016).
1178 30. Carette, J. E. *et al.* Haploid genetic screens in human cells identify host factors used by
1179 pathogens. *Science* **326**, 1231–1235 (2009).
1180 31. Beusch, I. *et al.* Targeted high-throughput mutagenesis of the human spliceosome reveals
1181 its in vivo operating principles. *Mol. Cell* **83**, 2578–2594.e9 (2023).
1182 32. Essletzbichler, P. *et al.* Megabase-scale deletion using CRISPR/Cas9 to generate a fully
1183 haploid human cell line. *Genome Res.* **24**, 2059–2065 (2014).
1184 33. Cerami, E. *et al.* The cBio cancer genomics portal: an open platform for exploring
1185 multidimensional cancer genomics data. *Cancer Discov.* **2**, 401–404 (2012).
1186 34. Groden, J. *et al.* Identification and characterization of the familial adenomatous polyposis
1187 coli gene. *Cell* **66**, 589–600 (1991).
1188 35. Joslyn, G. *et al.* Identification of deletion mutations and three new genes at the familial
1189 polyposis locus. *Cell* **66**, 601–613 (1991).
1190 36. Kinzler, K. W. *et al.* Identification of FAP locus genes from chromosome 5q21. *Science*
1191 **253**, 661–665 (1991).
1192 37. Miyoshi, Y. *et al.* Somatic mutations of the APC gene in colorectal tumors: mutation
1193 cluster region in the APC gene. *Hum. Mol. Genet.* **1**, 229–233 (1992).
1194 38. Miyoshi, Y. *et al.* Germ-line mutations of the APC gene in 53 familial adenomatous
1195 polyposis patients. *Proc. Natl. Acad. Sci. U. S. A.* **89**, 4452–4456 (1992).
1196 39. Miyaki, M. *et al.* Characteristics of somatic mutation of the adenomatous polyposis coli
1197 gene in colorectal tumors. *Cancer Res.* **54**, 3011–3020 (1994).
1198 40. Parsons, M. J., Tammela, T. & Dow, L. E. WNT as a driver and dependency in cancer.
1199 *Cancer Discov.* **11**, 2413–2429 (2021).
1200 41. Rubinfeld, B., Albert, I., Porfiri, E., Munemitsu, S. & Polakis, P. Loss of beta-catenin
1201 regulation by the APC tumor suppressor protein correlates with loss of structure due to
1202 common somatic mutations of the gene. *Cancer Res.* **57**, 4624–4630 (1997).
1203 42. Morin, P. J. *et al.* Activation of beta-catenin-Tcf signaling in colon cancer by mutations in
1204 beta-catenin or APC. *Science* **275**, 1787–1790 (1997).
1205 43. Smits, R. *et al.* Apc1638T: a mouse model delineating critical domains of the
1206 adenomatous polyposis coli protein involved in tumorigenesis and development. *Genes*
1207 *Dev.* **13**, 1309–1321 (1999).
1208 44. Wu, G. *et al.* Structure of a beta-TrCP1-Skp1-beta-catenin complex: destruction motif
1209 binding and lysine specificity of the SCF(beta-TrCP1) ubiquitin ligase. *Mol. Cell* **11**, 1445–
1210 1456 (2003).
1211 45. Huang, S.-M. A. *et al.* Tankyrase inhibition stabilizes axin and antagonizes Wnt signalling.
1212 *Nature* **461**, 614–620 (2009).
1213 46. Xing, Y. *et al.* Crystal structure of a full-length beta-catenin. *Structure* **16**, 478–487 (2008).

1214 47. Huber, A. H., Nelson, W. J. & Weis, W. I. Three-dimensional structure of the armadillo
1215 repeat region of beta-catenin. *Cell* **90**, (1997).
1216 48. Sampietro, J. *et al.* Crystal structure of a beta-catenin/BCL9/Tcf4 complex. *Mol. Cell* **24**,
1217 293–300 (2006).
1218 49. Sun, J. & Weis, W. I. Biochemical and structural characterization of β-catenin interactions
1219 with nonphosphorylated and CK2-phosphorylated Lef-1. *J. Mol. Biol.* **405**, 519–530
1220 (2011).
1221 50. Graham, T. A., Ferkey, D. M., Mao, F., Kimelman, D. & Xu, W. Tcf4 can specifically
1222 recognize beta-catenin using alternative conformations. *Nat. Struct. Biol.* **8**, 1048–1052
1223 (2001).
1224 51. von Kries, J. P. *et al.* Hot spots in beta-catenin for interactions with LEF-1, conductin and
1225 APC. *Nat. Struct. Biol.* **7**, 800–807 (2000).
1226 52. Graham, T. A., Weaver, C., Mao, F., Kimelman, D. & Xu, W. Crystal structure of a beta-
1227 catenin/Tcf complex. *Cell* **103**, 885–896 (2000).
1228 53. Daniels, D. L. & Weis, W. I. ICAT inhibits beta-catenin binding to Tcf/Lef-family
1229 transcription factors and the general coactivator p300 using independent structural
1230 modules. *Mol. Cell* **10**, 573–584 (2002).
1231 54. Eklof Spink, K., Fridman, S. G. & Weis, W. I. Molecular mechanisms of beta-catenin
1232 recognition by adenomatous polyposis coli revealed by the structure of an APC-beta-
1233 catenin complex. *EMBO J.* **20**, 6203–6212 (2001).
1234 55. Xing, Y. *et al.* Crystal structure of a beta-catenin/APC complex reveals a critical role for
1235 APC phosphorylation in APC function. *Mol. Cell* **15**, 523–533 (2004).
1236 56. Graham, T. A., Clements, W. K., Kimelman, D. & Xu, W. The crystal structure of the beta-
1237 catenin/ICAT complex reveals the inhibitory mechanism of ICAT. *Mol. Cell* **10**, 563–571
1238 (2002).
1239 57. Huber, A. H. & Weis, W. I. The structure of the beta-catenin/E-cadherin complex and the
1240 molecular basis of diverse ligand recognition by beta-catenin. *Cell* **105**, 391–402 (2001).
1241 58. Ha, N.-C., Tonozuka, T., Stamos, J. L., Choi, H.-J. & Weis, W. I. Mechanism of
1242 phosphorylation-dependent binding of APC to beta-catenin and its role in beta-catenin
1243 degradation. *Mol. Cell* **15**, 511–521 (2004).
1244 59. Poy, F., Lepourcelet, M., Shivdasani, R. A. & Eck, M. J. Structure of a human Tcf4-beta-
1245 catenin complex. *Nat. Struct. Biol.* **8**, 1053–1057 (2001).
1246 60. Tago, K. *et al.* Inhibition of Wnt signaling by ICAT, a novel beta-catenin-interacting protein.
1247 *Genes Dev.* **14**, 1741–1749 (2000).
1248 61. Li, K. *et al.* De novo mapping of α-helix recognition sites on protein surfaces using
1249 unbiased libraries. *Proc. Natl. Acad. Sci. U. S. A.* **119**, e2210435119 (2022).
1250 62. Fiedler, M., Mendoza-Topaz, C., Rutherford, T. J., Mieszczanek, J. & Bienz, M.
1251 Dishevelled interacts with the DIX domain polymerization interface of Axin to interfere with
1252 its function in down-regulating β-catenin. *Proc. Natl. Acad. Sci. U. S. A.* **108**, 1937–1942
1253 (2011).
1254 63. Sakanaka, C. & Williams, L. T. Functional domains of axin. Importance of the C terminus
1255 as an oligomerization domain. *J. Biol. Chem.* **274**, 14090–14093 (1999).
1256 64. Hsu, W., Zeng, L. & Costantini, F. Identification of a domain of Axin that binds to the
1257 serine/threonine protein phosphatase 2A and a self-binding domain. *J. Biol. Chem.* **274**,
1258 3439–3445 (1999).

1259 65. Kishida, S. *et al.* DIX domains of Dvl and axin are necessary for protein interactions and
1260 their ability to regulate beta-catenin stability. *Mol. Cell. Biol.* **19**, 4414–4422 (1999).
1261 66. Smalley, M. J. *et al.* Interaction of axin and Dvl-2 proteins regulates Dvl-2-stimulated TCF-
1262 dependent transcription. *EMBO J.* **18**, 2823–2835 (1999).
1263 67. Yamanishi, K. *et al.* A direct heterotypic interaction between the DIX domains of
1264 Dishevelled and Axin mediates signaling to β-catenin. *Sci. Signal.* **12**, eaaw5505 (2019).
1265 68. Morrone, S., Cheng, Z., Moon, R. T., Cong, F. & Xu, W. Crystal structure of a Tankyrase-
1266 Axin complex and its implications for Axin turnover and Tankyrase substrate recruitment.
1267 *Proc. Natl. Acad. Sci. U. S. A.* **109**, 1500–1505 (2012).
1268 69. Grossmann, T. N. *et al.* Inhibition of oncogenic Wnt signaling through direct targeting of β-
1269 catenin. *Proc. Natl. Acad. Sci. U. S. A.* **109**, 17942–17947 (2012).
1270 70. Yeste-Vázquez, A. *et al.* Structure-based design of bicyclic helical peptides that target the
1271 oncogene β-catenin. *Angew. Chem. Int. Ed Engl.* **63**, e202411749 (2024).
1272 71. Xing, Y., Clements, W. K., Kimelman, D. & Xu, W. Crystal structure of a beta-catenin/axin
1273 complex suggests a mechanism for the beta-catenin destruction complex. *Genes Dev.* **17**,
1274 2753–2764 (2003).
1275 72. Ji, L. *et al.* Identification of ICAT as an APC Inhibitor, Revealing Wnt-Dependent Inhibition
1276 of APC-Axin Interaction. *Mol. Cell* **72**, 37–47.e4 (2018).
1277 73. Yan, D. *et al.* Elevated expression of axin2 and hnkd mRNA provides evidence that
1278 Wnt/beta -catenin signaling is activated in human colon tumors. *Proc. Natl. Acad. Sci. U.*
1279 *S. A.* **98**, 14973–14978 (2001).
1280 74. Albuquerque, C. *et al.* The 'just-right' signaling model: APC somatic mutations are
1281 selected based on a specific level of activation of the beta-catenin signaling cascade.
1282 *Hum. Mol. Genet.* **11**, 1549–1560 (2002).
1283 75. Chang, L. *et al.* Systematic profiling of conditional pathway activation identifies context-
1284 dependent synthetic lethalities. *Nat. Genet.* **55**, 1709–1720 (2023).
1285 76. Beigl, T. B., Kjosås, I., Seljeseth, E., Glomnes, N. & Aksnes, H. Efficient and crucial
1286 quality control of HAP1 cell ploidy status. *Biol. Open* **9**, bio057174 (2020).
1287 77. Fuerer, C. & Nusse, R. Lentiviral vectors to probe and manipulate the Wnt signaling
1288 pathway. *PLoS One* **5**, e9370 (2010).
1289 78. Gaidatzis, D., Lerch, A., Hahne, F. & Stadler, M. B. QuasR: quantification and annotation
1290 of short reads in R. *Bioinformatics* **31**, 1130–1132 (2015).
1291 79. Liao, Y., Smyth, G. K. & Shi, W. The R package Rsubread is easier, faster, cheaper and
1292 better for alignment and quantification of RNA sequencing reads. *Nucleic Acids Res.* **47**,
1293 e47 (2019).
1294 80. Lawrence, M. *et al.* Software for computing and annotating genomic ranges. *PLoS*
1295 *Comput. Biol.* **9**, e1003118 (2013).
1296 81. Clement, K. *et al.* CRISPResso2 provides accurate and rapid genome editing sequence
1297 analysis. *Nat. Biotechnol.* **37**, 224–226 (2019).
1298 82. Lingeman, E., Jeans, C. & Corn, J. E. Production of Purified CasRNPs for Efficacious
1299 Genome Editing. *Curr. Protoc. Mol. Biol.* **120**, 31.10.1–31.10.19 (2017).
1300 83. Stirling, D. R. *et al.* CellProfiler 4: improvements in speed, utility and usability. *BMC*
1301 *Bioinformatics* **22**, 433 (2021).
1302 84. Abramson, J. *et al.* Accurate structure prediction of biomolecular interactions with
1303 AlphaFold 3. *Nature* **630**, 493–500 (2024).

Extended Data Fig.1

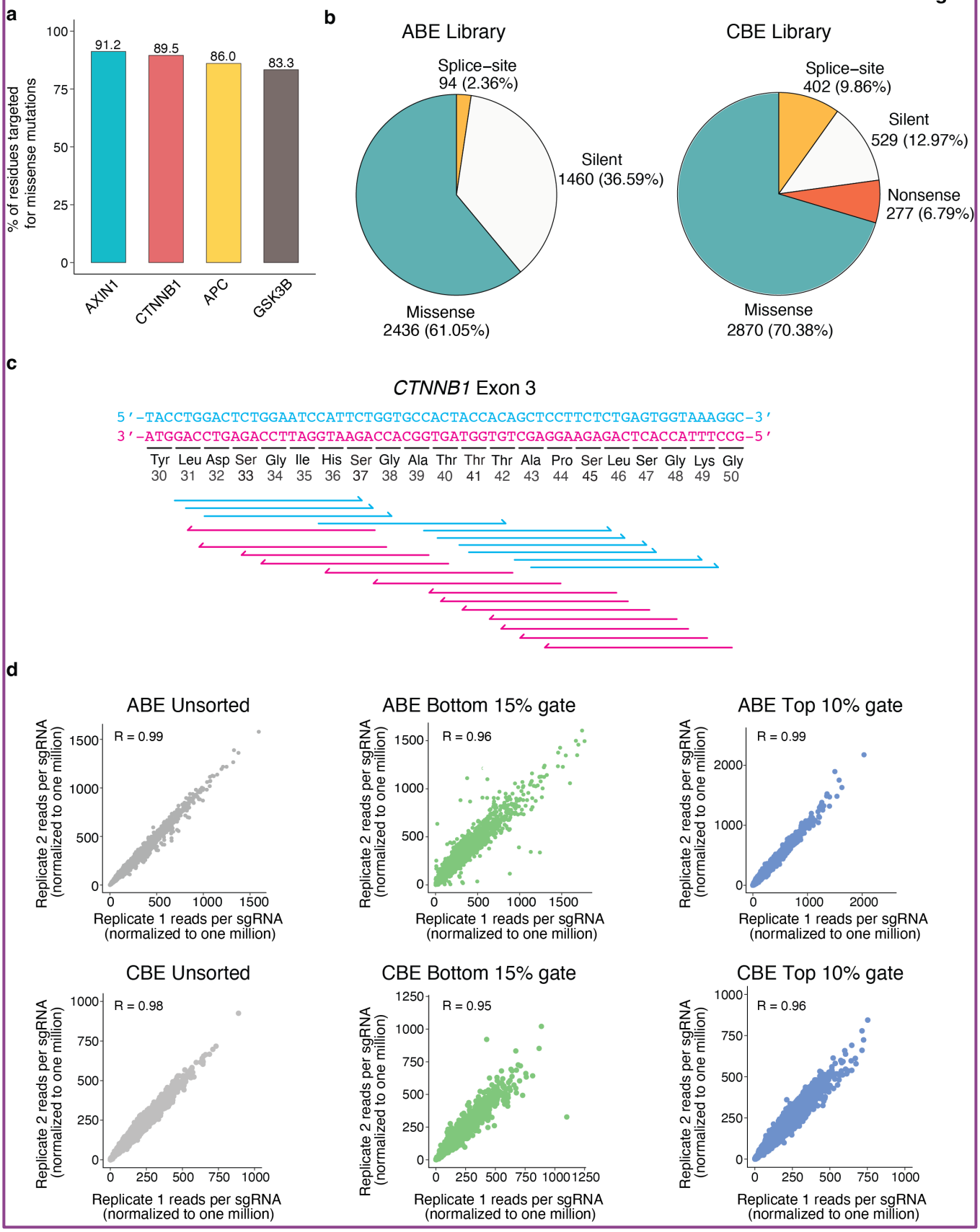

1304

1305

Extended Data Fig. 1. Design and quality control of ABE and CBE base editing screens targeting the β-catenin destruction complex (BDC). a, Bar graph summarizing the percent of amino acids in each BDC component predicted (i.e. located within the N3-N10 region of the protospacer) to be changed to a different amino acid by at least one sgRNA in our ABE and CBE libraries. **b,** Predicted proportion of missense, nonsense, silent, and splice-site mutations generated by the ABE (left) and CBE (right) libraries. Note that only CBE sgRNAs are predicted to generate nonsense mutations. **c,** The tiling nature of base editing libraries is illustrated using Exon 3 of *CTNNB1*. Arrows below the exon sequence show the position of sgRNA sequences, colored according to whether they hybridize to the top strand (red guides) or bottom strand (blue guides). Note that each codon in the exon is often targeted by multiple sgRNAs. **d,** Scatter plots showing the correlation of sgRNA read counts (per million total reads) between the two biological replicates for each of the six screens.
See also Supplementary Table 1

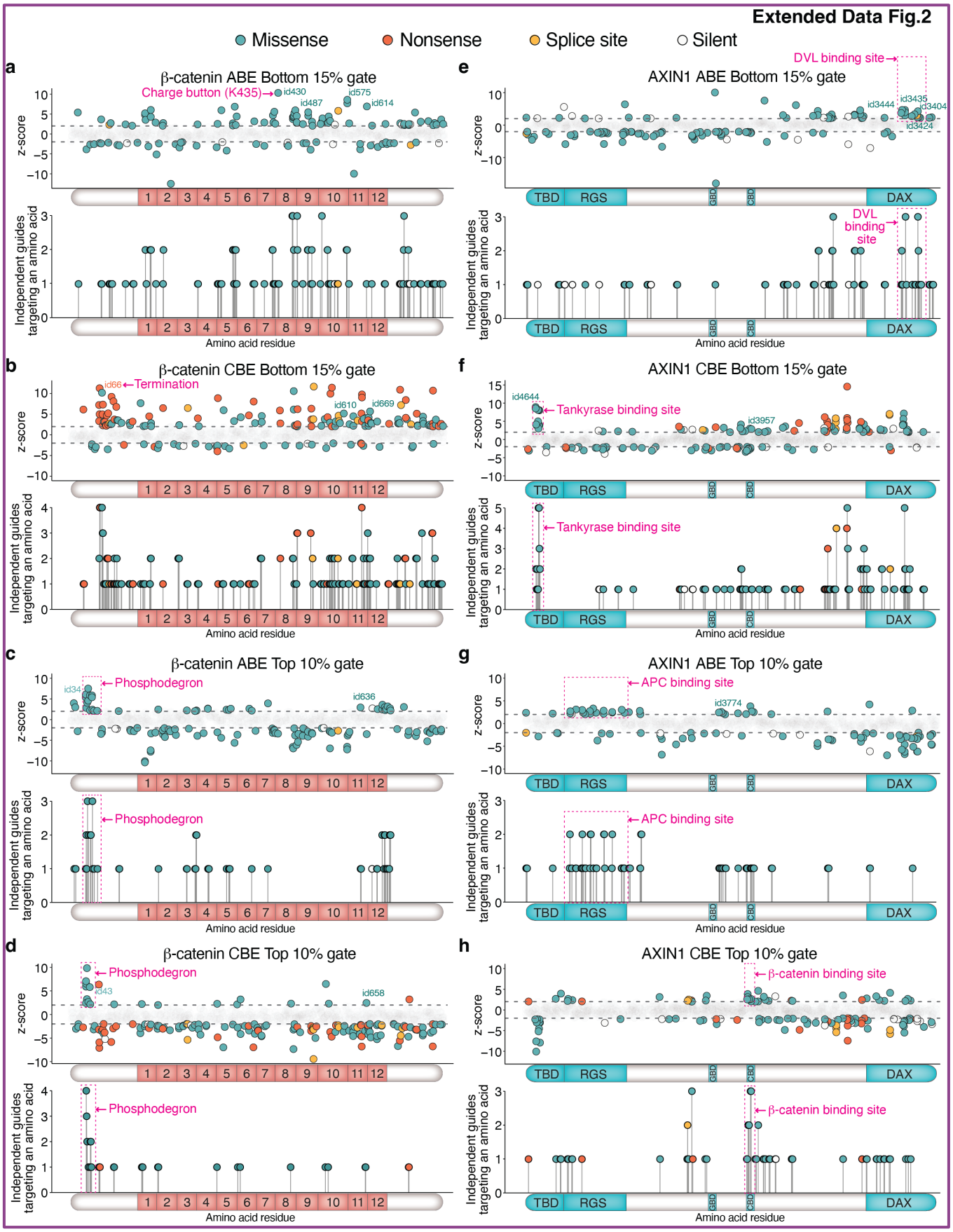
Extended Data Fig.2
Missense
Nonsense
Splice site
Silent
a
β-catenin ABE Bottom 15% gate
Charge button (K435)
id430
id487
id575
id614
b
β-catenin CBE Bottom 15% gate
id66
Termination
id610
id669
c
β-catenin ABE Top 10% gate
id34
Phosphodegron
id636
d
β-catenin CBE Top 10% gate
Phosphodegron
id43
id658
e
AXIN1 ABE Bottom 15% gate
DVL binding site
id3444
id3435
id3404
id3424
f
AXIN1 CBE Bottom 15% gate
id4644
Tankyrase binding site
id3957
g
AXIN1 ABE Top 10% gate
APC binding site
id3774
h
AXIN1 CBE Top 10% gate
β-catenin binding site
z-score
Independent guides targeting an amino acid
Amino acid residue
TBD
RGS
GBD
CBD
DAX

1306

1307

Extended Data Fig. 2. Sequence-function landscape of β-catenin and AXIN1 as mapped by tiled base editing screens. Each of the individual panels (**a-h**) show the position of all sgRNAs targeting the indicated protein using a z-score plot (top) and a lollipop plot (bottom). In the z-score plots, each sgRNA (represented by a point) is plotted based on its z-score for enrichment in the specified gate used for sorting (**Fig.1d**) on the y-axis and its amino acid position on the x-axis. For sgRNAs predicted to make multiple mutations, the most N-terminal residue is used as the position. A positive z-scores denotes enrichment in the indicated sorting gate; a negative z-score denotes depletion. sgRNAs with z-scores > 2 or < -2 (the criteria we used for statistical significance and follow-up) are shown as solid dots colored according to the type of predicted mutation (legend provided at the top of the figure). The target zone for each sgRNA was considered to span N3-N10 in its protospacer sequence. sgRNAs with -2< *z*-scores <2 are shown as faded dots and considered non-significant. In the lollipop plots, the y-axis represents the number of sgRNAs with z-scores ≥ 2 predicted to target a specific amino acid. In cases where an sgRNA was predicted to generate both missense and nonsense mutations, only the nonsense mutation is plotted. In all panels, magenta arrows and dotted squares point to known functional regions of the protein involved in key regulatory PTMs (e.g. the β-catenin phosphodegron) or PPIs. **a,b,** *z*-score and lollipop plots for β-catenin sgRNAs in the Bottom 15% gate (used to isolate mutant cells with reduced WNT/β-catenin signaling strength) from adenine (**a**, ABE) and cytosine (**b**, CBE) base editor screens. **c,d,** *z*-score and lollipop plots for β-catenin sgRNAs in the Top 10% gate (used to isolate mutant cells with elevated WNT/β-catenin signaling strength) from adenine (**c**, ABE) and cytosine (**d**, CBE) base editor screens. **e,f,** *z*-score and lollipop plots for AXIN1 sgRNAs in the Bottom 15% gate (used to isolate mutant cells with reduced WNT/β-catenin signaling strength) from adenine (**e**, ABE) and cytosine (**f**, CBE) base editor screens. **g,h,** *z*-score and lollipop plots for AXIN1 sgRNAs in the Top 10% gate (used to isolate mutant cells with elevated WNT/β-catenin signaling strength) from adenine (**g**, ABE) and cytosine (**h**, CBE) base editor screens.
See also Supplementary Table 1

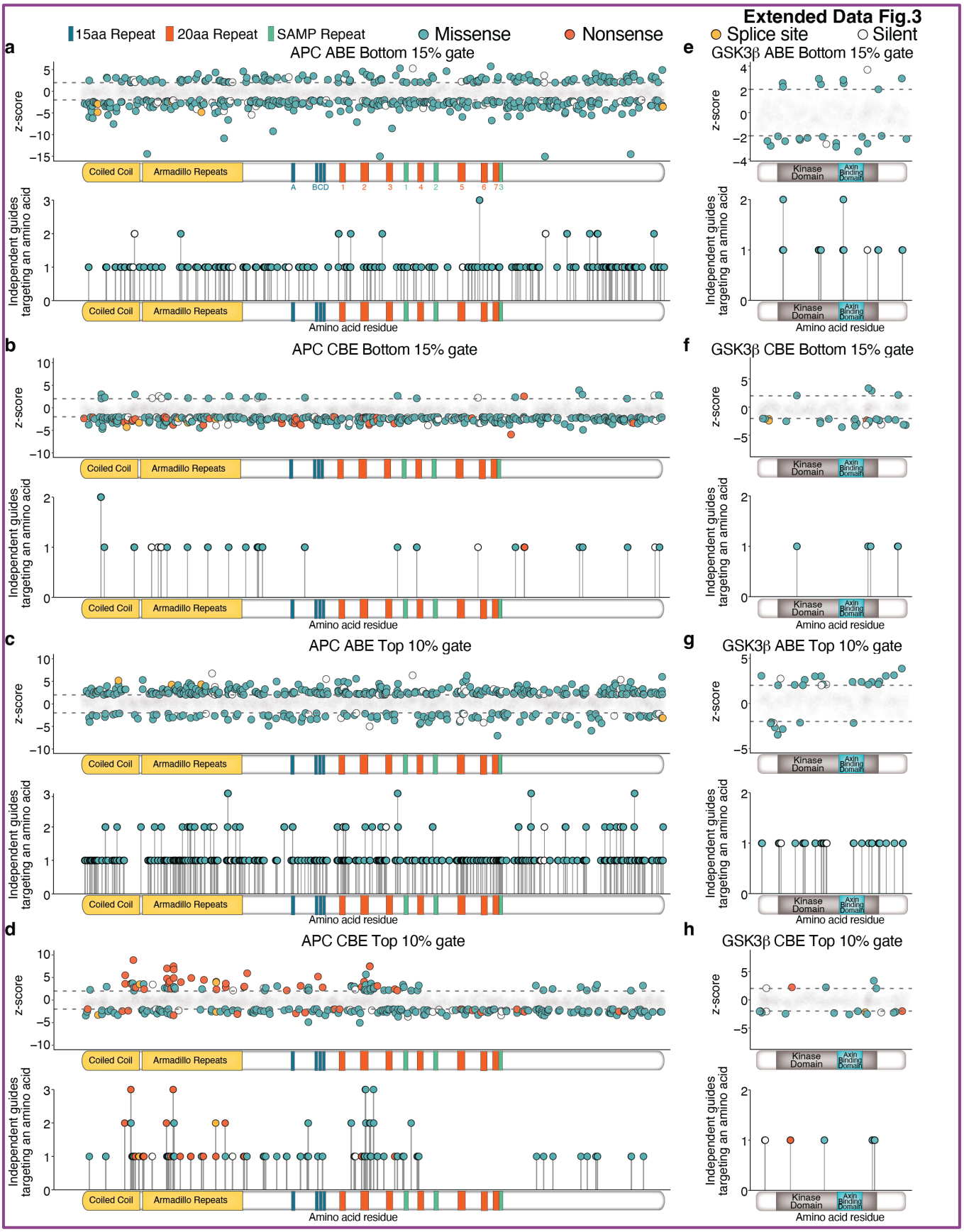
Extended Data Fig.3
15aa Repeat
20aa Repeat
SAMP Repeat
Missense
Nonsense
Splice site
Silent
a
APC ABE Bottom 15% gate
b
APC CBE Bottom 15% gate
c
APC ABE Top 10% gate
d
APC CBE Top 10% gate
e
GSK3β ABE Bottom 15% gate
f
GSK3β CBE Bottom 15% gate
g
GSK3β ABE Top 10% gate
h
GSK3β CBE Top 10% gate
z-score
Independent guides targeting an amino acid
Coiled Coil
Armadillo Repeats
Kinase Domain
Axin Binding Domain
Amino acid residue

1308

1309

Extended Data Fig. 3. Sequence-function landscape of APC and GSK3β as mapped by tiled base editing screens. Each of the individual panels (**a-h**) show the position of all sgRNAs targeting the indicated protein using a z-score plot (top) and a lollipop plot (bottom). In the z-score plots, each sgRNA (represented by a point) is plotted based on its z-score for enrichment in the specified gate used for sorting (**Fig.1d**) on the y-axis and its amino acid position on the x-axis. A positive z-scores denotes enrichment in the indicated sorting gate; a negative z-score denotes depletion. sgRNAs with z-scores < 2 or < -2 (the criteria we used for statistical significance and follow-up) are shown as solid dots colored according to the type of predicted mutation (legend provided at the top of the figure). The target zone for each sgRNA was considered to span N3-N10 in its protospacer sequence. sgRNAs with -2< *z*-scores <2 are shown as faded dots and considered non-significant. In the lollipop plots, the y-axis represents the number of sgRNAs with z-scores ≥ 2 predicted to target a specific amino acid. In cases where an sgRNA was predicted to generate both missense and nonsense mutations, only the nonsense mutation is plotted. **a,b,** *z*-score and lollipop plots for APC sgRNAs in the Bottom 15% gate (used to isolate mutant cells with reduced WNT/β-catenin signaling strength) from adenine (**a**, ABE) and cytosine (**b**, CBE) base editor screens. **c,d,** *z*-score and lollipop plots for APC sgRNAs in the Top 10% gate (used to isolate mutant cells with elevated WNT/β-catenin signaling strength) from adenine (**c**, ABE) and cytosine (**d**, CBE) base editor screens. **e,f,** *z*-score and lollipop plots for GSK3β sgRNAs in the Bottom 15% gate (used to isolate mutant cells with reduced WNT/β-catenin signaling strength) from adenine (**e**, ABE) and cytosine (**f**, CBE) base editor screens. **g,h,** *z*-score and lollipop plots for GSK3β sgRNAs in the Top 10% gate (used to isolate mutant cells with elevated WNT/β-catenin signaling strength) from adenine (**g**, ABE) and cytosine (**h**, CBE) base editor screens.

See also Supplementary Table 1

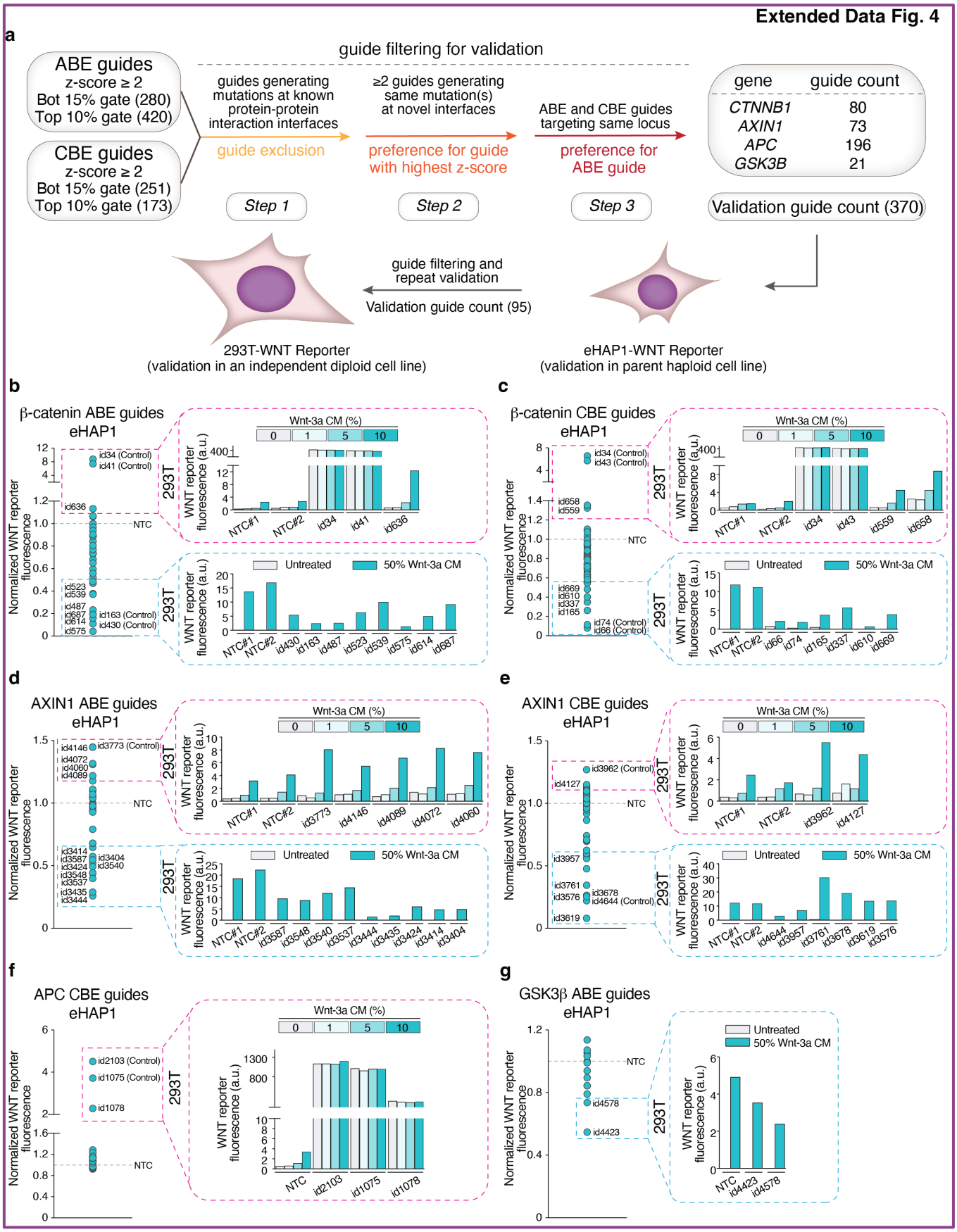
Extended Data Fig. 4
a
guide filtering for validation
ABE guides
z-score ≥ 2
Bot 15% gate (280)
Top 10% gate (420)
CBE guides
z-score ≥ 2
Bot 15% gate (251)
Top 10% gate (173)
guides generating mutations at known protein-protein interaction interfaces
guide exclusion
≥2 guides generating same mutation(s) at novel interfaces
preference for guide with highest z-score
ABE and CBE guides targeting same locus
preference for ABE guide
gene
guide count
CTNNB1 80
AXIN1 73
APC 196
GSK3B 21
Step 1
Step 2
Step 3
Validation guide count (370)
guide filtering and repeat validation
Validation guide count (95)
293T-WNT Reporter
(validation in an independent diploid cell line)
eHAP1-WNT Reporter
(validation in parent haploid cell line)
b
β-catenin ABE guides
eHAP1
c
β-catenin CBE guides
eHAP1
d
AXIN1 ABE guides
eHAP1
e
AXIN1 CBE guides
eHAP1
f
APC CBE guides
eHAP1
g
GSK3β ABE guides
eHAP1
Normalized WNT reporter fluorescence
WNT reporter fluorescence (a.u.)
Wnt-3a CM (%)
0
1
5
10
293T
NTC
Untreated
50% Wnt-3a CM

1310

1311

Extended Data Fig. 4. Validation strategy for hits from base editing screens. a, Outline of filtering and validation pipeline for sgRNAs with *z*-scores ≥ 2. After excluding most sgRNAs predicted to direct mutations at known PPI interfaces, remaining sgRNAs were individually introduced into eHAP1-7TS and HEK293T-7TS cells and WNT/β-catenin signaling strength assessed using the 7TS reporter. **b,c,** Validation of β-catenin sgRNAs from the ABE (**b**) and CBE (**c**) screens in both eHAP1-7TS and HEK293T-7TS reporter cells. sgRNAs were first tested for WNT/β-catenin signaling effects in eHAP1-7TS cells. Those that significantly increased (dotted magenta box) or decreased (dotted cyan box) reporter activity relative to non-targeting control sgRNA (NTC) were then retested in HEK293T-7TS cells (magenta and cyan insets). **d,e,** Validation of AXIN1 sgRNAs from the ABE (**d**) and CBE (**e**) screens, depicted like the β-catenin validation in **b** and **c**. **f,g,** Validation of *APC* sgRNAs from the CBE screen (**f**) and GSK3β sgRNAs from the ABE screen in both cell lines. eHAP1-7TS cells were treated with 25% Wnt-3a conditioned media (24h) before measuring 7TS reporter activity by flow cytometry. HEK293T-7TS cells carrying sgRNAs that decreased 7TS reporter activity were treated with 25% Wnt-3a conditioned media (24h). HEK293T-7TS cells carrying sgRNAs that increased 7TS reporter activity were treated (24h) with an increasing concentration of Wnt-3a conditioned medium (as shown in the magenta insets). All validated sgRNAs had directionally similar effects in both cell lines, except for AXIN1 CBE guides in panel **e** (ids: 3761, 3678, 3619, 3576), which were eliminated from consideration.
See also Supplementary Table 2.

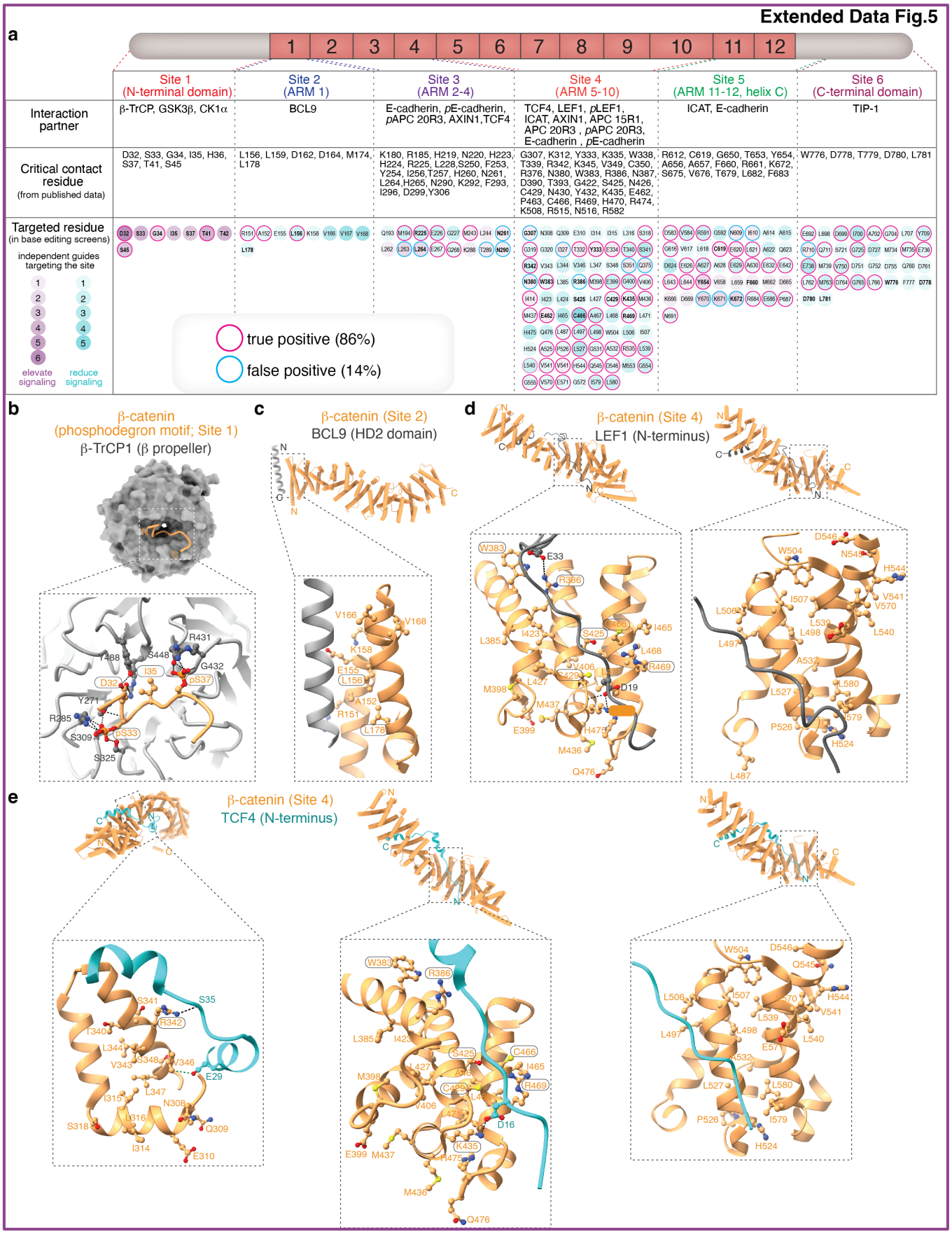
Extended Data Fig.5
a
1 2 3 4 5 6 7 8 9 10 11 12
Site 1 (N-terminal domain)
Site 2 (ARM 1)
Site 3 (ARM 2-4)
Site 4 (ARM 5-10)
Site 5 (ARM 11-12, helix C)
Site 6 (C-terminal domain)
Interaction partner
β-TrCP, GSK3β, CK1α
BCL9
E-cadherin, pE-cadherin, pAPC 20R3, AXIN1,TCF4
TCF4, LEF1, pLEF1, ICAT, AXIN1, APC 15R1, APC 20R3 , pAPC 20R3, E-cadherin , pE-cadherin
ICAT, E-cadherin
TIP-1
Critical contact residue (from published data)
D32, S33, G34, I35, H36, S37, T41, S45
L156, L159, D162, D164, M174, L178
K180, R185, H219, N220, H223, H224, R225, L228,S250, F253, Y254, I256,T257, H260, N261, L264,H265, N290, K292, F293, I296, D299,Y306
G307, K312, Y333, K335, W338, T339, R342, K345, V349, C350, R376, N380, W383, R386, N387, D390, T393, G422, S425, N426, C429, N430, Y432, K435, E462, P463, C466, R469, H470, R474, K508, R515, N516, R582
R612, C619, G650, T653, Y654, A656, A657, F660, R661, R672, S675, V676, T679, L682, F683
W776, D778, T779, D780, L781
Targeted residue (in base editing screens)
independent guides targeting the site
elevate signaling
reduce signaling
true positive (86%)
false positive (14%)
b
β-catenin (phosphodegron motif; Site 1)
β-TrCP1 (β propeller)
c
β-catenin (Site 2)
BCL9 (HD2 domain)
d
β-catenin (Site 4)
LEF1 (N-terminus)
e
β-catenin (Site 4)
TCF4 (N-terminus)

1312

1313

Extended Data Fig. 5. Validation of sgRNAs targeting β-catenin. a, Linear cartoon of β-catenin showing its 12 ARM repeats that form an extended ARM superhelix (see **Fig.2a**). An aligned table below shows the boundaries of Sites 1-6, known interaction partners at each Site (Row 1), β-catenin amino acids residues identified as playing a functional role at PPI interfaces in prior structural or biochemical studies (Row 2), and amino acid residues located in the N3-N10 segment of the protospacers of sgRNAs with a *z*-score ≥ 2 in our base editing screens (Row 3). Screen-identified residues are encircled by a dot colored teal for guides that reduce signaling and purple for guides that elevate signaling. The purple or teal shading intensity reflects the number of different sgRNAs predicted to target that amino acid residue (see scale in left-most column). Color of the ring surrounding each dot denotes whether it was a true positive (magenta) or false positive (blue) based on validation studies (**Extended Data Fig.4)**; dots without a surrounding ring were not validated. Bold lettering denotes amino-acid residues that have been implicated in β-catenin function in a prior publication (e.g. the charge button K435). **b**, Structural model of the complex between the β-catenin phosphodegron motif (PDB 2Z6H, sandy brown) and the beta-propeller domain of β-TrCP1 (PDB 1P22, dark grey)[44]. In the zoomed view, side chains of β-catenin residues targeted by sgRNAs that elevate WNT/β-catenin signaling (i.e. enriched in the Top 10% gate) are shown in ball-and-stick representation. **c**, Structural model of the complex between β-catenin (PDB 2Z6H, sandy brown) and the BCL9 HD2 domain (PDB 2GL7, dark grey)[48]. In the zoomed view, side chains of β-catenin residues targeted by sgRNAs that reduce WNT/β-catenin signaling (i.e. enriched in the Bottom 15% gate) are shown in ball-and-stick representation. **d**, Structural model of the complex between β-catenin (PDB 2Z6H, sandy brown) and the N-terminus of LEF1 (PDB 3OUX, dark grey)[49]. In the zoomed view, side chains of β-catenin residues targeted by sgRNAs that reduce WNT/β-catenin signaling (i.e. enriched in the Bottom 15% gate) are shown in ball-and-stick representation. **e**, Structural model of the complex between β-catenin (PDB 2Z6H, sandy brown) and the N-terminus of TCF4 (1JDH, blue)[50]. Zoomed views are used to show three different regions of this extended interaction interface. Side chains of β-catenin residues targeted by sgRNAs that reduce WNT/β-catenin signaling (i.e. enriched in the Bottom 15% gate) are shown in ball-and-stick representation.

Residues numbers circled by a rounded rectangle have been implicated in β-catenin function in prior structural or biochemical studies. Side chains of the partner proteins (β-TRCP, LEF1 or TCF4) are shown if they make a predicted contact with β-catenin. Dashed black lines show putative electrostatic interactions.

See also Supplementary Table 2.

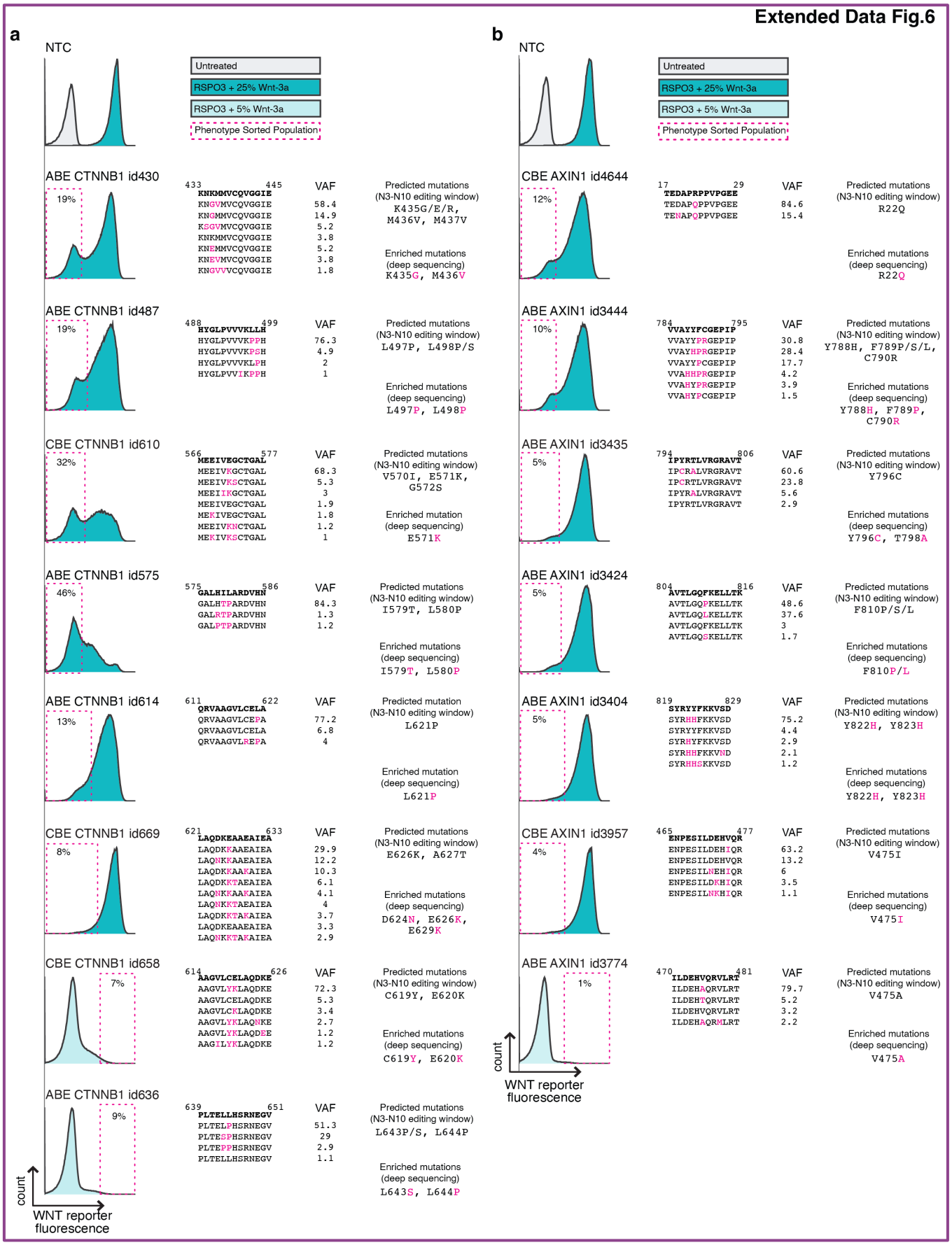
Extended Data Fig.6
a
NTC
Untreated
RSPO3 + 25% Wnt-3a
RSPO3 + 5% Wnt-3a
Phenotype Sorted Population
ABE CTNNB1 id430
19%
433 445 VAF
KNKMMVCQVGGIE
KNGVMVCQVGGIE 58.4
KNGMMVCQVGGIE 14.9
KSGVMVCQVGGIE 5.2
KNKMMVCQVGGIE 3.8
KNEMMVCQVGGIE 5.2
KNEVMVCQVGGIE 3.8
KNGVVVCQVGGIE 1.8
Predicted mutations (N3-N10 editing window) K435G/E/R, M436V, M437V
Enriched mutations (deep sequencing) K435G, M436V
ABE CTNNB1 id487
19%
488 499 VAF
HYGLPVVVKLLH
HYGLPVVVKPPH 76.3
HYGLPVVVKPSH 4.9
HYGLPVVVKLPH 2
HYGLPVVIKPPH 1
Predicted mutations (N3-N10 editing window) L497P, L498P/S
Enriched mutations (deep sequencing) L497P, L498P
CBE CTNNB1 id610
32%
566 577 VAF
MEEIVEGCTGAL
MEEIVKGCTGAL 68.3
MEEIVKSCTGAL 5.3
MEEIIKGCTGAL 3
MEEIVEGCTGAL 1.9
MEKIVEGCTGAL 1.8
MEEIVKNCTGAL 1.2
MEKIVKSCTGAL 1
Predicted mutations (N3-N10 editing window) V570I, E571K, G572S
Enriched mutation (deep sequencing) E571K
ABE CTNNB1 id575
46%
575 586 VAF
GALHILARDVHN
GALHTPARDVHN 84.3
GALRTPARDVHN 1.3
GALPTPARDVHN 1.2
Predicted mutations (N3-N10 editing window) I579T, L580P
Enriched mutations (deep sequencing) I579T, L580P
ABE CTNNB1 id614
13%
611 622 VAF
QRVAAGVLCELA
QRVAAGVLCEPA 77.2
QRVAAGVLCELA 6.8
QRVAAGVLREPA 4
Predicted mutation (N3-N10 editing window) L621P
Enriched mutation (deep sequencing) L621P
CBE CTNNB1 id669
8%
621 633 VAF
LAQDKEAAEAIEA
LAQDKKAAEAIEA 29.9
LAQNKKAAEAIEA 12.2
LAQDKKAAKAIEA 10.3
LAQDKKTAEAIEA 6.1
LAQNKKAAKAIEA 4.1
LAQNKKTAEAIEA 4
LAQDKKTAKAIEA 3.7
LAQDKEAAEAIEA 3.3
LAQNKKTAKAIEA 2.9
Predicted mutations (N3-N10 editing window) E626K, A627T
Enriched mutations (deep sequencing) D624N, E626K, E629K
CBE CTNNB1 id658
7%
614 626 VAF
AAGVLCELAQDKE
AAGVLYKLAQDKE 72.3
AAGVLCELAQDKE 5.3
AAGVLCKLAQDKE 3.4
AAGVLYKLAQNKE 2.7
AAGVLYKLAQDEE 1.2
AAGILYKLAQDKE 1.2
Predicted mutations (N3-N10 editing window) C619Y, E620K
Enriched mutations (deep sequencing) C619Y, E620K
ABE CTNNB1 id636
9%
639 651 VAF
PLTELLHSRNEGV
PLTELPHSRNEGV 51.3
PLTESPHSRNEGV 29
PLTEPPHSRNEGV 2.9
PLTELLHSRNEGV 1.1
Predicted mutations (N3-N10 editing window) L643P/S, L644P
Enriched mutations (deep sequencing) L643S, L644P
count
WNT reporter fluorescence
b
NTC
Untreated
RSPO3 + 25% Wnt-3a
RSPO3 + 5% Wnt-3a
Phenotype Sorted Population
CBE AXIN1 id4644
12%
17 29 VAF
TEDAPRPPVPGEE
TEDAPQPPVPGEE 84.6
TENAPQPPVPGEE 15.4
Predicted mutations (N3-N10 editing window) R22Q
Enriched mutations (deep sequencing) R22Q
ABE AXIN1 id3444
10%
784 795 VAF
VVAYYFCGEPIP
VVAYYPRGEPIP 30.8
VVAYHPRGEPIP 28.4
VVAYYPCGEPIP 17.7
VVAHHPRGEPIP 4.2
VVAHYPRGEPIP 3.9
VVAHYPCGEPIP 1.5
Predicted mutations (N3-N10 editing window) Y788H, F789P/S/L, C790R
Enriched mutations (deep sequencing) Y788H, F789P, C790R
ABE AXIN1 id3435
5%
794 806 VAF
IPYRTLVRGRAVT
IPCRALVRGRAVT 60.6
IPCRTLVRGRAVT 23.8
IPYRALVRGRAVT 5.6
IPYRTLVRGRAVT 2.9
Predicted mutations (N3-N10 editing window) Y796C
Enriched mutations (deep sequencing) Y796C, T798A
ABE AXIN1 id3424
5%
804 816 VAF
AVTLGQFKELLTK
AVTLGQPKELLTK 48.6
AVTLGQLKELLTK 37.6
AVTLGQFKELLTK 3
AVTLGQSKELLTK 1.7
Predicted mutations (N3-N10 editing window) F810P/S/L
Enriched mutations (deep sequencing) F810P/L
ABE AXIN1 id3404
5%
819 829 VAF
SYRYYFKKVSD
SYRHHFKKVSD 75.2
SYRYYFKKVSD 4.4
SYRHYFKKVSD 2.9
SYRHHFKKVND 2.1
SYRHHSKKVSD 1.2
Predicted mutations (N3-N10 editing window) Y822H, Y823H
Enriched mutations (deep sequencing) Y822H, Y823H
CBE AXIN1 id3957
4%
465 477 VAF
ENPESILDEHVQR
ENPESILDEHIQR 63.2
ENPESILDEHVQR 13.2
ENPESILNEHIQR 6
ENPESILDKHIQR 3.5
ENPESILNKHIQR 1.1
Predicted mutations (N3-N10 editing window) V475I
Enriched mutations (deep sequencing) V475I
ABE AXIN1 id3774
1%
470 481 VAF
ILDEHVQRVLRT
ILDEHAQRVLRT 79.7
ILDEHTQRVLRT 5.2
ILDEHVQRVLRT 3.2
ILDEHAQRMLRT 2.2
Predicted mutations (N3-N10 editing window) V475A
Enriched mutations (deep sequencing) V475A
count
WNT reporter fluorescence

1314

1315

Extended Data Fig. 6. Illumina sequencing strategy to identify sgRNA directed mutations in HEK293T-7TS cells used for mechanistic studies. This figure outlines the strategy for FACS-based enrichment and deep sequencing of base-edited HEK293T-7TS cells. Approximately 1 million cells transfected with pRDA plasmids encoding listed sgRNAs were sorted, expanded, and then subjected to deep sequencing of the targeted locus. **a**, FACS gates (indicated by a dotted magenta rectangle) are shown for cells transfected with sgRNAs targeting *CTNNB1*. Cells were treated with a high dose of ligand (RSPO3 + 25% Wnt-3a conditioned medium) to sort for mutants with reduced WNT reporter fluorescence, or a low dose (RSPO3 + 5% Wnt-3a conditioned medium) to sort for mutants with elevated WNT reporter fluorescence. The right panel shows the predicted mutations in the N3-N10 protospacer window and the measured frequencies of various alleles in the sorted cells (variant allele frequency or VAF). **b**, The same FACS gating strategy is shown for pooled AXIN1 base-edited cell lines.
See also Supplementary Table 3.

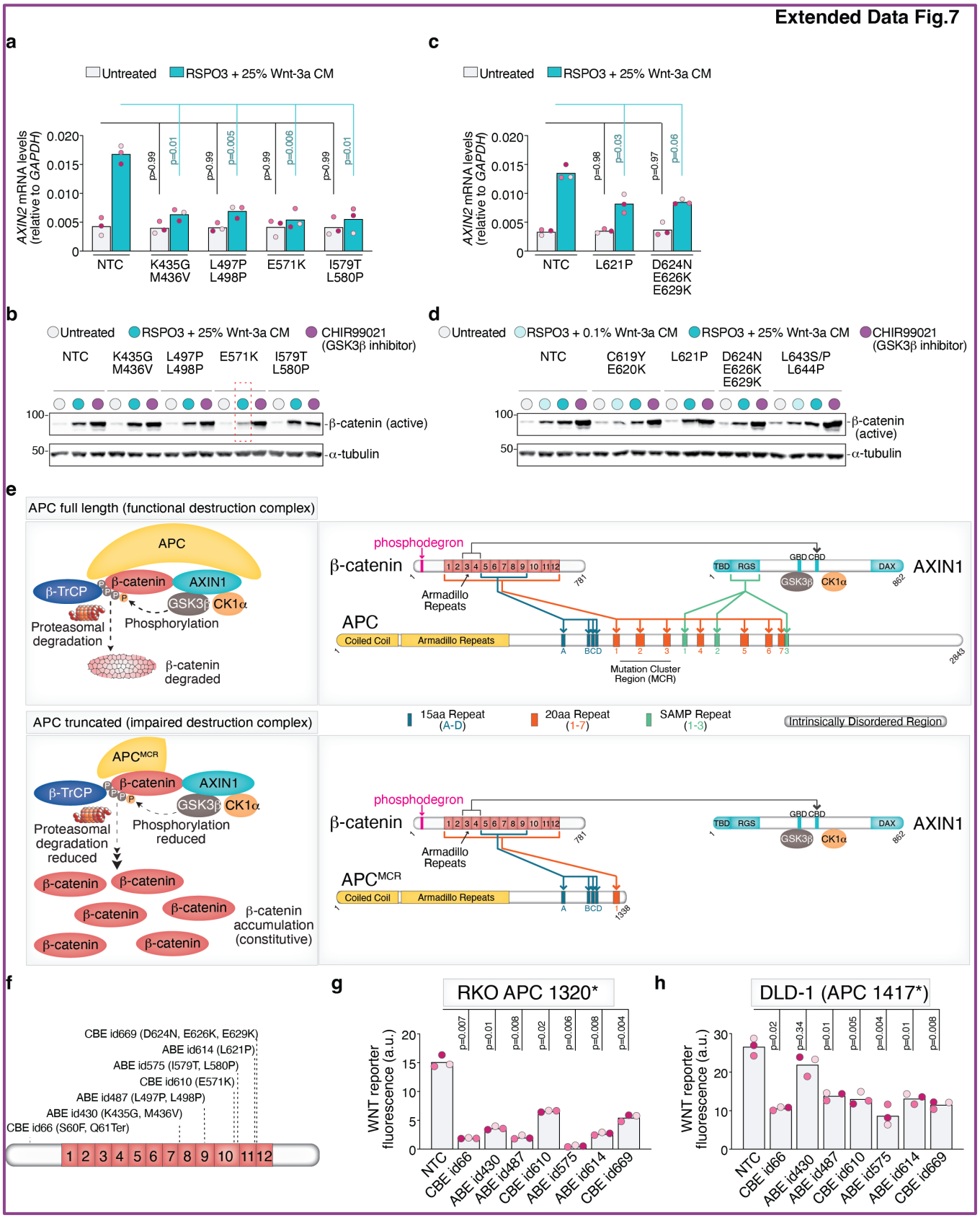
Extended Data Fig.7
a
Untreated
RSPO3 + 25% Wnt-3a CM
AXIN2 mRNA levels (relative to GAPDH)
NTC
K435G M436V
L497P L498P
E571K
I579T L580P
p>0.99
p=0.01
p=0.005
p=0.006
c
L621P
D624N E626K E629K
p=0.98
p=0.03
p=0.97
p=0.06
b
CHIR99021 (GSK3β inhibitor)
β-catenin (active)
α-tubulin
d
RSPO3 + 0.1% Wnt-3a CM
C619Y E620K
L643S/P L644P
e
APC full length (functional destruction complex)
APC
β-TrCP
β-catenin
AXIN1
GSK3β
CK1α
Proteasomal degradation
Phosphorylation
β-catenin degraded
phosphodegron
Armadillo Repeats
Coiled Coil
Mutation Cluster Region (MCR)
TBD
RGS
GBD
CBD
DAX
APC truncated (impaired destruction complex)
APCMCR
Proteasomal degradation reduced
Phosphorylation reduced
β-catenin accumulation (constitutive)
15aa Repeat (A-D)
20aa Repeat (1-7)
SAMP Repeat (1-3)
Intrinsically Disordered Region
f
CBE id669 (D624N, E626K, E629K)
ABE id614 (L621P)
ABE id575 (I579T, L580P)
CBE id610 (E571K)
ABE id487 (L497P, L498P)
ABE id430 (K435G, M436V)
CBE id66 (S60F, Q61Ter)
g
RKO APC 1320*
WNT reporter fluorescence (a.u.)
NTC
CBE id66
ABE id430
ABE id487
CBE id610
ABE id575
ABE id614
CBE id669
h
DLD-1 (APC 1417*)

1316

1317

Extended Data Fig. 7. Functional analysis of screen-identified mutations in β-catenin across assays and cell lines. This figure provides supporting data for **Fig. 3** and **Fig. 4**. As an alternative to the synthetic 7TS fluorescent transcriptional reporter (shown in **Fig.1c**), we tested whether sgRNA-induced mutations in β-catenin influence the induction *AXIN2*, an endogenous WNT target gene widely used as a metric for WNT/β-catenin signaling strength, or the abundance of β-catenin. Additionally, we tested whether selected mutations in β-catenin influence the constitutive oncogenic signaling seen in CRC cell lines carrying truncating mutations in APC. **a,c**, *AXIN2* mRNA levels were measured by quantitative reverse-transcription PCR (qRT-PCR) in HEK293T-7TS cells carrying the indicated mutations in β-catenin (confirmed by Illumina sequencing as shown in **Extended Data Fig.6**). Cells were left untreated or treated (24 h) with the indicated concentration of WNTs (RSPO3+Wnt-3a). **b,d,** the abundance of β-catenin protein in these same cell lines was measured by immunoblotting after a 4 h exposure to RSPO3 + Wnt-3a or GSK3β inhibitor (CHIR99021). α-tubulin serves as a loading control. The dashed red rectangle in **b** highlights a β-catenin mutation (E571K) with a defect in Wnt-3a-induced β-catenin accumulation but not CHIR99021-induced accumulation. **e**, PPIs between components of the wild-type, ligand-regulated BDC containing full-length APC (top) and the oncogenic BDC (bottom) containing truncating mutations in APC (APC^{mcr}). Colored lines indicate previously mapped PPIs between AXIN1-APC, APC-β-catenin, and AXIN1-β-catenin. Most oncogenic mutations in APC truncate the protein in the Mutation Cluster Region (MCR), eliminating all direct contacts between the APC SAMP motifs and the AXIN1 RGS domain and a subset of contacts between APC and β-catenin. TBD, tankyrase binding domain; DVL, Dishevelled; CBD, β-catenin binding domain of AXIN1; GBD, GSK3β-binding domain, DAX, Domain present in DVL and AXIN. See **Fig.1b** for further details. **f**, Linear cartoon representation of β-catenin showing the 12 ARM repeats and predicted mutations generated by sgRNAs tested in **g** and **h**. **g,h,** Activity of a WNT fluorescent reporter (7xTCF-GFP, same as the 7TS reporter **Fig.1c** but with GFP) in two CRC cell lines expressing the indicated sgRNAs (**f** shows predicted mutations). APC is truncated at amino acid residue 1320 in RKO cells (left) and residue 1417 in DLD1 cells (right), leading to constitutive, ligand-independent WNT/β-catenin signaling and high GFP fluorescence. Bars represent the mean of three biological replicates (n=3, each denoted using a different pink shade). Each data point represents the mean fluorescence from approximately 10,000 cells measured by flow cytometry. In **a,c,g,h,** statistical significance was determined using Brown-Forsythe and Welch ANOVA followed by Dunnett's T3 multiple comparisons test for pairwise comparisons between groups.

Extended Data Fig.8

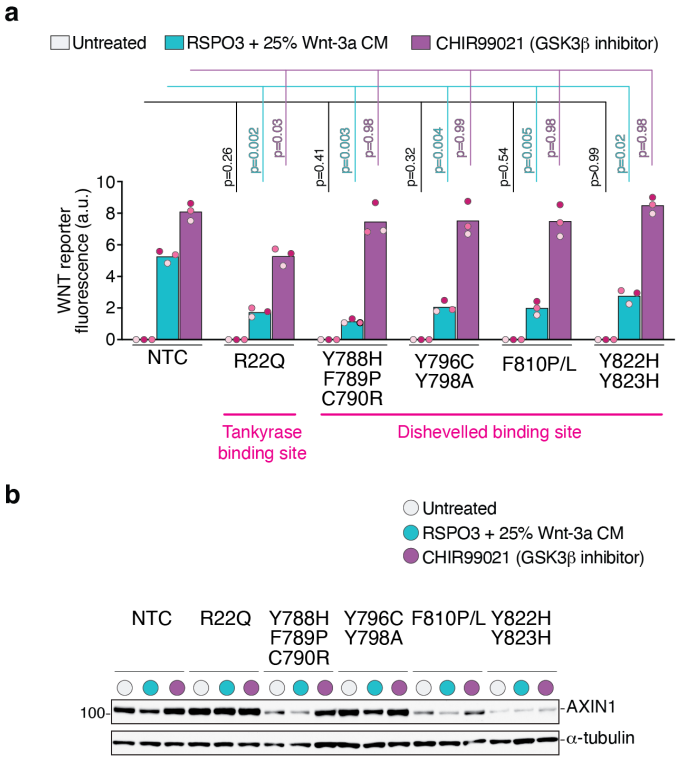

1318

1319

Extended Data Fig. 8. Functional analysis of screen-identified mutations in AXIN1. This figure provides supporting data for **Fig.5**. **a,** WNT/β-catenin signaling strength was measured in HEK293T-7TS cells carrying the indicated mutations in AXIN1 (confirmed by Illumina sequencing as shown in **Extended Data Fig.6**). Cells were left untreated or treated (24 h) with RSPO3 + Wnt-3a or a GSK3β inhibitor (CHIR99021). Bars represent the mean of three biological replicates, with each replicate indicated by a different pink shade. Each data point represents the mean fluorescence from approximately 10,000 cells. Amino acid residues previously known to be critical for the interaction of AXIN1 with Tankyrase 1 (TNKS1) and amino acid residues predicted to be important for the interaction with the DIX domain of Dishevelled are denoted. These amino acid residues are shown on the structural models in **Fig. 5b** and **5c**. Statistical significance was determined using Brown-Forsythe and Welch ANOVA followed by Dunnett's T3 multiple comparisons test for pairwise comparisons between groups. **b**, AXIN1 abundance was measured in these same cell lines after cells were left untreated or treated (5 h) with RSPO3 + Wnt-3a or a GSK3β inhibitor (CHIR99021). α-tubulin serves as a loading control.

Extended Data Fig.9

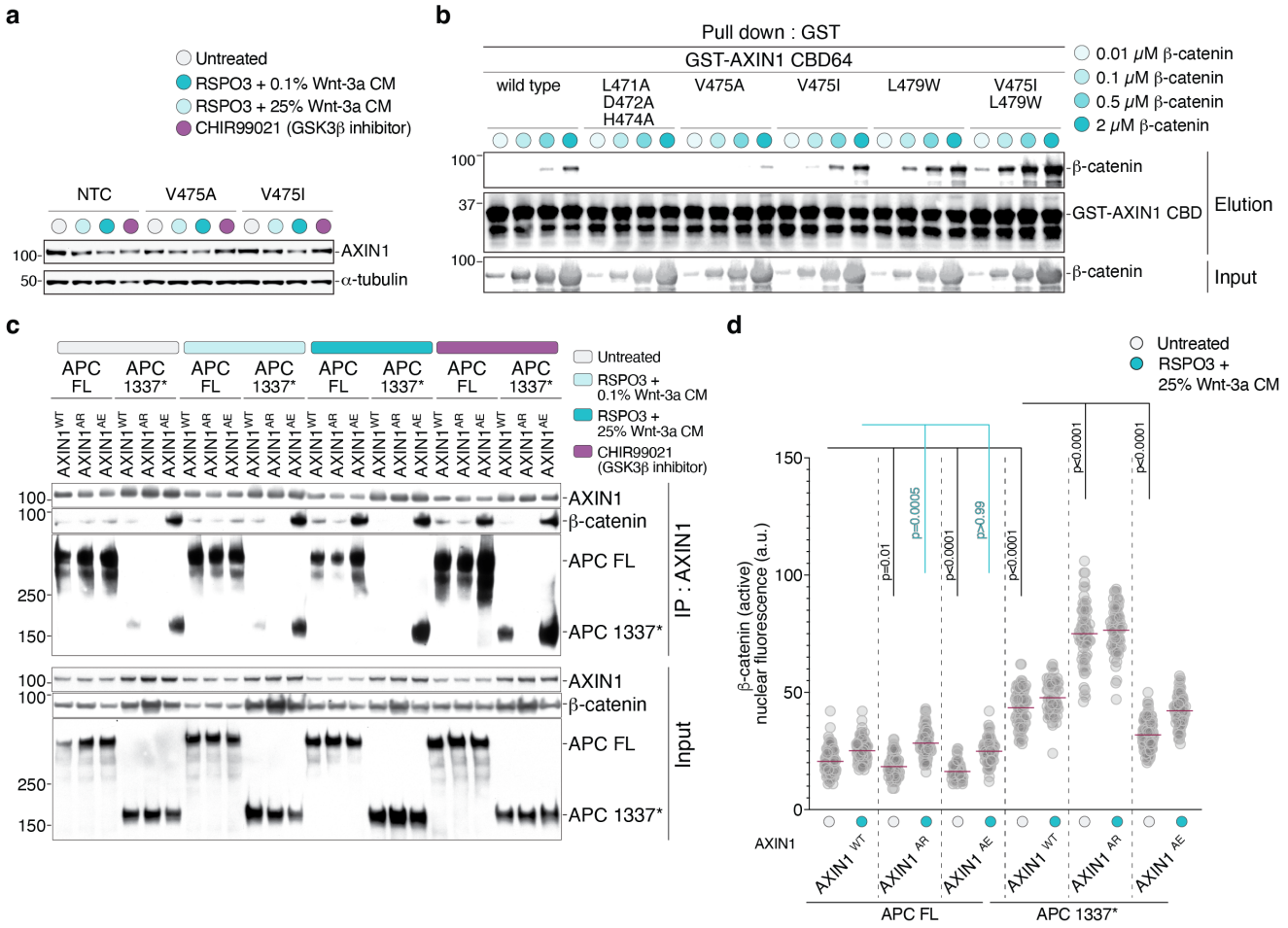

1320

1321

Extended Data Fig. 9. Characterization of AXIN1 mutations in its β-catenin binding domain (CBD). This figure provides supporting data for **Fig. 6** and **Fig. 7**. **a**, AXIN1 protein abundance in HEK293T-7TS cells carrying the indicated mutations (verified by Illumina sequencing) left untreated or treated (5 h) with RSPO3 + Wnt-3a or a GSK3β inhibitor (CHIR99021). α-tubulin serves as a loading control. **b**, An affinity pulldown assay was used as an alternative to Biolayer Interferometry (BLI, **Fig.6d**) to measure the interaction of purified β-catenin with AXIN1 CBD fragments containing the indicated mutations. GST-tagged AXIN1 CBD fragments (1 μM), expressed and purified from *E. coli*, were immobilized on glutathione beads and incubated with increasing concentrations of untagged, full-length, purified β-catenin. β-catenin abundance in the input (5%) and β-catenin captured on the beads (10%) was measured by immunoblotting. **c**, Association of endogenous AXIN1 with APC and β-catenin in extracts from clonal eHAP1 cells measured using an AXIN1 IP followed by immunoblotting. Sequence verified clonal cell lines (**Extended Data Fig.10**) contained the indicated combinations of full-length APC (APC FL) or truncated APC (APC 1337) and one of three AXIN1 variants-- $AXIN1^{WT}$, $AXIN1^{AE}$ (V775I/L479W) and $AXIN1^{AR}$ (L471A/D472A/H474A)-- with varying affinities for β-catenin (see **Fig.6d**). Extracts were made from untreated cells or cells treated (1h) with low-dose Wnt-3a, high-dose Wnt-3a or CHIR99021. This experiment is identical to the one shown in **Fig.7a** but performed using an independent set of clonal cell lines. **d**, Nuclear abundances of active (non-phosphorylated) β-catenin were measured by immunofluorescence and quantitative image analysis in clonal cell lines carrying the indicated combinations of *APC* and *AXIN1* alleles (same cell lines as those used in **Fig.7a** for IP experiments). Measurements were performed in untreated cells or cells treated with RSPO3 + Wnt-3a for 2 h. Statistical significance was determined using Brown-Forsythe and Welch ANOVA followed by Dunnett's T3 multiple comparisons test for pairwise comparisons between groups.

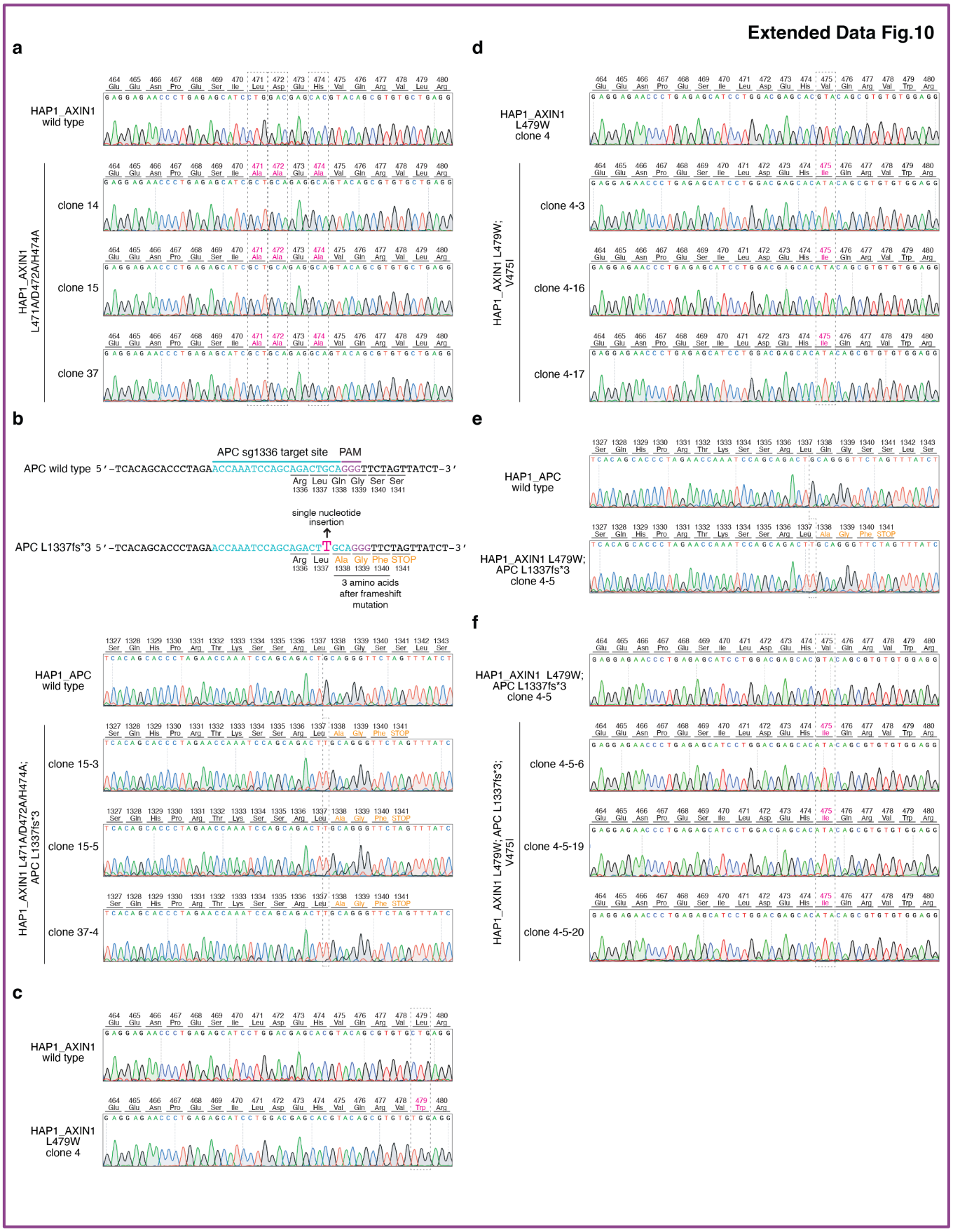
Extended Data Fig.10
a
HAP1_AXIN1 wild type
HAP1_AXIN1 L471A/D472A/H474A
clone 14
clone 15
clone 37
b
APC sg1336 target site
PAM
APC wild type 5′-TCACAGCACCCTAGAACCAAATCCAGCAGACTGCAGGGTTCTAGTTATCT-3′
Arg Leu Gln Gly Ser Ser
1336 1337 1338 1339 1340 1341
single nucleotide insertion
APC L1337fs*3 5′-TCACAGCACCCTAGAACCAAATCCAGCAGACTTGCAGGGTTCTAGTTATCT-3′
Arg Leu Ala Gly Phe STOP
1336 1337 1338 1339 1340 1341
3 amino acids after frameshift mutation
HAP1_APC wild type
HAP1_AXIN1 L471A/D472A/H474A; APC L1337fs*3
clone 15-3
clone 15-5
clone 37-4
c
HAP1_AXIN1 wild type
HAP1_AXIN1 L479W clone 4
d
HAP1_AXIN1 L479W clone 4
HAP1_AXIN1 L479W; V475I
clone 4-3
clone 4-16
clone 4-17
e
HAP1_APC wild type
HAP1_AXIN1 L479W; APC L1337fs*3 clone 4-5
f
HAP1_AXIN1 L479W; APC L1337fs*3 clone 4-5
HAP1_AXIN1 L479W; APC L1337fs*3; V475I
clone 4-5-6
clone 4-5-19
clone 4-5-20

1322

1323

Extended Data Fig. 10. Generation and sequence verification of clonal eHAP1 cell lines carrying various combinations of *AXIN1* and *APC* alleles (used in Fig.7 and Extended Data Fig.9). All mutations were introduced into the single *APC* and *AXIN1* alleles in eHAP1 cells using a combination of CRISPR/Cas9-mediated non-homologous end joining (NHEJ), homology-directed repair (HDR), and base editing. **a**, Sanger sequencing traces confirming the presence mutations (L471A/D472A/H474A) generated using HDR that reduce AXIN1-β-catenin affinity ($AXIN1^{AR}$, **Fig.6c-d**) in three clonal cell lines. **b**, Position of the sgRNA target site and associated PAM sequence in the *APC* gene used to generate an APC truncation mutant (APC 1337*, **Fig.7a**) using NHEJ. Sanger sequence traces from three clonal cell lines show insertion of a single T nucleotide that shifts the translational frame, leading to an in-frame stop codon three amino acids after Leu 1337. **c**, Sanger sequencing trace of a clonal line harboring one of the two mutations (L479W, **Fig.6c-d**) used to generate the affinity-enhancing $AXIN1^{AE}$ variant using HDR. Although only one trace is shown, four additional clonal lines were generated with similar WNT/β-catenin signaling phenotypes. **d**, Sanger sequencing traces of clonal lines harboring both mutations (V475I/L479W) used to generate the affinity-enhancing $AXIN1^{AE}$ variant (**Fig.6c-d**). The V475I mutation was introduced using base-editing of the cell line shown in **c**. **e**, Sanger sequencing traces of a clonal line edited using NHEJ to introduce an APC truncating mutation (APC 1337*) in the background of the *AXIN1* L479W mutation (from **c**). Although only one trace is shown, seven additional clonal lines were generated with similar WNT/β-catenin signaling phenotypes. **f**, Sanger sequencing traces of clonal lines base edited to introduce the V475I mutation in the background of the AXIN1 L479W and APC 1337* mutations (from panel **e**).